UNIVERSITÀ DI PISA

Scuola di Dottorato in Ingegneria "Leonardo da Vinci"

Corso di Dottorato di Ricerca in
Ingegneria dell'Informazione

Tesi di Dottorato di Ricerca

About the Use of Adaptive Antennas in 60 GHz UWB-OFDM Personal Area Network Transceivers

Autore:

Domenico A. Fittipaldi _____

Relatori:

Prof. Marco Luise _____

Anno 2008

Abstract

The recent opening of unlicensed spectrum around 60 GHz has raised the interest in designing gigabit Wireless Personal Area Networks (WPANs). Since at 60 GHz the signal attenuation is strong, this band is basically suitable for short range wireless communications. It is understood that directional antennas can be employed to compensate for the path loss and combat the waste of power due to the scatter phenomena characteristic of these high frequencies.

This thesis studies the use of adaptive array systems in 60 GHz Ultra Wide Band-Orthogonal Frequency Division Multiplexing (UWB-OFDM) personal area network transceivers. The study has been conducted by simulations and theoretical analysis. Two sensor arrangements have been considered, the Uniform Linear Arrays (ULA) and the Uniform Circular Arrays (UCA), in the simple case of the Line of Sight (LOS) transmission scenario.

On the one hand we have designed a IEEE 802.15.3c Medium Access Control (MAC) phased-array controller throughput using Direction of Arrival (DOA) estimation to perform beamsteering. We have simulated the MAC controller with the network simulator ns-2. The impact of the array controller performance onto the achievable throughput of the wireless links has been studied to draw the requirements about the standard deviation of the DOA estimator.

On the other hand, we have found the Cramér-Rao Bound (CRB) for DOA estimation of impinging 60 GHz OFDM sources. The requirements of the standard deviation of the DOA estimator are analysed against the CRB for DOA to validate the design of the directional 60 GHz UWB-OFDM transceivers.

The comparison reveals that directional 60 GHz UWB-OFDM transceivers can achieve high wireless throughput with a number of pilot subcarriers and for a Signal to Noise Ratio (SNR) operating range typical of next generation WPANs.

Summary

Chapter I. Introduction: Millimeter Wave PANs 1

1.1 The 60 GHz Challenge 1

1.2 Smart Antennas Overview 3

1.3 Advantages of Directional Antennas for 60 GHz WPANs 4

1.4 Adaptive Arrays Controller 6

1.5 Goal and Contributions 7

1.6 Outline 8

Chapter II. Antenna Arrays Fundamentals 11

2.1 Array Processing 11

2.3 Reference Antenna System 14

2.4 Narrow Band Antenna Model 16

2.5 Uniform Linear Array Model 16
2.5.1 Array Factor of ULA Systems 19

2.6 Uniform Circular Antenna Model 25
2.6.1 Array Factor of UCA Systems 26

2.7 Antenna Directivity. 28
2.7.1 Directive Gain of ULA Systems 29
2.7.2 Directive Gain of UCA Systems 29

2.8 Beamsteering 30
2.8.1 Beamsteering of ULA Systems 30
2.8.2 Beamsteering of UCA Systems 33

2.9 Half Power Beamwidth of ULA Systems 35

Chapter III. Simulation Analysis with IEEE 802.15.3c MAC 37

3.1 General Description of IEEE 802.15.3 37

3.2 Adapting IEEE 802.15.3c MAC for the Use of Phased Array Antennas 41
3.2.1 DOA Estimation on the PHY Preamble 41
3.2.2 Frame Driven Beamsteering in IEEE 802.15.3c MAC 43

3.3 Simulation Background 46

3.4 Simulations Analysis with ULA Systems 48

3.5 Simulations Analysis with UCA Systems *54*

Chapter IV. CRB for DOA Estimation of Narrow Band Data Signals **57**

4.1 CRB on DOA Estimation of Narrow Band Signals. *57*

4.2 Derivation of the **FIM** *from the Sufficient Statistic* *60*

4.3 CRB for DOA with ULA Systems *61*

4.4 CRB for DOA with UCA Systems *64*

4.5 Extension of the Observation Time to more Symbol Intervals *66*

4.6 Derivation of the FIM *from the Continuous Time Observation Space* *67*

4.7 MCRB: Estimation with Unknown Data Symbols *67*

Chapter V. CRB for DOA of OFDM Data Signals **71**

5.1 CRB of Parameter Estimation with Waveforms having Orthogonal Derivatives *71*

5.2 DOA Estimation of OFDM Signals over AWGN Channel *75*

5.2.1 Numerical Example: IEEE802.15.3c OFDM 81

5.2.2 Comparison between OFDM Signals and Monocarrier Signals 84

5.3 DOA Estimation of OFDM Signals over Frequency Selective Channel *87*

5.4 Comparison of the CRB for DOA with the Simulation Analysis Results *93*

Conclusions and Developments **96**

Appendix A: Analytic White Gaussian Noise **99**

Appendix B: FIM Computation **101**

B.1 Derivation of the FIM *from the sufficient statistic z of narrow band signals* *101*

B.2 Derivation of the FIM *from the analytic signal y(t) of narrow band signals* *106*

B.3 Derivation of the FIM *for OFDM Signals in the case of Frequency Selective Channels* *111*

References **114**

Chapter I. Introduction: Millimeter Wave PANs

1.1 The 60 GHz Challenge

Wireless personal area network (WPANs) are used to convey information over relatively short distances among a relatively few participants through connections involving little or no infrastructure. This allows, small power efficient, inexpensive solutions to be implemented for a wide range of wireless devices. The millimeter-wave PANs will be the Gbps evolution of the wireless personal area network technology. The first WPAN standard is IEEE 802.15.1 which is commonly known with the name of Bluetooth, while the latest standard of this wireless family is IEEE 802.15.3a which operates in the 2.4 GHz Industrial Scientific and Medical (ISM) Band [1].

The recent opening of massive unlicensed spectrum around 60 GHz fosters the design of WPANS with a target date rate up 5 Gbps whilst the ones operating at 2.4 GHz reaches 55Mbps at most. The abundance of bandwidth available and the signal propagation phenomena typical of these frequencies make the 60GHz band appealing for the even growing market of the short range wideband applications when the other unlicensed bands are or are becoming crowded.

Two organizations that have driven the 60 GHz radios are the IEEE 802.15.3 standard body [2] and the WiMedia Alliance [3], an industrial association. The IEEE 802.15.3 Task Group 3c (IEEE 802.15.3c) is developing a *mm*-wave-based alternative physical layer to the existing 802.15.3 WPAN standard IEEE-Std-802.15.3-2003. The WiMedia Alliance is pushing a 60GHz WPAN industrial standard based on Orthogonal Frequency-Division Multiplexing (OFDM) [4]. Figure 1. 1 and Table 1. 1 show the worldwide availability of bandwidth around 60 GHz and the most recent regulatory results for this band.

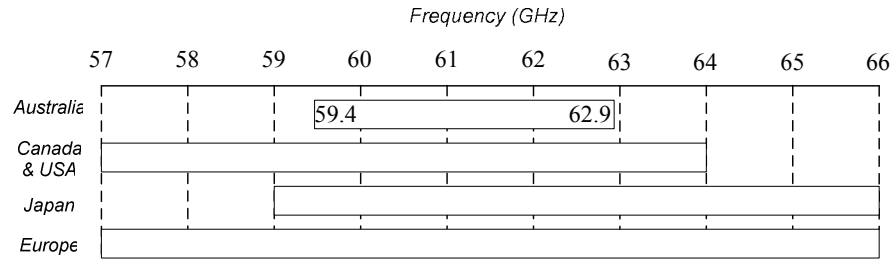

Figure 1. 1- Spectra available around 60 Hz

Table 1. 1 - Emission power requirements

Region	Output Power	Other Considerations
Australia Canada and USA	10 mW into antenna 500 mW peak	150 W peak EIPR min. BW = 100MHz
Japan	10 mW into antenna +50, -70% power change OT and TTR	47 dB_i max. ant. Gain
Europe	+ 55 dBm EIPR	min. BW = 500 MHz

The core of the design of the millimeter WPANs lies at the physical layer (PHY) and the Medium Access Control (MAC) layer. At PHY the wireless channel reliability is the issue to face in order to make the high data rates of the millimetre WPANs realistically achievable. Probably, OFDM is the most suitable technique for high speed data transmission at 60 GHz. This technique partitions a high frequency selective wideband channel to a group of nonselective channel, which makes it robust against large delay spreads while preserving orthogonality in the frequency domain. Another property of OFDM that makes it very attractive for wideband applications is its easy scalability to different environment, bandwidth and bit rates. Our study assumes OFDM as the data modulation technique of the millimeter WPANs [2].

Another important feature of these frequencies is the strong attenuation that the signals undergo in free space propagation and trough materials. Directional antennas are the candidate PHY capability to compensate for the path loss. In Section 1.3 we review the *Smart Antennas* in general and in

Section 1.3 we discuss the potential benefits of the adaptive antennas in the specific case of the *mm*-wave WPANs by taking into account the features of the wireless channel at the frequencies of interest.

On the other hand, the use of directional antennas raises the problem of designing the beamforming intelligence that steers the main lobe of the antenna to point the right direction at the right time. The design usually involves PHY and MAC, although it could touch other network layers at the cost of more end-to-end delay in the case of data delivery failure and more compatibility problems among different standards. In Section 1.4 we discuss the guidelines of designing adaptive array controllers in more detail.

1.2 Smart Antennas Overview

Smart antennas are directional antennas that use signal processing both in space and time to sense the neighbour electromagnetic environment and to adjust their radiation patterns subsequently according to a given transmission\receive strategy. This mechanism through which the wireless devices become aware of the surrounding environment and react to it when transmitting\receiving constitutes the intelligence of the smart antennas. This intelligence is usually categorized into: *Switched Beam Antennas* and *Adaptive Array*s [5].

- *Switched Beam Antennas* are designed with a fixed set of radiation patterns. This type of smart antennas can be created by using multiple directive elements each pointing towards different sectors. Basically, the outputs of the radiation patterns of the directive elements are continuously sampled, and the output statistics are composed by selecting (maximum signal) or combined (maximum ratio, equal gain) the output samples. Perfect match between the antenna beams and direction of arrival is realized only in a limited number of directions, those of the single antenna patterns. When plotting the received signal strength versus the Direction of Arrival (DOA), one notices that the plot

marks the antenna pattern with even nulls in the nulls of the antenna pattern. This roll-off behavior is known as *scalloping*.

- *Adaptive Arrays* are antenna systems where the signals at the input(output) of the antenna elements are multiplied by complex weights that are called *weighting elements*. These coefficients can be controlled both in amplitude and in phase by an array processor network. If the array processor is designed to control the phases of the signals at each array element but not their magnitudes, the adaptive array is specifically called *Phased Array*. Phased Arrays provide *beamsteering* only, that is, the main array beam is steerable in any direction. If the array processor control the amplitudes of the weighting elements as well, the adaptive array system is capable of performing *beamforming* which is beamsteering and *null placing* together. Nulls can be placed in the look angles of interfering sources.

Switched-beam antennas are cheaper than adaptive array antennas but the later outperform the former in co-channel interference spatial filtering and direction tracking. This difference is of great importance in mobile applications.

1.3 Advantages of Directional Antennas for 60 GHz WPANs

As for the matter of power, there two main points that is worth highlighting. Array antenna systems relax the requirements for power amplifiers and enlarge the operational coverage of the radio link with respect to isotropic antennas.

According to reports from BWRC, CMOS amplifier gain at 60 GHz is below 12 dB [6], which raises a concern about limited transmitted power. If each branch can emit a certain amount of power, an M-branch transmitter can emit roughly $20\log_{10}(M)$ more power compared to the case of a single antenna transmitter **[7]**.

On the other hand, the radio coverage increases because the random multipath reflections are suppressed and the power is focused in one

intended direction. This, on the one hand, reduces the delay spread with respect to omni antennas. On the other hand, a comparable spatial outage reduction would be highly power consuming in the 60GHz band if performed by omni antennas. In fact the free space path loss of the millimeter waves is $(60/5)^2$ (21.6dB) times the one at 5 GHz and $(60/2.4)^2$ or (27.96 dB) higher than that at 2.4 GHz. High gain directional antennas compensate for the high propagation loss with the antenna gain instead of increasing the power emission. This also limits the generation of co-channel interference. The attenuation of the millimeter waves is also strong trough materials. It is understood that walls of a building act like reliable cell boundaries and WPANs in the 60GHz band will be deployed as in-room, -corridor or -hall cells with hot spot communications.

Another advantage of having a set of antenna elements comes with the application of diversity techniques to resolve the dominant path(s) in a space-time domain for the purpose of improving the link quality/reliability. Diversity antenna schemes require low cross correlation among the diversity channels. In spatial diversity, the cross correlation of the signals received at the array elements is a function of the array element spacing and the power angle profile. Placing the array elements at the distance of many times the wavelength (λ=5mm at 60 GHz) creates low correlation among the channels of the antennas composing the array.

The replicas of the signal may be also uncorrelated in the case of a significant angle spread so that multiple antenna beams receive distinct paths. Angle diversity is expected to provide significant gain improvement in rich scatter environments. In [8] it has been shown that at 60 GHz the angular spread is quite rich for room and obstructed indoor propagation while for Line of Sight (LOS) applications the LOS component is 10 dB above the first order reflections if no strong reflectors are present. In this case Array Processing can be applied to acquire the LOS direction in order to establish directional communication by practicing beamsteering or more

in general beamforming. Beamforming increases the network throughput by reducing the interference generation/affection in unintended directions.

1.4 Adaptive Arrays Controller

The design of smart antennas controllers is considered as part of the overall design of the MAC protocols, and the realizable gains of smart antennas for a specific network depend on the control algorithms in use. Lots of work can be found in the literature about the basic mechanisms of employment of the smart antennas in WLANs and Mobile Ad Hoc Networks (MANETs) for the purpose of reducing the typical collision rates of many contention-based MAC access protocols like Aloha, CSMA, CSMA/CA and TDMA [9 - 19]**.**

The advantages of the smart antennas come with the narrow beam signal transmission and/or reception. The main issue related to such narrow beams consists in the knowledge of the pointing direction and in the coordination of antenna steering at both ends prior to accomplishing data transfer among devices. Information about the steering direction toward the intended device is provided through neighbour discovery algorithms which are carried out before the link establishment. There are two basic categories of neighbour discovery techniques with smart antennas in ad-hoc self-configuring wireless networks. One category is composed of those algorithms that do not make use of omni receive operations at any stage. These algorithms are classified as *scan-based* algorithms, [15] [17]. When using this class of algorithms, devices in the network are synchronized and follow a predefined scan sequence to discover neighbours and point the right direction at the right time. On the other hand, the other class of neighbours discovery strategy is based on the capability provided by the array processing of estimating the angle of arrival of a radio source impinging on the array system. Direction of arrival information is subsequently exploited for space diversity access to the shared radio medium. A thorough characterization of the direction of arrival estimation capability is thus of paramount

importance to validate the use of array sensors as realistically viable. In [20] the authors raise the issue of the antenna controller accuracy with highly directive antenna systems. They study the throughput behaviour versus the steering error in a Time Division Multiple Access (TDMA) link and show that significant throughput degradation may be caused by a pointing error of a few degrees. Again the actual benefits of the smart antennas in a specific network depend on the antenna control system whose performance is directly bound to the one of the algorithms of DOA estimation in use.

1.5 Goal and Contributions

The goal of this thesis is to study the use of adaptive antennas in 60 GHz Ultra Wide Band (UWB)-OFDM wireless personal network transceivers. It has been conducted as follows.

We have studied the network throughput of the 60 GHz WPANs with an extended version of the IEEE 80215.3a MAC supporting the use of directional antennas. The antenna controller that we have developed for this purpose, makes use of DOA estimation capability to perform neighbour discovery. The antenna controller protocol has been implemented into the network simulator ns-2 [21] and software simulations have been run for the sake of assessing the impact of the antenna pointing error onto the network throughput performance for several configurations of antenna directivity. With the simulation analysis we have drawn the requirements regarding the pointing controller of the array system. To validate the use of the adaptive antennas in general, and of our MAC protocol in particular, we have compared these requirements against the Cramér-Rao Bound (CRB) for DOA estimation of OFDM wireless signals detected by array systems. The derivation of this CRB represents the second contribution of our work. The CRB on DOA estimation is well documented in the literature for narrowband signals and many typologies of array systems, but not much is done for wideband sources. Moreover, the available research for wideband applications is limited to the model of the zero mean stochastic Gaussian

wideband source with the analysis being conducted in the spectral domain [22 - 23]. Further research can be done in this direction to cover the gap of specific signal formats in lieu of the generic Gaussian source model. In our work we have focused on broadband OFDM sources with a carrier frequency around 60 GHz and a channel bandwidth is 1-5 Gbps. Thus, the hypothesis of the wideband Gaussian source has been dropped and the CRB on the DOA estimation of the OFDM incident signal has been approached according to the estimation model of the deterministic signals [24].

List of Publications:

[C3] **Antonio Fittipaldi**, Stan Skafidas, Marco Luise
IEEE 802.15.3c Medium Access Controller Throughput for Phased Array Systems
PIMRC 07, September 2007, Athens, Greece

[C2] **Antonio Fittipaldi**, Marco Luise
Game Theory-based Power control Criteria in CDMA Wireless Ad Hoc Network
Med-Hoc-Net 2006, June 2006, Lipari, Italy

[C1] **Antonio Fittipaldi**, Marco Luise
Power-Saving and Capacity-Maximizing Power control Criteria in CDMA Wireless Ad Hoc Networks
15th IST Mobile & Wireless Communications Summit, June 2006, Mykonos, Greece

1.6 Outline

This thesis is organized as follows. In Chapter II we review the topic *Array Processing* to fix the background needed to develop our analysis. Two models of antenna arrays have been considered throughout the thesis, the Uniform Linear Antenna (ULA) model and the uniform circular antenna (UCA) model. In Chapter III we first describe the MAC mechanism to control phased-antennas with IEEE 802.15.3 MAC and then discuss the simulation analysis of our phase array controller throughput which has been conducted with the network simulator ns-2. Chapters IV and V are

dedicated to the study of the CRB for DOA estimation. In Chapter IV we provide the mathematical formalism to develop the analysis and review the CRB inferior limit for narrow band signal sources. In Chapter V, we step into the domain of the OFDM wideband signals. The general results of this section are further analysed in the case of the UWB-OFDM signals of the 60 GHz PANs.

Conclusions and considerations for future development conclude the work.

Chapter II. Antenna Arrays Fundamentals

2.1 Array Processing

In this paragraph we introduce the topic *Array Processing* with the aim of understanding how our work covers the issues that are typical of the array processing theory. Moreover, this introduction serves to fix some basic assumptions of our analysis. Four main issues of interest related to the array processing that we briefly discuss are:

A Applications
B Spatial and temporal characteristics of the signal
C Spatial and temporal characteristics of the interference
D Array configuration
E Objective of the array processing

Array processing plays an important role in many application areas such as

A1 Radar
A2 Radio astronomy
A3 Sonar
A4 Communications
A5 Direction-finding
A6 Seismology
A7 Medical diagnosis and treatment

The problems treated in this work falls in the application areas A1, A4 and A5. The second issue is the spatial and temporal structure of the signal. In the temporal domain we can highlight the following categories

T1 Known signals
T2 Signals with unknown parameters
T3 Signals with known structure (e.g. QPSK)
T4 Random signals

In the spatial domain, the cases of interest are

S1 Plane-wave signals from known directions

S2 Plane-wave signals from unknown directions

S3 Spatially spread signals

In this regard, this work covers the combinations T2-S2 and T3-S2.

The third issue is the spatial and temporal structure of the noise (or interference). We will always include "a sensor noise" component that consists of a white Gaussian noise disturbance that is statistically independent from sensor to sensor. A complete treatment of the noise would also include external sources of interference and provide for them a characterization both temporal that spatial. In this work we neglect this class of interference and limit our analysis to the noise having thermal origin only.

Array configuration consists of two parts. The radiation pattern of the antenna array in the far field $\mathbf{E}(\theta,\varphi)$ can be expressed as the product of two factors, the array factor $AF(\theta,\varphi)$ and the element factor $\mathbf{EF}(\theta,\varphi)$. The array factor depends on the amplitudes and phases of the signals feeding the array elements, and on the arrangement of the elements in the array. The element factor depends on the physical dimensions and electromagnetic characteristics of the radiating elements. The array geometries can be divided into three categories:

G1 Linear

G2 Planar

G3 Volumetric (3-D)

and for each category other classes of sub-division are of interest

U1 Uniform spacing

U2 Non-uniform spacing

U3 Random spacing

In this work we focus on Uniform Linear Array (ULA) systems and Uniform Circular Array (UCA) systems. They belong to the classes G1-U1 and G2-U1, respectively.

As for the Element Factor, for the sake of argument, consider two of the mostly widely used antennas, namely the short dipole and a half-wave patch antenna. When positioned along the *z*-axis their element patterns are given by

$$EF(\theta,\varphi) = E(\theta,\varphi) = \frac{\cos\left(\pi/2\cos(\theta)\right)}{\sin^2(\theta)} \qquad half\ \ wave\ dipole$$

and

$$EF(\theta,\varphi) = E(\theta,\varphi) = \cos\left(\frac{\pi L}{\lambda}\sin(\theta)\right) \qquad half\ \ wave\ patch$$

where $L \approx 0.49\,\lambda/\sqrt{\varepsilon_r}$ is the resonant length of a half-wave patch and ε_r indicate the dielectric constant [25].

In the following we restrict our analysis to the 2-D case and consider that the plane waves lie in the azimuth plane $(\pi/2,\phi)$. Thus, the phase the radiation patterns becomes

$$EF(\theta,\varphi) = 1 \qquad half\ \ wave\ dipole \tag{2.1}$$

and

$$EF(\theta,\varphi) = \cos\left(\frac{0.49\pi}{\sqrt{\varepsilon_r}}\right) \qquad half\ \ wave\ patch \tag{2.2}$$

From (2.1) and (2.2) one gets that under the assumption of identical and isotropic sensors, the element factors of the sensors are all equal to a constant, so that, without loss of generality, such a constant can be supposed to be unity and the sensors of the array can be supposed to be half-wave dipoles all, without loss of generality.

The fourth issue of interest is the objective of the array processing theory. A representative list of objectives is:

- O1 Detect the presence of a signal in the presence of noise and interference
- O2 Demodulate the signal and estimate the information waveform in the presence of noise and interference.

O3 Detect the information sequence of a digital communication arriving over multiple paths

O4 Estimate the Direction of Arrivals (DOAs) of multiple plane-wave signals in the presence of noise

O5 Direct the transmitted signal to a specific spatial location.

In this work we will focus on O4 and O5.

In general, the terms that define the detection/estimation problems may vary significantly application to application and many combination of the aspects listed as above are possible. An example is the temporal model of the signal that is processed at the receiver. It may be strictly identified with the particular application area. As for the DOA estimation of a plane wave impinging on an array system, we may state that in telecommunications systems, area A4, the model of the received signal is usually the one of a known deterministic source that bears random parameters to estimate such as the DOA or the channel phase and amplitude. This is the modelling that we have adopted in our work. When instead we deal with physical phenomena, like in sonar or seismology, the signal source is usually considered as a random process whose description is given in terms of power spectral density that contains the parameters to estimate.

2.3 Reference Antenna System

The antenna array model is composed of M sensors placed at the positions

$$\mathbf{p}_m = x_m\hat{\mathbf{x}} + y_m\hat{\mathbf{y}} + z_m\hat{\mathbf{z}}, \qquad m = 0,...,M\text{-}1$$

The reference coordinate system we refer to is scratched in Figure 2. 1. The array sensors are assumes to be isotropic and identical to each other. Consider a narrow band plane wave that impinges on the array from the direction (θ,φ), where θ and φ indicate the azimuth and elevation angle, respectively. In the following the angle pair (θ,φ) is called *Angle of Arrival* (AOA) or *Direction of Arrival* (DOA) of the plane wave. The assumption of a plane wave holds when the signal source is in the far field of the receive antenna which implies that the radius of the wave front is much bigger than

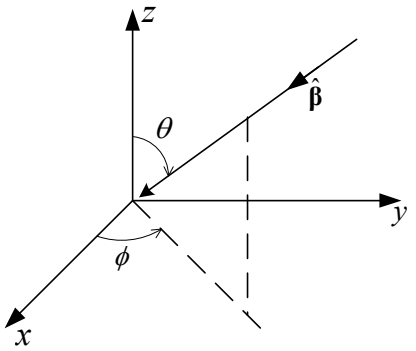

Figure 2. 1 - Coordinate System

the physical size of the antenna array. We indicate the phase propagation factor of a wave at the wavelength λ with $\boldsymbol{\beta}$

$$\boldsymbol{\beta} = -\frac{2\pi}{\lambda}\left(\cos\phi\sin\theta\hat{\mathbf{x}} + \sin\phi\sin\theta\hat{\mathbf{y}} + \cos\theta\hat{\mathbf{z}}\right) = \frac{2\pi}{\lambda}\hat{\boldsymbol{\beta}}$$

where $\hat{\boldsymbol{\beta}}$ denotes a unity vector in the direction of propagation of the plane wave. As said our analysis is 2-D and the DOA of the plane wave lies in the azimuth plane $(\pi/2, \phi)$. Thus, the phase propagation factor simplifies

$$\boldsymbol{\beta} = -\frac{2\pi}{\lambda}\left(\cos\phi\hat{\mathbf{x}} + \sin\phi\hat{\mathbf{y}}\right)$$

The appearance of the elevation angle θ in the formulas that follow is to be interpreted as an intended reminder that the concepts we come across are true in the volumetric space in general. The phase difference between the received signals at the *m*-th element of the array and the origin of the coordinate system ($x = y = z = 0$) is

$$\Delta\psi_m = -\boldsymbol{\beta}\cdot\mathbf{p}_m$$

with $\cdot$ that indicates inner product. Accordingly, the propagation time of the wave to propagate from the array element *m* to the origin of the coordinate system is

$$\tau_m = -\frac{\hat{\boldsymbol{\beta}}\cdot\mathbf{p}_m}{c}$$

where c is the speed of propagation of the plane wave front.

2.4 Narrow Band Antenna Model

In this work we are interested in studying the use of the antenna arrays in telecommunications systems. Thus, We point out the fundamentals of the array processing theory for digital communications applications. In the following we explain the narrow band antenna model in depth. It models the signal reception of narrow band digital information signals by antenna arrays. The reference quantity of the digital signal is the signalling interval which is to be compared with the propagation time that the wave front of the plane wave takes to propagate over the inter element spacing of the array system. If one can assume that the signalling interval of narrow band digital signal is much larger than the characteristic propagation time, thus, at any time epoch t all the sensors in the array system receive the same symbol time. Moreover, the signals captured by the array sensors have the same amplitude but different phases. These phases are the only quantities of the received signal that contain the information of the direction of arrival. Then, direction of arrival estimation can be carried out by manipulating the signal phases at the array sensors output. This concept is formulated in detail in the subsequent sections for the two spatial distributions of array sensors that we have study in this work, that is ULA and UCA.

2.5 Uniform Linear Array Model

The antenna elements of ULA systems are positioned along a linear direction, which is the axis x in our study, with a uniform element spacing d , Figure 2. 2. The m-th element location is

$$\mathbf{p}_m = x_m \hat{\mathbf{x}} = md\hat{\mathbf{x}} \qquad m = 0,...,M\text{-}1$$

We indicate with $r(t)$ the analytic narrow band impinging signal at the origin of the coordinate system. $r(t)$ is referred to as the reference signal impinging on the array system throughout this document. Its general expression is

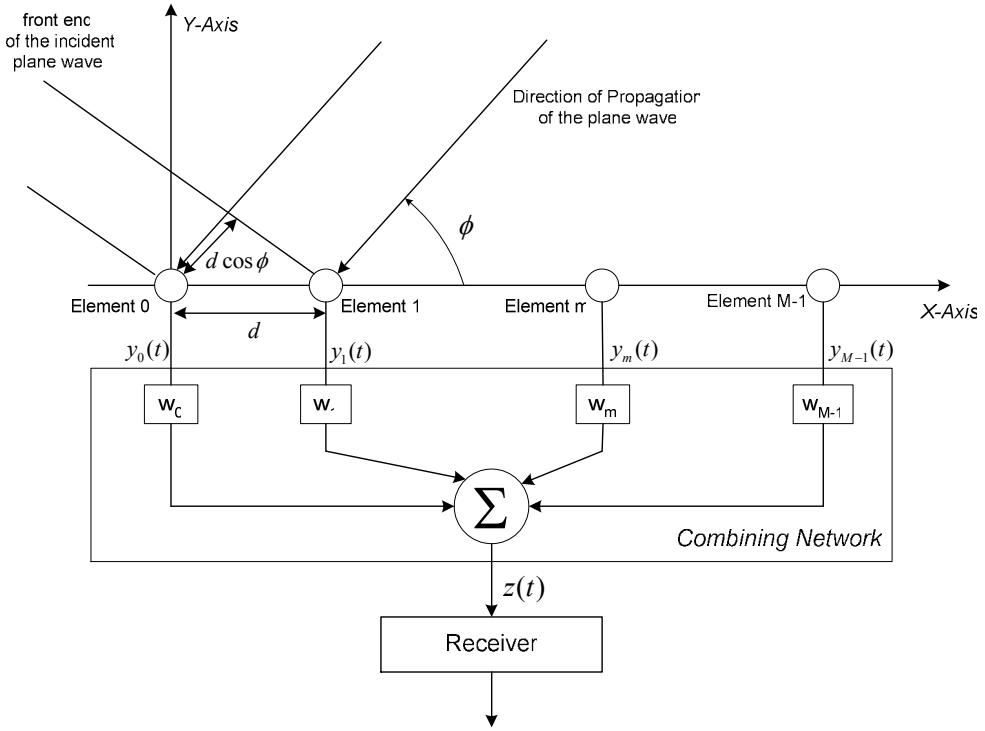

Figure 2. 2 - ULA Reference System

$$r(t) = \mu(t)e^{j2\pi f_c t} \tag{2.3}$$

where f_c is the carrier frequency and $\mu(t)$ is a narrow band signal bearing the data modulation signal. The *m*-th array element produces the signal

$$r_m(t) \triangleq r(t+\tau_m) = \mu(t+\tau_m)e^{j2\pi f_c(t+\tau_m)} = \mu(t+\tau_m)e^{j(2\pi f_c t+\Delta\psi_m)}$$

where *m* represents the element index in the array $m = 0,...,M\text{-}1$. In the remainder of this work, the range of *m* will be omitted.

If the impinging complex modulation signal $\mu(t)$ does not vary significantly over

$$\max\{\tau_m\} = \frac{d(M-1)}{c}$$

which is the propagation time from one end-sensor to the opposite end-sensor of a plane wave impinging from $\phi = 0°$ or $\phi = 180°$, the simplification

$$\mu(t + \tau_m) \simeq \mu(t)$$

holds for all the array elements. For a data-modulated signal this means that

$$\max\{\tau_m\} \ll T$$

where T is the signal interval of a data symbol.

Under this condition, the signal captured by the antenna element *m* differs from the reference signal $r(t)$ by a phase offset only

$$r_m(t) \simeq \mu(t) e^{j(2\pi f_c t + \Delta\psi_m)} = r(t) e^{j\Delta\psi_m} \tag{2.4}$$

Indicating with ψ_o the phase of narrow band incident signal at the origin of the coordinate system, the signal phase at the output of the m-*th* array branch is

$$\psi_m = \psi_o + \Delta\psi_m = \psi_o - \boldsymbol{\beta} \cdot \mathbf{p}_m = \psi_o + \frac{2\pi}{\lambda} md \cos\phi = \psi_o + m\Delta\psi$$

The phase offset $\Delta\psi = \beta d \cos\phi$ between the signals of two adjacent sensors is called the *electrical angle* and contains the DOA information.

We define the vector of the received signals by the array elements as

$$\mathbf{y}(t) = [y_0(t), y_1(t), ..., y_m(t), ..., y_{M-2}(t), y_{M-1}(t)]^T$$

whose *m*-th entry can be expressed as

$$y_m(t) = r(t) e^{-j\boldsymbol{\beta}\cdot\mathbf{r}_m} + n_m(t) = r(t) e^{jm\Delta\psi} + n_m(t)$$

$n_m(t)$ is the noise captured at the array element *m* and is a complex sample function from an analytic white Gaussian noise process with power spectral density $2N_0$ around f_c (see Appendix A). By introducing the *steering vector* or *array manyfold* of uniform linear arrays of isotropic sensors $\mathbf{a}_{ULA}(\phi)$

$$\mathbf{a}_{ULA}(\phi) = [1, e^{j\Delta\psi}, ..., e^{j(M-1)\Delta\psi}]^T \tag{2.5}$$

and defining the noise vector $\mathbf{n}(t)$ as

$$\mathbf{n}(t) = [n_0(t), n_1(t), ..., n_{M-2}(t), n_{M-1}(t)]^T$$

whose covariance matrix is

$$\mathbf{R}_{\mathbf{n}} = E\left\{\mathbf{n}(t)\mathbf{n}^H(u)\right\} = 2N_0\mathbf{I}\delta(t-u)$$

the vector $\mathbf{y}(t)$ of the signals captured at the array sensors can be conveniently rearranged as

$$\mathbf{y}(t) = r(t)\mathbf{a}_{ULA}(\phi) + \mathbf{n}(t) \tag{2.6}$$

The vector notation (2.6) will be used late when we will deal with the DOA estimation. From (2.6), one sees that the noiseless signal at the array output $z(t)$ is

$$z(t) = \sum_{m=0}^{M-1} w_m y_m(t) = r(t)\sum_{m=0}^{M-1} w_m e^{jm\beta d\cos\phi} = r(t)f(\theta,\phi) \tag{2.7}$$

The factor $f(\theta,\phi)$ is termed *array factor*. It represents the ratio of the received signal which is available at the array output, $z(t)$, to the signal input $r(t)$, measured at the reference element of the array, as a function of the DOA (θ,ϕ). $f(\theta,\phi)$ is lied to the steering vector $\mathbf{a}_{ULA}(\theta,\phi)$ as

$$f(\theta,\phi) = \mathbf{w}^T \cdot \mathbf{a}_{ULA}(\theta,\phi) \tag{2.8}$$

where ***w*** is the vector of the weighting coefficients

$$\mathbf{w} = \left[w_0,...,w_m,...,w_{M-1}\right]^T$$

From (2.8) it is evident that by adjusting the set of weights $\{w_m\}$ it is possible to direct the maximum of the main beam of the antenna factor in any desired direction (θ_0,ϕ_0). This is the basic mechanism on which to design antenna controllers that performs beamsteering by exploiting the estimates of the DOA of the received signal. This is the approach that we have followed in this work and that will be explained later with more details.

2.5.1 Array Factor of ULA Systems

From the analysis of the array factor one can understand the directional properties of the antenna arrays. The parameters of interest are the number of antenna elements in the array *M* and the inter-element spacing *d*. We

rearrange the expression of the array factor given in (2.8) for the case of unity weighting coefficients as

$$f(\theta,\phi) = e^{j\frac{M-1}{2}\beta d\cos\phi}\frac{\sin\left(\frac{M\beta d\cos\phi}{2}\right)}{\sin\left(\frac{\beta d\cos\phi}{2}\right)} \tag{2.9}$$

In Figure 2. 3a and 1.3b, we have plotted the amplitude of the array factor (2.9) normalised to *M*, for different values of *M*. It is evident that increasing *M* determines the following effects on the radiation patterns:

- The width of the main lobe of the radiation pattern reduces. This is crucial for applications where smart antennas are employed to track a mobile device with a single narrow beam. This point will be highlighted later when analysing the system requirements of the antenna controller.
- The number of sidelobes increases. At the same time, the level of the sidelobes decreases compared with the one of the main lobe. Sidelobes are important in wireless systems communication since they represent radiated or received power, in unwanted directions.
- The number of nulls in the patter increases. In interference cancellation applications, the directions of those nulls as well as the null depth has to be optimized.

The inter element spacing *d* also has a significant impact on the shape of the radiation pattern. It is known that the directional properties of the antenna array depend on the array size. Increasing the array size by increasing the number of sensors *M* gets better characteristics of the radiation pattern as far as its shape and degrees of freedom. But, the array size can be increased also by increasing the inter-element separation *d*. By playing on *d* we can customize the design of antenna arrays. The main observation that we draw when analysing the normalized array factor versus *d* is the appearance of replicas of the main beam which are names *gratings lobes*. In Figures 2.4 we have plotted the array pattern of a 8-element antenna array for different

values of d. As is seen when d is $\lambda/4$ or $\lambda/2$, Figure 2. 4a and Figure 2. 4b respectively, the array pattern is composed of one main lobe at 90° and a few sidelobes. The main lobe of the array pattern is termed *boresight*. When d is λ, Figure 2. 4c, a grating lobe appears at 0°. When d becomes greater than λ more grating lobes appear as shown in Figure 2. 4d. To see this, consider that from (2.9), the maxima of the array factor are the solutions in the ϕ of the equation

$$\sin\left(\frac{\beta d\cos\phi}{2}\right)=0$$

which gives

$$\cos\phi=\frac{\lambda}{d}$$

whose solutions exist only if $d\geq\lambda$.

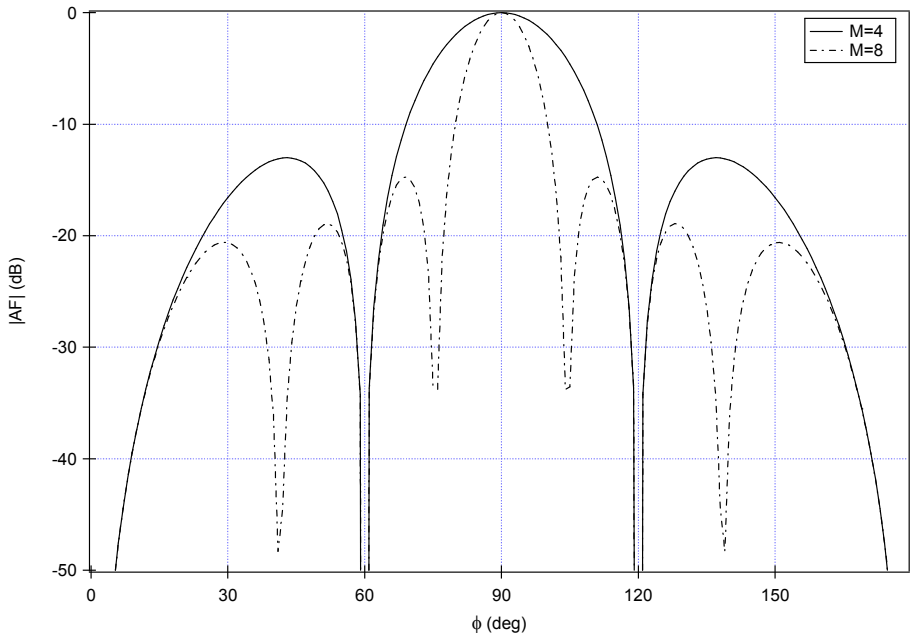

Figure 2. 3a - Radiation Pattern of ULA Systems with d=λ/2

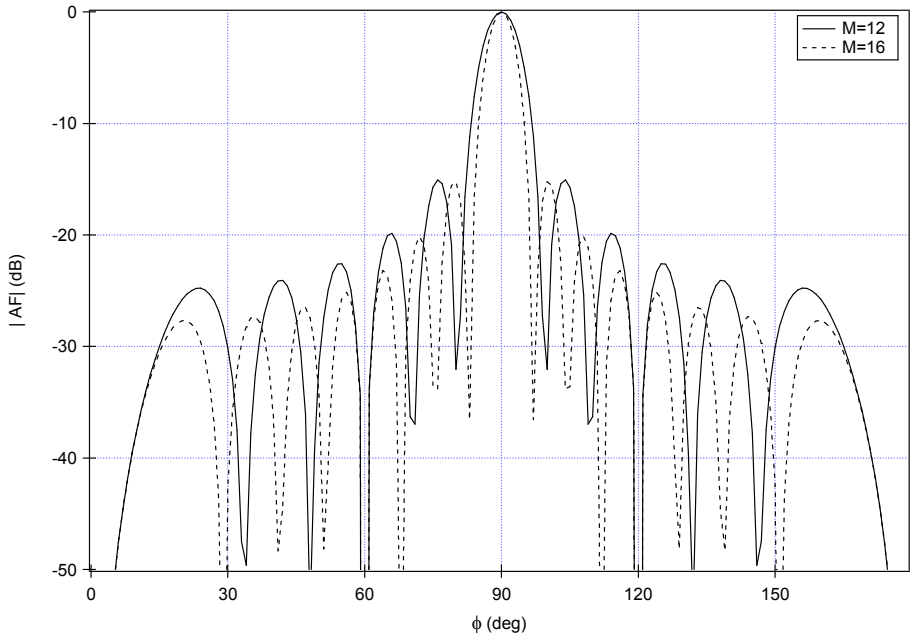

Figure 2.3b - Radiation Pattern of ULA Systems with d=λ/2

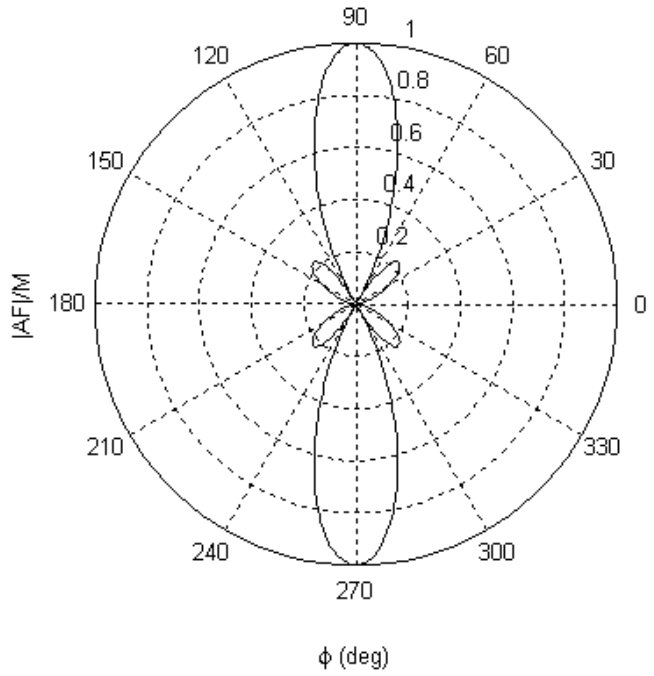

Figure 2. 4a - Polar Radiation Pattern of ULA Systems with d=λ/4

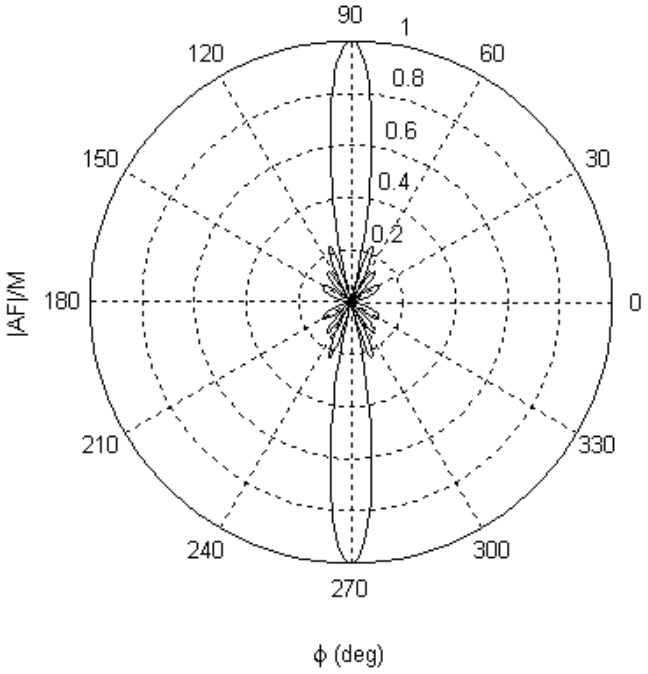

Figure 2.4b - Polar Radiation Pattern of ULA Systems with d=λ/2

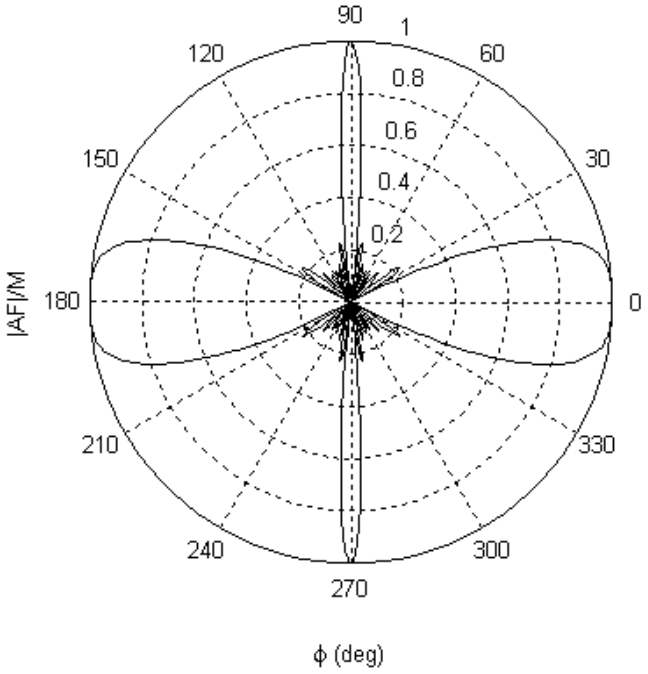

Figure 2.4c - Polar Radiation Pattern of ULA Systems with d=λ

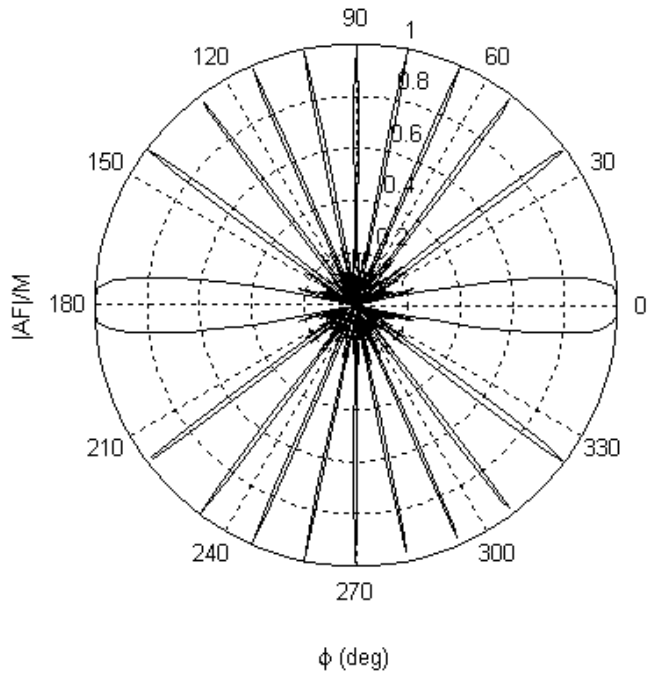

Figure 2.4d - Radiation Pattern of ULA Systems with d=5λ

Notice that the grating lobes differ from the sidelobes because they have the same magnitude of the gain as the main lobes. Thus in applications where we intend to apply *transmit diversity* to combat the fading effects we can intentionally use antenna arrays designed with d up to 10λ to exploit the angle spread of the fading. In applications where the aim is the array directivity only, grating lobes are very difficult to deal with since they produce a significant waste of power emitted in unintended directions and more interference captured than the sidelobes. As a general rule, in this class of applications, d is chosen to be less than λ but more than $\lambda/2$ to limit the mutual coupling effects among the sensors. In practice, $\lambda/2$ is the usual inter-element distance and an array having the elements spaced of $\lambda/2$ is said *standard* array. In the following we will refer to standard arrays unless otherwise specified.

2.6 Uniform Circular Antenna Model

Uniform Circular Array systems are composed of sensors which are disposed along a ring with a uniform angle separation of $2\pi/M$, Figure 2. 5. The *m*-th sensor position is

$$\mathbf{p}_m = R(\cos\phi_m \hat{\mathbf{x}} + \sin\phi_m \hat{\mathbf{y}})$$

where *R* is the radius of the circle and ϕ_m is the azimuth angle of the *m*-th sensor

$$\phi_m = m\frac{2\pi}{M}$$

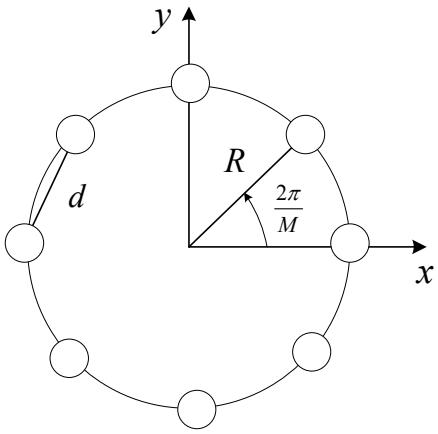

Figure 2. 5 – 8-element UCA Reference System

With *d* that indicates the inter element distance, the relationship between *R*, *M* and *d* is

$$R = \frac{d/2}{\sqrt{\left(1-\cos\left(\frac{\pi}{M}\right)^2\right)}} \tag{2.10}$$

As with ULA systems, indicating with $r(t)$ the analytic narrow band incident signal at the origin of the coordinate system and with ψ_o its phase, if it is possible to assume that

$$|r(t)| \simeq |r(t-\tau_m)| \qquad \forall m$$

which happens if $|r(t)|$ does not vary significantly over a time lag of

$$\max\{\tau_m\} = \frac{2R}{c}$$

the noisy signal available at the output of the *m*-th array element can be written as

$$y_m(t) = r(t)e^{-j\boldsymbol{\beta}\cdot\mathbf{r}_m} + n_m(t)$$

whose phase is

$$\psi_m = \psi_o - \boldsymbol{\beta}\cdot\mathbf{p}_m = \psi_o + R\frac{2\pi}{\lambda}(\cos\phi\cos\phi_m + \sin\phi\sin\phi_m)$$

The steering vector of UCA systems can be defined as

$$\mathbf{a}_{UCA}(\phi) = \begin{bmatrix} e^{j\beta R\cos(\phi-\phi_0)} \\ \vdots \\ e^{j\beta R\cos(\phi-\phi_{M-1})} \end{bmatrix} \tag{2.11}$$

and the vector $\mathbf{y}(t)$ of the signals available at the array output can be expressed similarly to (2.6)

$$\mathbf{y}(t) = r(t)\mathbf{a}_{UCA}(\phi) + \mathbf{n}(t)$$

2.6.1 Array Factor of UCA Systems

The array factor of ULA systems with unity weighting coefficients is

$$f(\theta,\phi) = \sum_{m=0}^{M-1} e^{j\beta R\cos(\phi-\phi_m)} \tag{2.12}$$

The advantage of a circular array is that it creates only one man beam that can be swept fully around the circle. Similar to linear arrays, the number of elements in the array determines the width of the meanbeam and the element spacing determines the entity of the sidelobes. In ULA system the choice of keeping the element spacing lower than half a wavelength is dictated by the appearance of grating lobes. In UCA systems a similar choice is made in order to limit the *pattern ripple* [26], a possible criterion is to keep below 1 dB. The pattern ripple is measured by the ratio of the maximum array factor to the minimum array factor. The more the pattern ripple the more the array pattern deviates from the omnidirectional radiation when the sensors are fed

with equal phases and amplitudes as seen in Figure 2. 6 for a 8 element array with $kR = 5.2$.

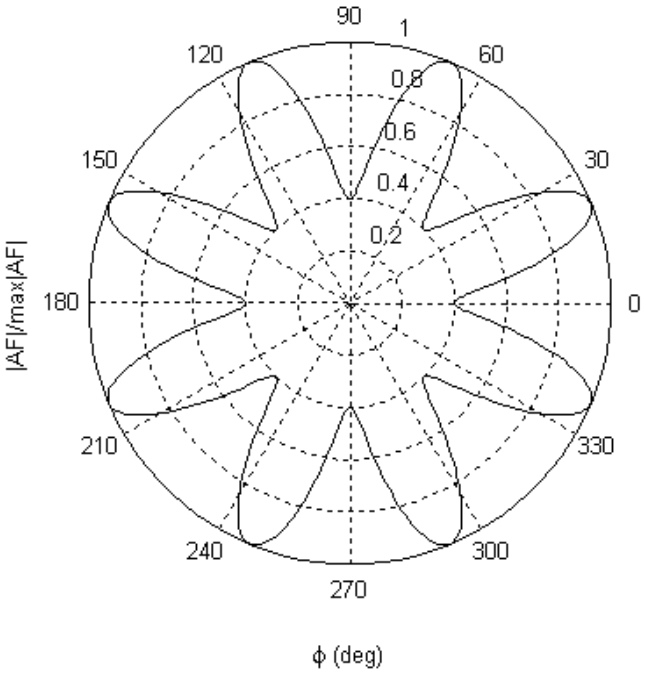

Figure 2. 6 - Polar Radiation Pattern of a 8 element UCA with *kR*=5.2

The pattern ripple of the array of Figure 2. 6 amounts to

$$10\log\left(\frac{1}{0.4}\right)^2 \simeq 8dB$$

In Table 2. 1 we have reported the calculated ripple by using (2.12) as resulting from the sensor arrangement $d = \lambda/2$.

M	***kR***	***Ripple dB***
8	4.10469	0.4
12	6.0691	0.1262
16	8.05164	0.01861

Table 2. 1– Ripple values for the sensor arrangement $d = \lambda/2$

As is seen the more *M*, the less the ripple. For M less than 8 instead, *d* has to be less than $\lambda/2$. For instance with 4 elements, $d = 0.35\lambda$ gives 0.97 dB ripple.

2.7 Antenna Directivity.

The power density, having units of W/rad^2, for a particular direction (θ,ϕ) is given by $U(\theta,\phi)$. It is of practical interest the relationship between the power density $U(\theta,\phi)$ and the array factor $AF(\theta,\phi)$ so as to derive the antenna directivity from the geometry of the array system. $U(\theta,\phi)$ as a function of the array factor $AF(\theta,\varphi)$ is

$$U(\theta,\phi) = \left|AF(\theta,\phi)\right|^2 \tag{2.13}$$

The total power transmitted in all directions is

$$P_{rad} = \int_{\phi=0}^{2\pi}\int_{\theta=0}^{\pi} U(\theta,\varphi)\sin\theta d\theta d\phi$$

The average power density, U_{ave}, is

$$U_{ave} = \frac{P_t}{4\pi} = \frac{1}{4\pi}\int_{\phi=0}^{2\pi}\int_{\theta=0}^{\pi} U(\theta,\varphi)\sin\theta d\theta d\phi \tag{2.14}$$

When the antenna transmits power equally in all directions, the antenna is said to be *isotropic*. Isotopic antennas are often used as a reference case. Antenna arrays have the ability to concentrate the radiated power in a particular angular direction in space. This ability is measured by the *directive gain* defined as

$$D(\theta,\varphi) = \frac{U(\theta,\phi)}{U_{ave}} \tag{2.15}$$

The directive gain in the direction of the maximum radiation density is referred to as the *directivity*, D, and is given

$$D = \frac{\max\limits_{\theta,\phi}\{U(\theta,\phi)\}}{U_{ave}}$$

The *antenna gain* is instead given by

$$G(\theta,\varphi)=\frac{4\pi U(\theta,\phi)}{P_{in}}$$

where P_{in} is the total input power to the array. By defining the *antenna efficiency* η, which accounts for losses, as

$$\eta=\frac{P_{rad}}{P_{in}}$$

it follows that

$$G(\theta,\phi)=\eta D(\theta,\phi)$$

In our work, the antenna is assumed to be lossless and perfectly matched, so as we will interchangeably refer to the antenna gain or antenna directivity.

2.7.1 Directive Gain of ULA Systems

The directive gain of ULA systems can be found as follows. We first substitute (2.9) in (2.13) to write the power density. We then substitute (2.13) in (2.14) and (2.13)-(2.14) in (2.15). The final expression is

$$D(\theta,\phi)=\frac{4\pi\sin^2\left(\frac{M\beta d\cos\phi\sin\theta}{2}\right)\Big/\sin^2\left(\frac{\beta d\cos\phi\sin\theta}{2}\right)}{\int_0^{2\pi}\int_0^{\pi}\sin^2\left(\frac{M\beta d\cos\phi\sin\theta}{2}\right)\Big/\sin^2\left(\frac{\beta d\cos\phi\sin\theta}{2}\right)\sin\theta d\theta d\phi} \tag{2.16}$$

2.7.2 Directive Gain of UCA Systems

The derivation of the directive gain of UCA systems is similar to ULA systems with the only difference that (2.9) replaces (2.12). The directive gain is

$$D(\theta,\phi)=\frac{4\pi\left|\sum_{m=0}^{M-1}e^{j\beta R\sin\theta\cos(\phi-\phi_m)}\right|^2}{\int_0^{2\pi}\int_0^{\pi}\left|\sum_{m=0}^{M-1}e^{j\beta R\sin\theta\cos(\phi-\phi_m)}\right|^2\sin\theta d\theta d\phi} \tag{2.17}$$

2.8 Beamsteering

Beamsteering is the simplest form of beamforming. It can be achieved by a delay-and-sum beamformer with all its weights equal in magnitude and the phases selected to steer the antenna boresight in any wanted direction ϕ_0 known as the *look direction*. As an example, this goal can be achieved with these choices of weighting coefficients

$$w_m = \frac{1}{M} e^{-j\beta md\cos\phi_0} \tag{2.18}$$

and

$$w_m = \frac{1}{M} e^{-j\beta R\cos(\phi_0-\phi_m)} \tag{2.19}$$

for ULA and UCA systems respectively.

2.8.1 Beamsteering of ULA Systems

To see the effect of this operation we write the array factor or equivalently the directive gain of ULA systems by introducing the weighting coefficients (2.18) in (2.8). The resulting expression of the array factor is

$$f(\theta,\phi) = e^{j\frac{M-1}{2}\beta d(\cos\phi-\cos\phi_0)} \frac{\sin\left(\frac{M\beta d(\cos\phi-\cos\phi_0)}{2}\right)}{\sin\left(\frac{\beta d(\cos\phi-\cos\phi_0)}{2}\right)} \tag{2.20}$$

which is straightforwardly comparable with (2.9). In Figure 2. 7 we have plotted (2.20) for $\phi_0 = 30°$ and $\phi_0 = 60°$ for an 8-element linear-phased standard array. In particular when $\phi_0 = 0°$ the array is said *end-fir*e whereas when $\phi_0 = 90°$ the array is said *broadside*. Figure 2. 8 depicts the directive gain of a standard linear-phased array with weighting elements (2.18) in the plane *x*-*y* and ϕ ranging in [0°,180°), for *M* equal to 8 (9 dBi), 12 (10.79 dBi) and 16 (12 dBi) and for three values of the scanning angle ϕ_0, 0°, 45° and 90°, respectively. As said, increasing the number of elements determines a higher antenna directivity and a narrower mainlobe beamwidth. We point out that the reduction of the mainlobe beamwidth due

to an increasing M has a different importance if analysed versus the pointing direction ϕ_0. In fact in general, for a fixed M, the beamwidth of uniform linear antenna arrays is narrower if the array is broadside and becomes broader outwards with the maximum at end-fire. Such a variation is more noticeable with M that increases. It can be observed that an increase of M up to 16 leaves the beamwidth still large if $\phi_0 = 0°$ whereas it gives a sharp and narrow mainlobe if $\phi_0 = 90°$. The behaviour of the beamwidth for ULA systems is treated in more details in the next section.

The steering process is similar to steering the array mechanically in the look direction, except that it is done electronically by adjusting the phases of the signals at the array elements outputs. This later is also referred to as electronic steering, and phase shifters are used to adjust the phases. The phase offset form one element to the next in ULA systems is

$$\pi \cos\phi_0$$

which amounts to 0° for broadside and to π for end-fire.

If ϕ_0 is the AOA of the far field source, we want to point the antenna in the AOA of the impinging signal to receive the signal. Said $\mathbf{a}_{ULA}(\phi_0)$ the steering vector of the ULA system in the AOA of the impinging source, the weighting coefficients vector (2.18) is

$$\mathbf{w} = \frac{1}{M}\mathbf{a}^*_{ULA}(\phi_0)$$

The array with these weights has unity response in the look direction, that is, the mean output power of the processor due to a source in the look direction is the same as source power. Assume that the data modulation signal $\mu(t)$ in (2.3) has mean power p_μ, from (2.7) one gets the mean output power

$$P(\mathbf{w}) = E\left[z^H(t) \cdot z(t) \right] = p_\mu$$

Thus, the mean output power of the beamformer steered in the look direction is equal to the power of the signal in the look direction. In the special case where the system is dominated by uncorrelated noise, $\mathbf{R_n} = \sigma_n^2\mathbf{I}$, and no interference exists in the look direction, this beamformer provides maximum SNR. In fact, the noise output power is

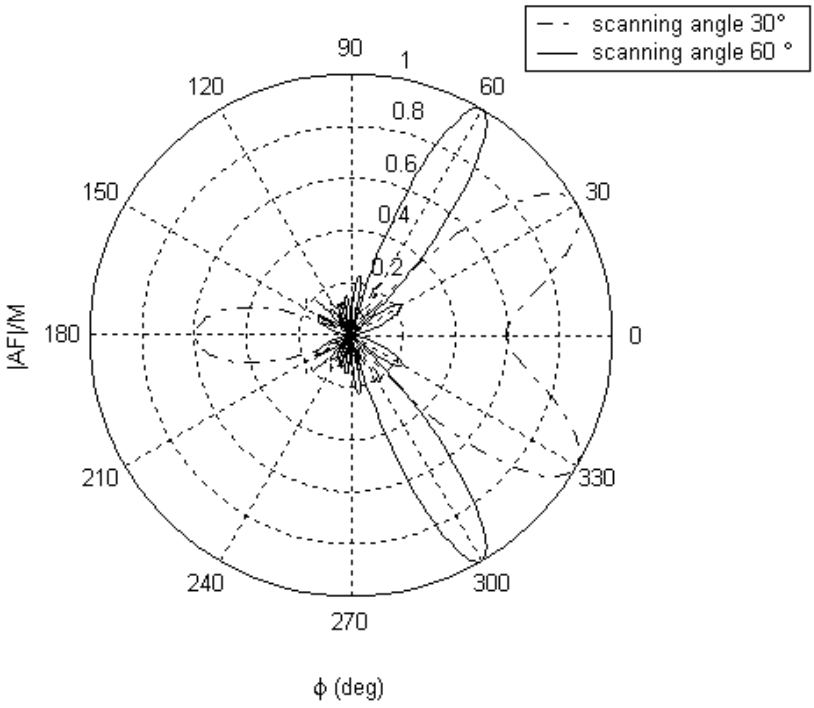

Figure 2. 7 - Beamsteered 8-element standard ULA System

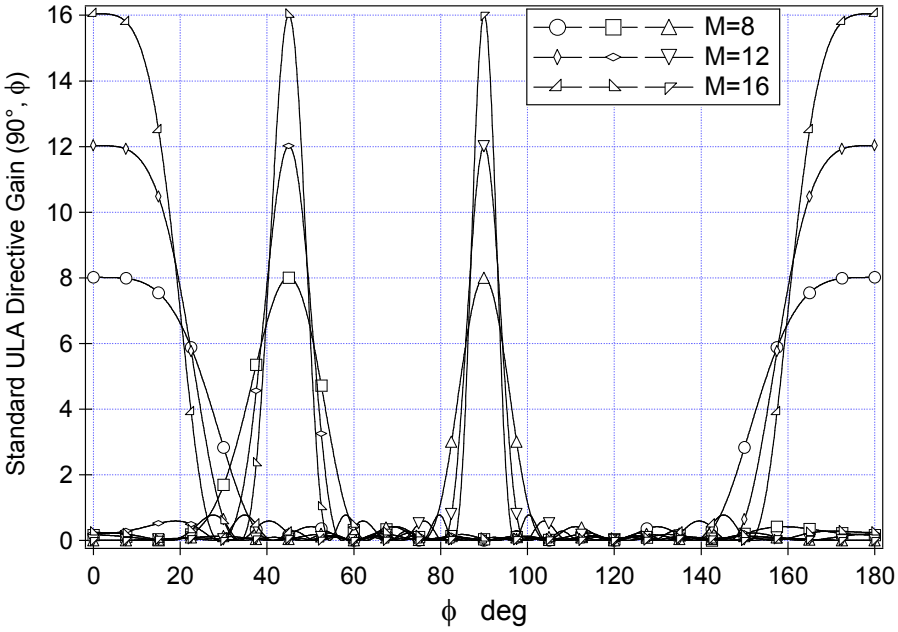

Figure 2. 8 - Standard ULA Directive Gain, ϕ_0=0°, 45°, 90°

$$\mathbf{P_n} = \mathbf{w}^T \mathbf{R_n} \mathbf{w} = \frac{\sigma_n^2}{M}$$

The processor with unity gain in the direction of the source has reduced the uncorrelated noise by a factor *M*, yielding an output SNR

$$SNR_{out} = M \frac{p_\mu}{\sigma_n^2}$$

when the input SNR is

$$SNR_{in} = \frac{p_\mu}{\sigma_n^2}$$

This beamformer provides an array gain, which is defined as the ratio of the output SNR to the input SNR, equal to the number of elements in the array *M*.

This beamformer requires some prior knowledge about the look direction ϕ_0 to be applied. In this work we study the CRB for DOA estimation and the impact of the accuracy of those estimates onto the goodput performance of phased array controllers that use DOA estimates for beamsteering.

2.8.2 Beamsteering of UCA Systems

In this section we analyse the normalized array factor of UCA systems with the substitution of (2.19) in (2.12) for beamsteering with an inter element separation of half a wavelength. Figure 2. 9a refers to a 8-element array pointing two directions, $\phi_0 = 45°$ and $\phi_0 = 22°$, respectively. We have also plotted the case of a 12-element array to show the increase in directivity due to more elements in the array, Figure 2. 9b. For the 8 element array we note the presence of a relevant back lobe compared to the 8-element standard linear array of Figure 2. 7. As said UCA systems can scan all the azimuth circle with only one beam. However we note that the relative direction of the beam compared to the location of the sensors can cause a nonsymmetric pattern and the appearance of some relatively large sidelobe. For instance, in Figure 2. 9a one notices that the sidelobe at 150° of the array pattern when $\phi_0 = 45°$ becomes bigger when the look angle moves towards 22°.

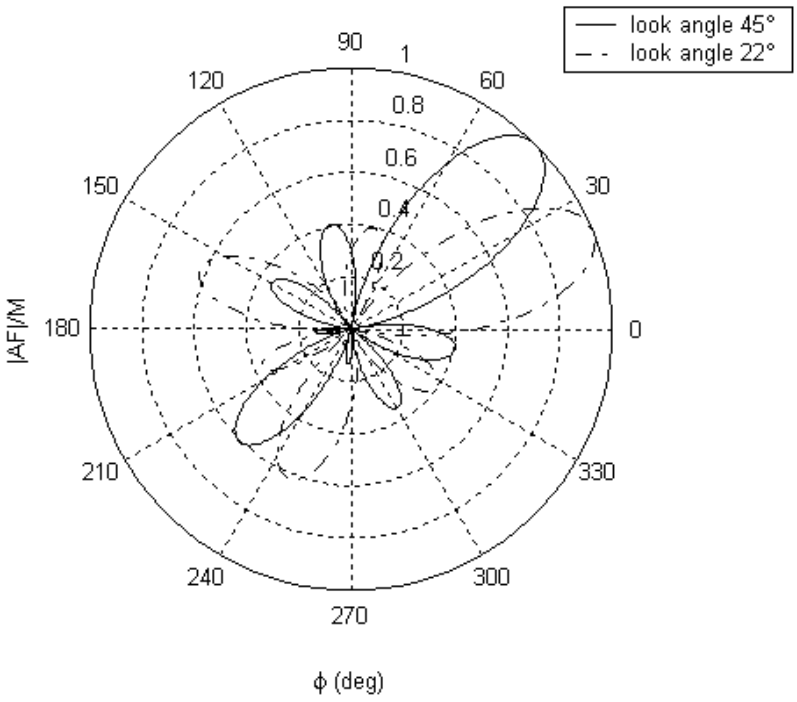

Figure 2. 9a - 8-element UCA System steered at 45°

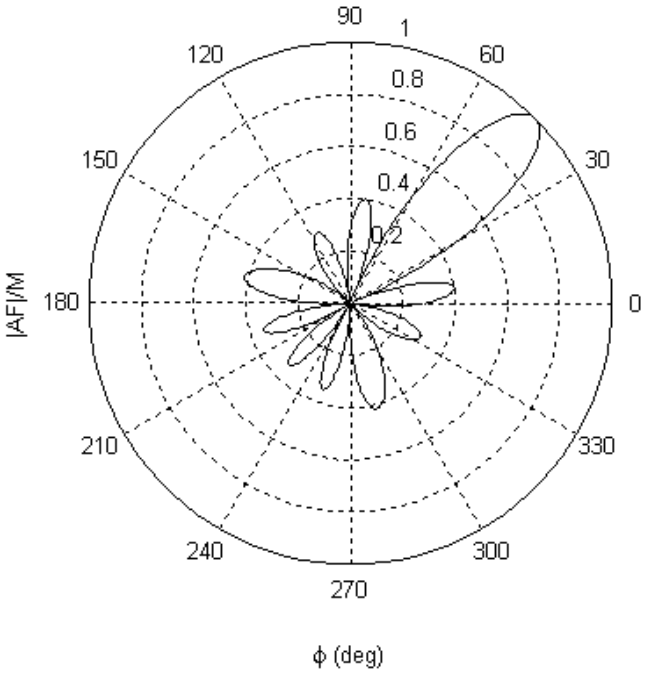

Figure 2. 9b - 12-element UCA System steered at 45°

2.9 Half Power Beamwidth of ULA Systems

The *half-power beamwidth* (HPBW) or simply *beamwidth* is defined as: "In a plane containing the direction of the maximum of a beam, the angle between the two directions in which the radiation intensity is one-half the maximum value of the beam". Thus the term beamwidth is implicitly reserved to indicate -3dB beamwidth. An important indication provided by the beamwidth if the resolution capacity of the antenna that is the capacity of the antenna to distinguish between to sources. Two sources separated by angular distances equal or greater than HPBW can be resolved [27].

A general formula for the beamwidth of a linear-phased array is [28]

$$HPBW = \cos^{-1}\left[\cos\phi_o - 0.443\frac{\lambda}{Md}\right] - \cos^{-1}\left[\cos\phi_o + 0.443\frac{\lambda}{Md}\right] \quad (2.21)$$

which is valid for a wide range of scanning angles but not for end-fire. In Figures 2.10a and 2.10b we notice the same behaviour for the beamwidth when we increase *d* and M. Figure 2.10c demonstrates that the beamwidth of a linear-phased array of a given size is not constant but rather it depends on the scanning angle.

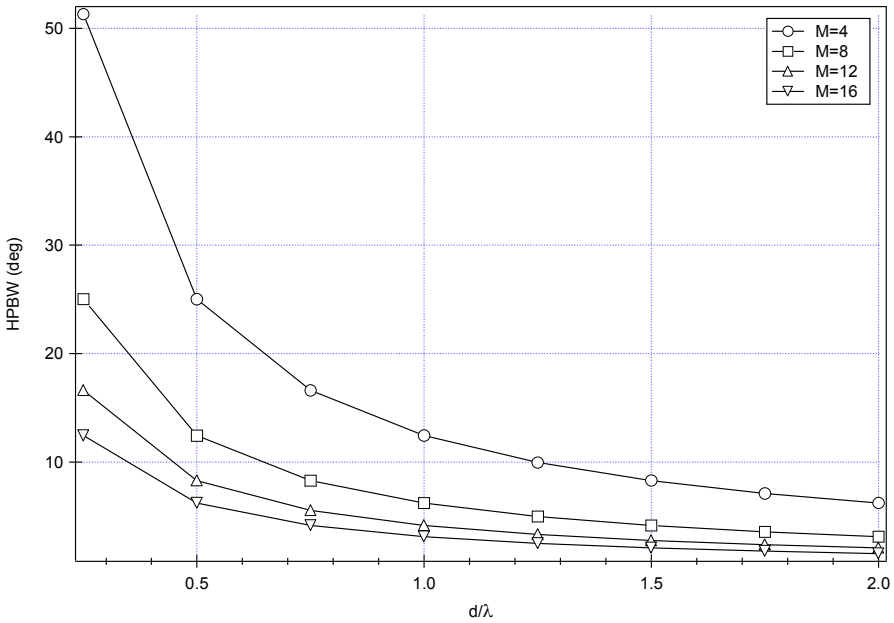

Figure 2. 10a - Beamwidth of ULA systems as a function of d/λ

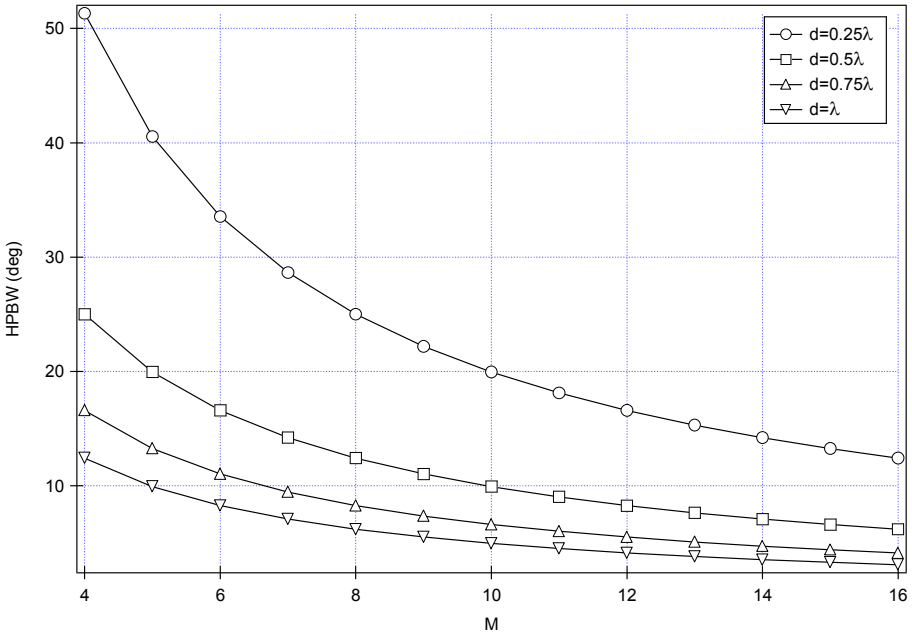

Figure 2.10b - Beamwidth of ULA systems as a function of M

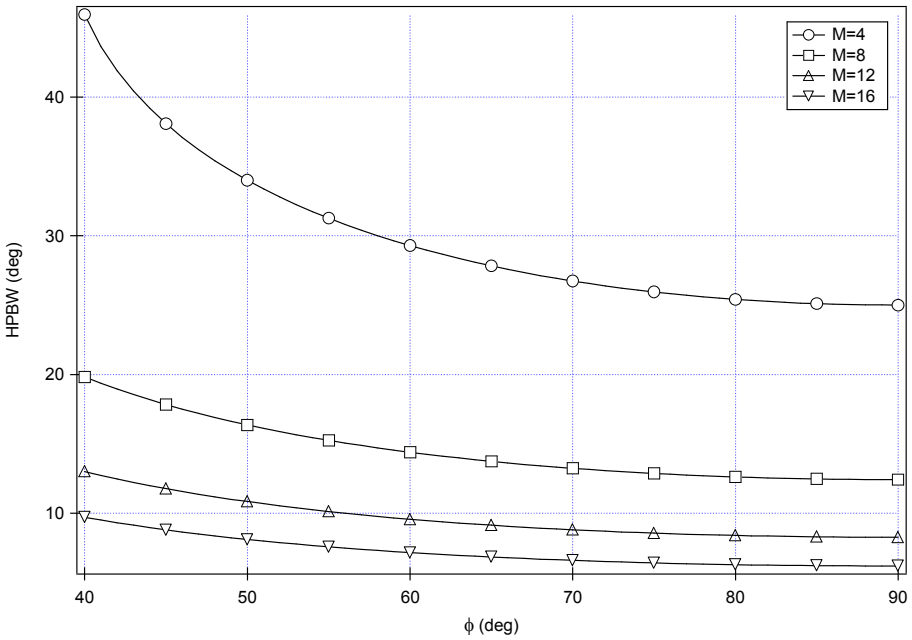

Figure 2.10c - Beamwidth of ULA systems as a function of the look angle ϕ

Chapter III. Simulation Analysis with IEEE 802.15.3c MAC

3.1 General Description of IEEE 802.15.3

In this section we provide a brief description of the IEEE 802.15.3 standard. In that, we have picked up those features of the standard that serve to set the background for the explanation of the design of the IEEE 802.13.3 phased array controller throughput, which is our aim in this chapter.

A piconet is a wireless ad hoc data communication system which allows a number of devices (DEVs) to communicate with each other. A piconet differs from other data networks in that communications are confined to a limited area around a person or an object. The target radio coverage of the *mm*-wave WPANs goes from desktop and body applications to the in-room like applications. A 802.15.3-based piconet consists of several components. The main are shown in Figure 3. 1. One DEV is required to assume the role of the coordinator of the piconet (PNC). It provides the basic timing for the piconet with the beacon. Additionally, the PNC manages the QoS requirements, power saving modes, and access control to the piconet. Because 802.15.3 networks form without pre-planning and only for as long as the piconet is needed, this type of operation is classified as an ad hoc network. 802.15.3 specifies allocation of a subsidiary piconet generally referred to as dependent piconet. In our work we have neglected allocation of dependent piconets.

Timing in the 802.15.3 piconet is based on the superframe, which is illustrated in Figure 3. 2. The superframe is composed of three parts:

- The *beacon* is used to set the time timing allocations and to communicate management information for the piconet.

- The *contention access period* (CAP) is used to communicate commands and/or asynchronous data if it present in the superframe.
- The *channel allocation period* (CTAP) is composed of channel time allocations (CTAs), including management CTAs (MCTAs). CTAs are used for commands, isochronous streams and asynchronous data connections.

The CAP uses CSMA/CA for the medium access. The CTAP uses a standard TDMA protocol where the DEVs have specified time windows. MCTAs are either assigned to a specific source /destination pair and use TDMA for medium access or shared CTA that use slotted aloha protocol. In this work MCTAs are neglected.

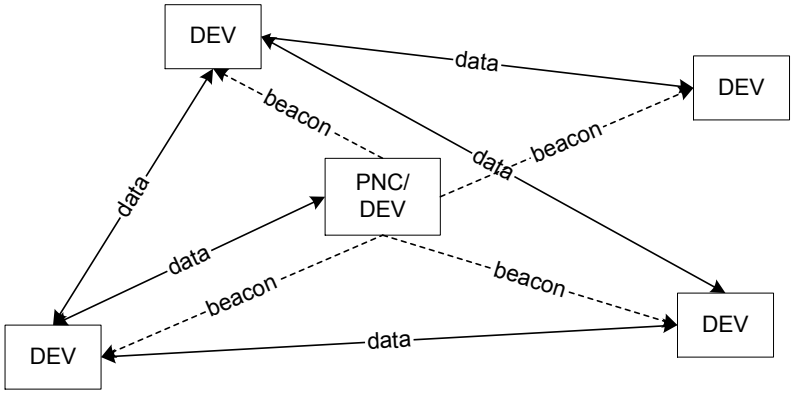

Figure 3. 1 - Piconet components

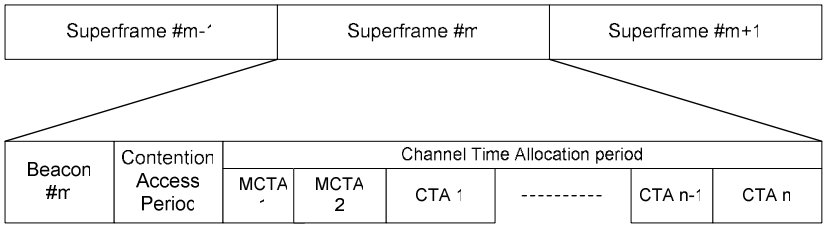

Figure 3. 2 - Superframe composition

All data in the 802.15.3 piconet data are exchanged in a peer-to-peer manner.

There three methods for communicating data among DEVs in a piconet:

1) Sending asynchronous data in the CAP, if present. DEVs can send small amounts of data without having to allocate channel time.
2) Allocating channel time for isochronous streams in the CTAP. This kind of communication is requested by a DEV that needs time allocation on a regular basis. If the resources are available the PNC reserves a CTA for the DEV. The isochronous CTAs can be either static or pseudo-static. If a DEV misses a beacon, the DEV cannot use the CTA in the next superframe if the CTA is of the first type. If the CTA request is of the second type, the device can still use the CTA in the subsequent superframe up to a *mMaxLostBeacons* of missed beacons.
3) Allocating asynchronous channel time in the CTAP. Unlike isochronous allocation, it corresponds to a request for a total amount of time needed to transfer a given bulk of data. The PNC schedules channel time for this communication according to the current channel time requests.

In this work, we have taken into consideration isochronous communications only, and pseudo-static CTAs only.

To verify the delivery of frame the standard specifies three types of ACKs to enable different applications.

1) The *no-ACK* policy is appropriate for frames that do not require guaranteed delivery where the retransmitted frame would arrive too late or where an upper layer protocol is handling a the ACK and the retransmission.
2) The *Immediate-ACK* (Imm-ACK) policy is an ACK process in which each frame is individually acknowledged after the reception of the frame.
3) With the *Delayed-ACK* (Del-ACK) frames are acknowledged in groups. The ACK is sent when requested by the source DEV. This ACK policies decreases the overhead with respect to the Imm-ACK while ensuring t the source DEV the verification of a successful transmission.

In this work we have considered the Imm-ACK policy only.

As seen, the MAC mechanisms included in this standard make it sufficiently flexible to operate with a wide range of wireless applications having different QoS requirements, bandwidth demands and traffic types. Table 3. 1**Errore. L'origine riferimento non è stata trovata.** shows how this MAC standard fits the wireless applications that are envisaged to be operative in the 60 GHz band.

Table 3. 1- MAC related System Attributes

#	Application	MAC Related Systems Attributes
1	Uncompressed HDTV Video/Audio streaming [DVD players and other power-line operated devices]	a) Isochronous b) High throughput efficiency c) Point-to-Point d) Support for high gain antennas for Data Transmission e) Device discovery f) Moderate latency g) Minimum reserved bandwidth
2	HDTV Video/Audio streaming [video camera/mobile devices and other battery operated devices]	a) Isochronous b) High throughput efficiency c) Maintain link throughput while in motion jitter d) Point-to-Point e) Support for moderate gain antennas for Data Transmission f) Automatic device discovery g) Moderate latency h) Minimum reserved bandwidth i) Multiple nearby data transmissions
3	Internet bulky music and video downloading [computing devices]	a) Asynchronous b) High throughput efficiency c) Point-to-Point d) Support for moderate gain antennas for Data Transmission e) Device discovery (Automatic preferred)
4	Internet bulky music and video downloading [mobile devices]	a) Asynchronous b) High throughput efficiency c) Point-to-Point d) Support for moderate gain antennas for Data Transmission e) Device discovery (Automatic preferred) f) Multiple nearby data transmissions g) Power saving mode
5	Internet small size file transfer (email, web, chat)	a) Asynchronous b) Point-to-Point c) Support for moderate gain antennas for Data Transmission d) Device discovery (Automatic preferred) e) Multiple nearby data transmissions f) Power saving mode g) Fast connect
6	Local file transfer for printing, document and small size file	a) Asynchronous b) Point-to-Point c) Support for moderate gain antennas for Data Transmission d) Device discovery (Automatic preferred) e) Multiple nearby data transmissions f) Power saving mode

7	Local file transfer for bulky music and video, point-to-point connection (photo/video camera and photo/video handy phone, mp3 player)	a) Asynchronous b) Point-to-Point c) Support for moderate gain antennas for Data Transmission d) Device discovery (Automatic preferred) e) Multiple nearby data transmissions f) Power saving mode
8	Wireless docking station	a) Isochronous b) High throughput efficiency c) Maintain link throughput while in motion jitter d) Point-to-Point e) Support for moderate gain antennas for Data Transmission f) Device discovery (Automatic preferred) g) Moderate latency h) Minimum reserved bandwidth i) Multiple nearby data transmissions
9	Video supply, Environment bus, train, airplane	a) Isochronous b) High throughput efficiency c) Broadcast, multicast and unicast capable d) Minimum reserved bandwidth e) QoS support f) Low delay jitter (<100 ms) g) Moderate latency (< 100 ms) h) Support of asymmetric data rates and gaming i) Cumulative acknowledgements and unacknowledged streaming j) Infrastructure mode (non ad-hoc) k) Secondary (fallback) PHY for 100% coverage and uplink

3.2 Adapting IEEE 802.15.3c MAC for the Use of Phased Array Antennas

In this section we describe the extension of the IEEE 802.15.3 MAC for the use of phased array antennas. The array system does include the omni directional operating mode. Omni operations are directly involved into this directional protocol and ensure compatibility with devices that are not equipped with array antennas. For this reason, our protocol can be thought as an extension to the PHY-MAC functionalities of IEEE 802.15.3c when directional antennas are used. In the following we first explain the basic mechanism of our neighbour discovery protocol which is based on DOA estimation of the incoming frames. We then illustrate how this mechanism is employed to establish both PNC-DEV and DEV-DEV wireless links.

3.2.1 DOA Estimation on the PHY Preamble

In this section we show a revisited modelling approach first proposed in [29] for directional antenna adaptation. Figure 3. 3 shows the timeline of a

received frame. It composes of a PHY part and a MAC part. DOA estimation can be carried out on the preamble of the PHY of the received frame. The physical preamble is assumed to be a known OFDM long training sequence added to aid receiver algorithms of synchronization, carrier-offset recovery and channel equalization. In particular, as far as the DOA estimation is concerned, we simplify the modelling of a training sequences as one OFDM symbol having both the number and the positions of the pilot subcarriers known. DOA estimation is accomplished in the PHY preamble time T_{pp} and the DOA estimate is used to point the main beam in the direction of arrival of the frame during the remainder of the frame receive time T_{frame} - T_{pp}. If frame reception is successful, the DOA estimate is cached and the DEV switches to the narrow beam communication. The DEV can use the DOA just acquired either to reply to the sending DEV directionally or as the expected DOA of the next frame from the same source. In this second case then, the next frame is received with a receive antenna already beam steered to the DOA of the frame.

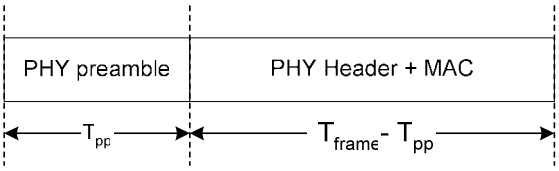

Figure 3. 3 - Data frame exploitation for antenna adaptation

It should be noted that:

1) DOA estimation with no DOA information cached occurs during the T_{pp}. of the first frame of a wireless communication or after a protocol reset, for instance due to the loss of the direction toward the intended DEV. With reference to Figure 2. 2, DOA estimation in these conditions is actually performed on the signals vector $\boldsymbol{y}$ at the output of the array sensors, before the multiplication by the weighting elements $\boldsymbol{w}$.
2) DOA estimation performed with a receive antenna already pointed benefits from a maximum SNR as explained in Section 1.9.1. In this

case the signals vector used for estimation is $\boldsymbol{z}$ at the output of the array sensors after the multiplication by the weighting elements $\boldsymbol{w}$.

3) DOA estimation could be carried out, let us say *refreshed* or *refined*, during the symbol times composing T_{frame} - T_{pp}. Concentrating the estimation in T_{pp} can be thought as representative of the performance estimation achievable on whatever number of symbols in the interval T_{frame}.

3.2.2 Frame Driven Beamsteering in IEEE 802.15.3c MAC

In a piconet there are two kinds of wireless links. One is the PNC-DEV link, The other id the DEV-DEV link.

- *Antenna steering on beacon time.* All the DEVs set their local timing information upon receiving the beacon. Beacon reception serves as a time reference for clock synchronization in the network. Beacon transmission is intrinsically broadcast to keep the differences of the instants at which the beacon is received at the DEVs within the guard intervals fixed by the standard and avoid time differences due to the protocol. The wireless link PNC-DEVs as far as the beacon transmission is concern is omni at the PNC and can be directional at the DEVs. That is, the PNC-DEVs links antenna gain is exploited at the receiver only. To overcome the link gain asymmetry, the MAC beacons are transmitted at a lower rate. The lower rate transmission rate results in a lower SNR requirement that with less antenna gain in the link should end up with the same probability of correct frame reception. This mechanism represents a form of MAC-PHY *cross-layer* optimization that can be implemented with the addition of a few PHY-SAP (Service Access Point) primitives. For instance consider the current IEEE 802.15.3 PHY specification. To achieve $FER \leq 8\%$ with a transmission rate of 55 Mb/s and 64-QAM-TCM, we need

$SNR \geq 20\ dB$. Assume that we transmit the MAC beacon at 22 Mb/s using DQPSK. The same FER of 8% is achieved with $SNR \geq 13\ dB$. That is we can lose about 7 dB in antenna gain. Using the lower transmission rate causes a throughput overhead since we need more time to transmit the beacon per superframe. The throughput reduction is negligible anyway because the increase in beacon transmission time is a very small portion of the overall superframe. During the reception of the beacon frame all the DEVs perform DOA estimation on the PHY training sequence of the beacon. The DOA estimates drive beam steering to carry out beacon reception. If reception is successful the DOA estimate is used as the expected DOA of the beacon of the subsequent superframe.

- *Antenna steering on data frame and ACK*. The DEV-DEV wireless link can be directional in both directions. The mechanism to establish a directional-directional link during the data-ACK frame exchange is explained with the aid of Figure 3. 4. Transmit devices do not know the angular position of the intended receivers at the start. So a transmit DEV, DEV1, starts by sending a training frame omni directionally to DEV2 at a lower data rate. This operation has been denoted with E1 in Figure 3. 4. The receive DEV, DEV2, estimates the DOA of the frame on the PHY preamble of the data frame. The DOA estimate becomes the pointing direction of the antenna boresight during the remaining frame receive time, and in case of successful frame reception also the pointing direction to acknowledge DEV1 directionally. This sequence of operations is indicated with E2 in Figure 3. 4. DEV1 estimates the DOA toward DEV2 upon receiving the ACK MAC frame and, if the reception succeeds, uses it for the directional transmission to DEV2 during the subsequent CTA. E3 is the conclusion of the DEV-DEV handshake ending with the establishment of a directional-directional wireless link.

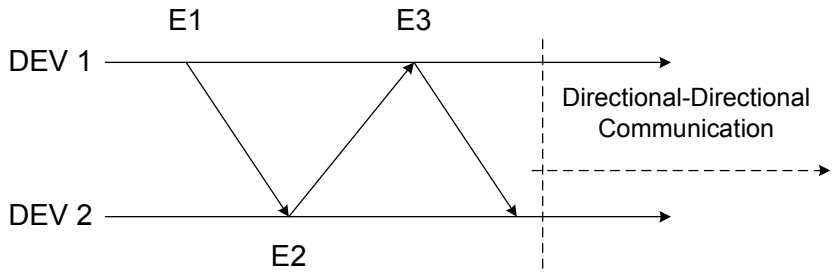

Figure 3. 4 - Directional-Directional communication in DEV-DEV link

In principle the directional-directional link may take place after one DATA-ACK exchange only. For the PNC-DEV it would be after one beacon frame only, namely in one superframe time only. Indeed, how fast and successful this strategy is depends on the capacity of estimating the DOA. To have a comparison regarding the potential speed of acquiring the directional communication, let us make the example of a DEV that enters the network and scans the space around directionally in search of the beacon. Indicating with $\phi_{beam}/2\pi$ the probability that the DEV points a particular direction with a beam of beamwidth ϕ_{beam}, the probability P that the DEV points the direction of the PNC when the PNC is sending the beacon is

$$P = \frac{\phi_{beam}}{2\pi}\frac{T_{beacon}}{T_{\sup erframe}}$$

Since the ratio of the beacon time T_{beacon} to the superframe time $T_{\sup erframe}$ is likely a very small value, P is a very small quantity indicating that lots of superframe would be needed to acquire the direction to the PNC on average. Figure 3. 5 shows the flowchart of a DEV1 having a packet to transmit to DEV2. If DEV1 does not receive the Imm-ACK, it retransmits the unacknowledged data frame by performing beamsteering with the last DOA estimate available (if any) for a maximum number of times *retry_count_limit*. After *retry_count_limit* retransmissions the data frame is discarded and the DOA estimate (if any) is assumed to be invalid. The antenna of the DED1 is then unlocked and a switch to the omni hearing

occurs. Failure in delivering a MAC frame may be due to an estimation error of either or both transmit and receive DEVs.

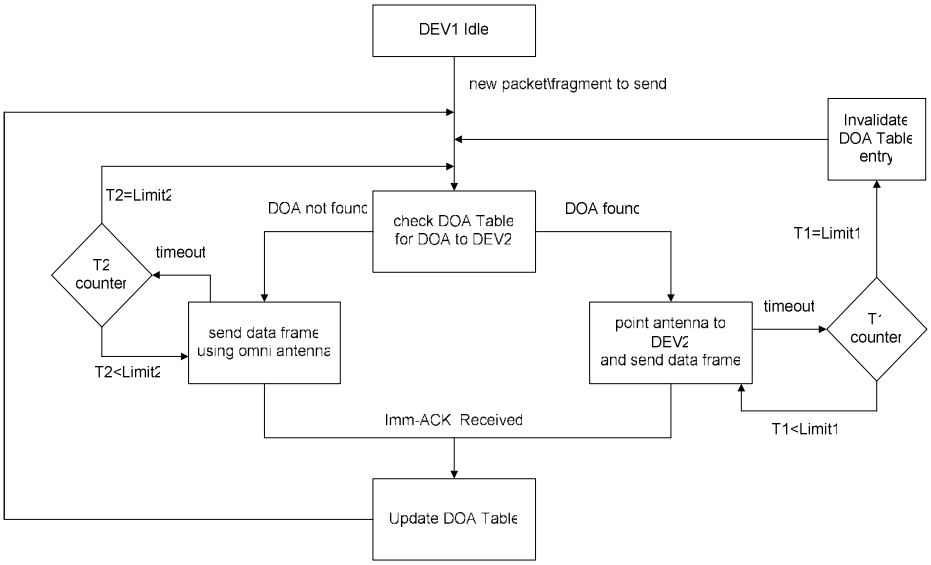

Figure 3. 5 - Flowchart of a DEV having a packet to transmit

3.3 Simulation Background

The MAC protocol for phased array antenna controllers described in Chapter II has been studied by means of computer simulations carried out with the network simulator ns-2 [21]. In this section we describe the model of the directional wireless link that we have simulated. The main assumption is the existence of a dominant LOS component and the absence co-channel interference. Such a channel model holds at 60GHz for room applications with no strong reflectors [8]. If a LOS exists and under the reasonable assumption that the DOA estimator used by the antennas is unbiased, the DOA estimates are noisy estimates of the LOS direction. The estimation error represents an alignment error to the LOS direction between transmitting and receiving antennas as can be seen with the aid of Figure 3.

6. The alignment error has been modelled as a Gaussian random variable with a zero mean and a given variance that we have indicated with σ_G^2. Hereafter, the DOA estimation is referred to as the Gaussian DOA estimator (GDOA) which represents the generator of a Gaussian error indeed.

We notice that the abstraction of schematic DOA estimation processing allows the generalization of the use of phased array antennas with 802.15.3 MAC regardless of the PHY. Such a simplification makes sense in that it enables us to gain insight into the relationship between the pointing accuracy and the antenna beamwidth/directivity of the antennas, and may

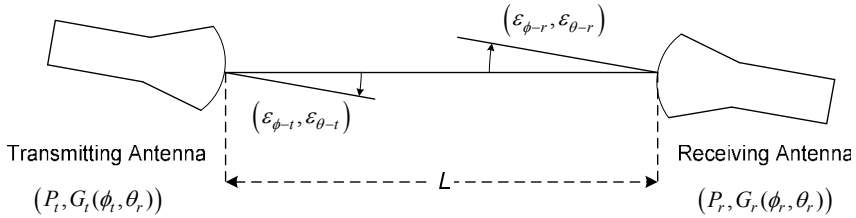

Figure 3. 6 - Geometrical orientation of transmitting and receiving antennas for Friis propagation equation.

serve as a reference analysis for specific DOA estimation algorithms and specific signal modulation techniques.

The propagation equation corresponding to our link model is given by

$$P_t = \overline{PL}(L) G(\phi_t, \theta_t) G(\phi_r, \theta_r) \mathrm{P_r} \tag{3.1}$$

(3.1) relates the power delivered to the load of the receiving antenna P_r to the input power of the transmitting antenna P_t. The term $\overline{PL}(L)$ is the average path loss measured at the distance L. $\overline{PL}(L)$ as a function of the distance L is

$$\overline{PL}(L)[dB] = \underbrace{PL_0}_{\substack{\text{free space path loss at} \\ \text{reference distance } L_0}} + 10 \cdot n \cdot \log_{10}\left(\frac{L}{L_0}\right); \qquad L \geq L_0 \tag{3.2}$$

In our simulations the parameters of (3.2) have been taken from a measurement campaign regarding the *mm*-waves [30].

The reference distance L_0 is 1 m, the corresponding path loss $\overline{PL}_0$ is 71.1 dB and the path loss exponent n equal to 1.53. (ϕ_t, θ_t) and (ϕ_r, θ_r) in (3.1) are the reciprocal angles of view of the antennas. For instance ϕ_r is given by

$$\phi_r = \underbrace{\phi_{LOS}}_{\text{anzimuth of LOS}} + \underbrace{\varepsilon_{\phi-r}}_{\substack{\text{error component with} \\ \text{Gaussian statistics}}} \tag{3.3}$$

In (3.3) ϕ_{LOS} is assumed to be a known quantity whereas $\varepsilon_{\phi-r}$ is generated by the GDOA.

3.4 Simulations Analysis with ULA Systems

Six nodes, five DEVs communicating to a PNC, compose the network. The DEVs are allocated the same CTAP duration. The main simulation parameters are shown in Table 3. 2. In particular we have simulated a physical capacity of 192 Mbps capable of a 157 Mbps throughput with 802.15.3 MAC. The PCN has been placed at the center of the network and the DEVs are located at the same radial distance L but with a progressive angle ϕ_{0i} with respect to the PCN, Figure 3. 7. The distance L varies from 1 up to 5 meters. To simplify, we have assumed that the antenna of any device (DEVi's x-axis) is parallel to the PCN's antenna so that the PCN and the DEVi see each other with look angles, ϕ_{0i} and ϕ_{i0} respectively, that give the same antenna patterns, see Table 3. 3. The metrics that we have investigated are the mean value, reported in Figures 3.8a,b,c and 3.9a,b,c, and the goodput standard deviation which is reported in Figures 3.10a,b,c, of all the PCN-DEVi links recorded separately. Simulation results are shown for σ_G of 4° and 5°, respectively. Statistics have been acquired by running 200 simulations of 20 seconds each, per network configuration. It is worth recalling that increasing values of ϕ_0 and M correspond to increasing antenna directivity, i.e. decreasing values of beamwidth. From now on, we will mainly refer to ϕ_0 and M to indicate the antenna directivity.

Table 3. 2 - Main simulation parameters

short interframe space	2.304 μs	transmit power	3 mW
guard time	72 ns	rx threshold	-70 dBm
retry_count_limit	4	packet length	2000 Bytes
path loss exponent	1.53	transport agent	UDP
reference distance , d_0	1 m	CTAP duration	2 ms
path loss at d_0	71.1 dB	packet error rate	1%
channel bandwidth	500 MHz	traffic source	CBR
central beamwidth freq.	60 GHz	channel capacity	192 Mbps

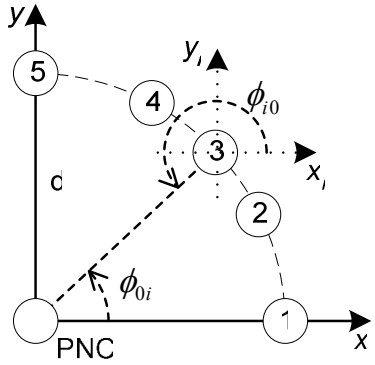

Figure 3. 7 - Device placement

Table 3. 3 - Look direction PNC-DEVi

DEV_i	ϕ_{0i}	ϕ_{0i}
1	0°	180° (0°)
2	30°	210° (30°)
3	45°	225° (45°)
4	60°	240° (60°)
5	90°	270° (90°)

From the figures regarding the goodput mean value, it emerges that:

i) Only the link PCN-DEV1, which corresponds to the end-fire pointing direction $\phi_0 = 0°$, always achieves the maximum goodput of about 30.85 Mbps regardless of *M*, the distance *L* and the variance of GDOA estimator.

ii) For values of the look angle far from end-fire, $\phi_0 \geq 30°$, the mean goodput decreases progressively as ϕ_0 grows. This is noticeable for any *M*, *L* and σ_G

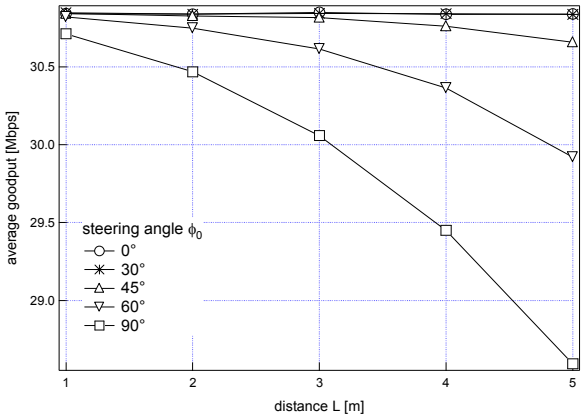

Figure 3. 8a - mean goodput, σ_G = 4°, M=8

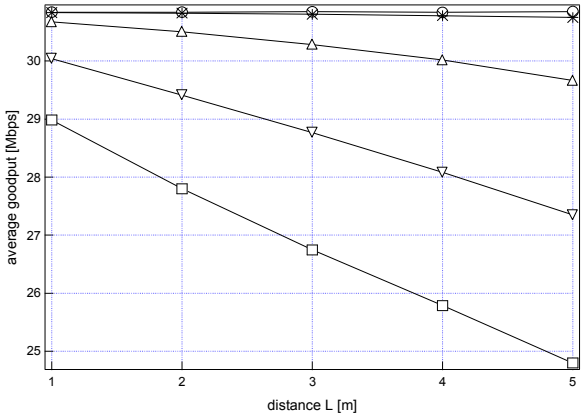

Figure 3.8b - mean goodput, σ_G = 4°, M=12

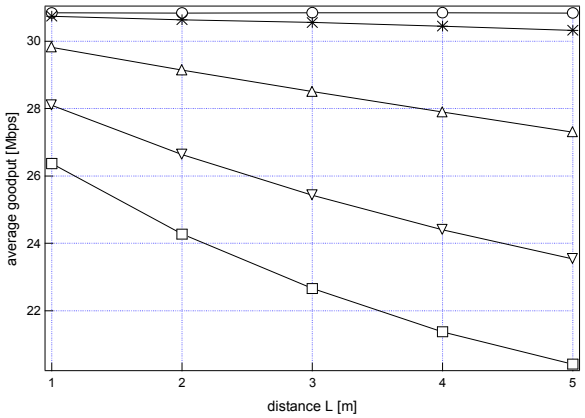

Figure 3.8c - mean goodput, σ_G = 4°, M=16

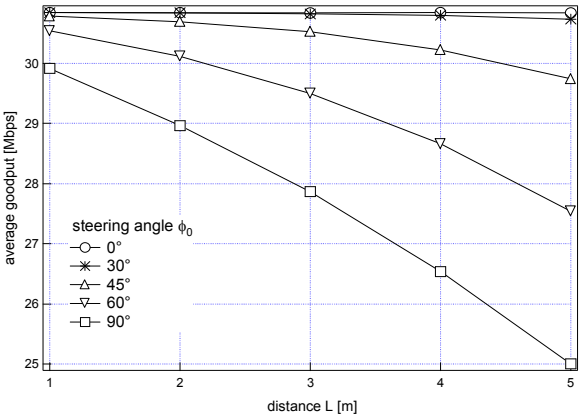

Figure 3. 9a - mean goodput, σ_G = 5°, M=8

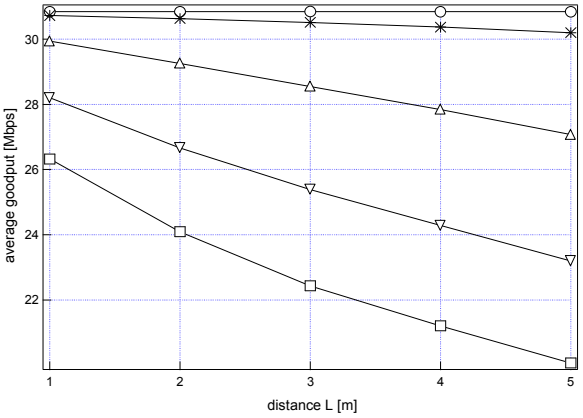

Figure 3.9b - mean goodput, σ_G = 5°, M=12

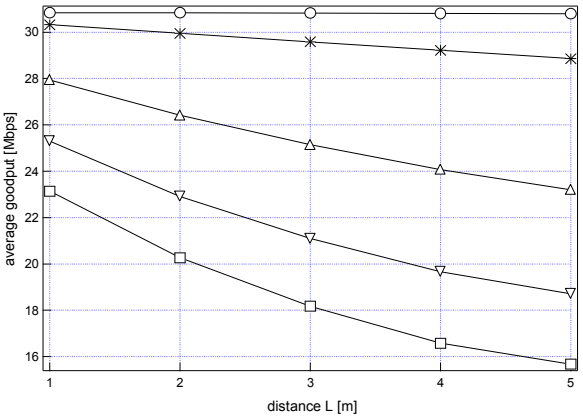

Figure 3.9c - mean goodput, σ_G = 5°, M=16

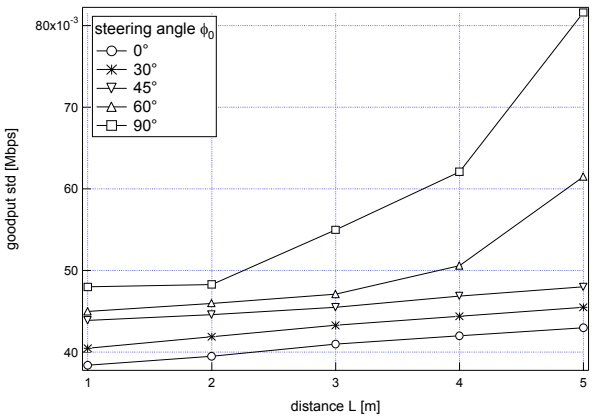

Figure 3. 10a – goodput std, $\sigma_G = 4°$, M=8

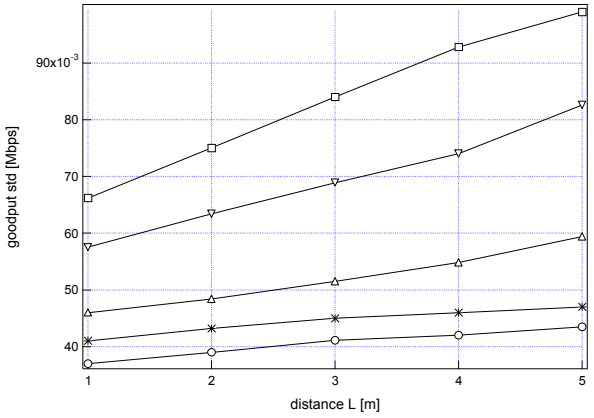

Figure 3.10b – goodput std, $\sigma_G = 4°$, M=12

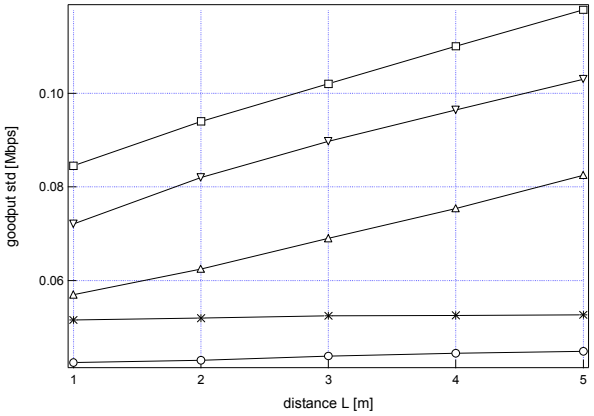

Figure 3.10c – goodput std, $\sigma_G = 4°$, M=16

iii) For look angles far from end-fire, the mean goodput diminishes as L goes from 1 to 5 meters. This happens for any M and both values of σ_G.

iv) For a given GDOA estimator variance, we note that increasing the antenna size M causes an increasing goodput loss. For instance, with $\phi_0 = 90°$ and L=5 the goodput mean value passes from 28.59 Mbps in Figure 3.8a where M=8 (low directivity) to 20.4 Mbps in Figure 3.8c where M =16 (high directivity). Again, this behaviour is clear for look angles far from end-fire.

v) As expected, the GDOA estimator variance affects the goodput. By comparing Figures 3.9.a,b and c with the corresponding Figures 3.8a,b and c, one notices that one degree more of standard deviation leads to a goodput loss which increases as the antenna directivity M increases. For instance with M=8, $\phi_0 = 90°$ and L=5 the goodput mean value passes from 28.59 Mbps in Figure 3.8a to 25 Mbps in Figure 3.9a. With M=16, $\phi_0 = 90°$ and L=5 the goodput from 20.4 Mbps reduces to 15.68 Mbps, Figures 3.8c and 3.9c respectively.

From the analysis of the goodput standard deviation we derive observations compliant with the mean value analysis:

i) The goodput standard deviation increases progressively with ϕ_0 going from 0° to 90°, for any value of M and L.

ii) the goodput standard deviation increases with L, for any M and ϕ_0.

iii) For any fixed geometry (ϕ_0 ,L) the goodput standard deviation increases as M increases.

iv) As expected, simulations run with other values of σ_G confirm that the goodput standard deviation increases as the GDOA estimator performance decreases.

Simulations have shown that σ_G has to be smaller than 2.8° and 2.3° to limit the goodput loss to less than 5% of the maximum goodput at a distance L=5 m for M=12 and M=16, respectively.

The indication that we draw is that high gain directional antennas expose the wireless link to significant goodput degradations in terms of mean value and fluctuations when the alignment error exceeds the requirement. This is the rule except for pointing configurations close to the end-fire. In general, the grater the antenna bandwidth, the higher and more stable the link goodput. Hence, the performance requirements of any algorithm for DOA estimation can be fixed by referring to the broadside pointing.

3.5 Simulations Analysis with UCA Systems

Regarding UCA systems, we have conducted a similar investigation to ULA systems. In particular, bearing in mind that for these latter a mispointing standard deviation around 2°-3° represents the upper boundary to achieve a network throughput negligibly below the maximum throughput of the ideal conditions of no pointing error, we have replicated the same analysis to compare the same kind of boundary for UCA against ULA. Figure 3. 11a and b show the average goodput of UCA systems composed of 8 and 16 elements, respectively. The simulation parameters are the same of Table 3. 2 and the device placement of Figure 3. 7 is simplified to one wireless link only, the one corresponding to PNC – DEV1, being the UCA antenna pattern uniform with the look orientation in the azimuth angle.

As is seen from Figures 3.6 no remarkable degradation appears up to the most directive array of 16 elements even with $\sigma_G = 5°$. The achieved goodput is 31 Mbps roughly, irrespectively of M and σ_G. This result stems from the feature of the UCA directive pattern of providing the same gain as the ULA systems in the direction of the maximum gain, but, unlike ULA, with a boresight beamwidth still large enough also for high directive antenna configurations. As argued in the previous paragraph in fact, the high directional gain of ULA comes together with a very narrow beamwidth that stresses the required pointing precision and may cause goodput losses.

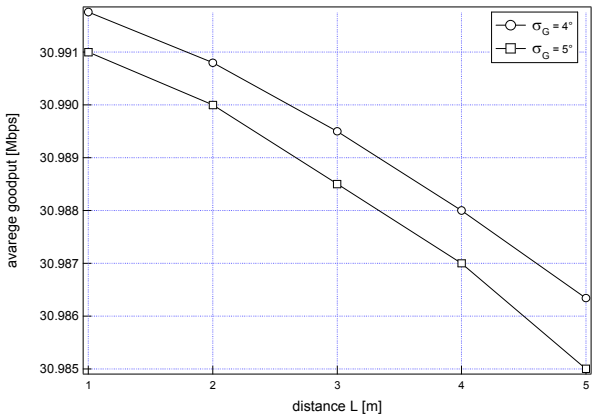

Figure 3. 11a- mean goodput M=8

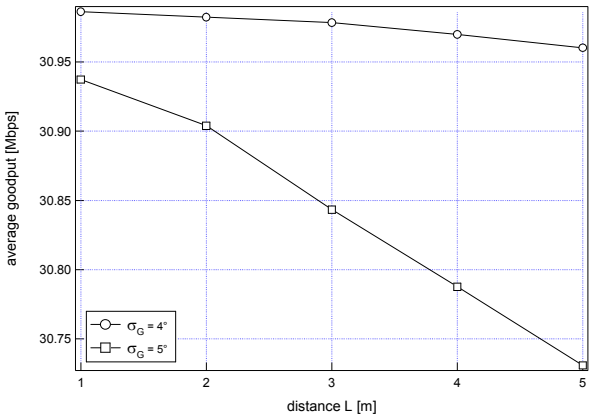

Figure 3.11b - mean goodput, M=16

The characterization of the wireless channel with UCA systems is then exempted from the inclusion of the antenna orientation and also from the antenna pattern provided that the antenna controller performance is below a given threshold. This threshold amounts to $\sigma_G = 5,5°$ and $\sigma_G = 6°$ for *M*=8 and *M*=12, respectively. These values of the standard deviation ensure goodput losses inferior to 5% of the maximum as observed by simulation. Such a boundary for UCA is then less strict than for ULA.

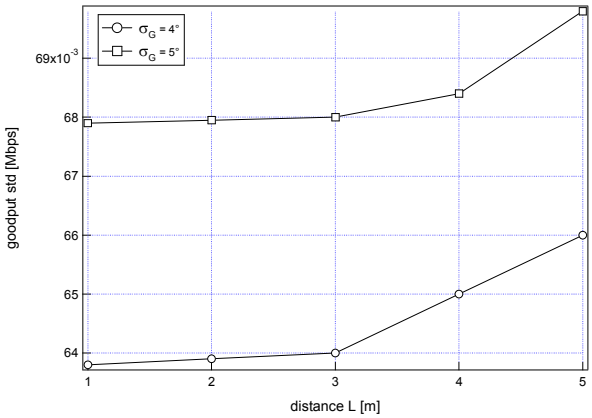

Figure 3. 12a – goodput std, M=8

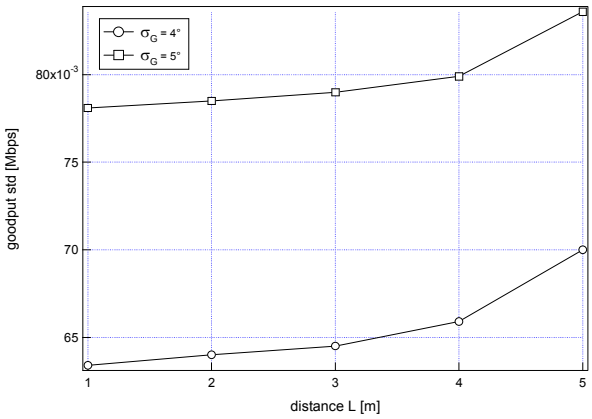

Figure 3. 12b – goodput std, M=16

The behaviour of the curves regarding the goodput standard deviation of Figures 3.12 is self-explanatory. We only notice that the amount of the increase of the fluctuation around the mean value, due to a high antenna directivity, M=16, is negligible and is less than ULA systems as can be observed by comparing Figure 3. 12b with Figure 3. 10c. This is an another proof of the stability of the performance achievable with highly directional UCA systems.

Chapter IV. CRB for DOA Estimation of Narrow Band Data Signals

4.1 CRB on DOA Estimation of Narrow Band Signals.

In this section we derive the CRB of the direction of arrival estimation of narrow band sources propagating over an AWGN channel. The complex transmitted signal $s(t)$ has the following expression

$$s(t) = \sqrt{2P_s}\sum_k c_k g_T(t-kT)e^{j2\pi f_c t} \tag{4.1}$$

where P_s denotes the transmit power, $\{c_k\}$ are the constellation points transmitted at the symbol rate $1/T$. They are zero mean independent random variables with

$$E\{c_k c_i^*\} = \begin{cases} E_c & i = k \\ 0 & otherwise \end{cases}$$

and $g_T(t)$ is the transmit (ideal) shaping filter

$$g_T(t) = \begin{cases} 1 & 0 \le t \le T \\ 0 & elsewhere \end{cases} \tag{4.2}$$

The channel impulse response is

$$h(t;\tau) = \alpha\delta(t-\tau)$$

The channel propagation delay τ is considered known, i.e. perfect timing recovery is assumed to be carried out; $\alpha = \rho e^{jb}$ instead, is an unknown complex-valued attenuation. Thus, the reference analytic signal $r(t)$ incident on the array system assumes the form

$$\begin{aligned} r(t) &= \alpha e^{-j2\pi f_c\tau}\sum_k c_k g_T(t-kT-\tau)e^{j2\pi f_c t} = \\ &= \rho e^{j\psi}\sqrt{2P_s}\sum_k c_k g_T(t-kT-\tau)e^{j2\pi f_c t} \end{aligned} \tag{4.3}$$

in which we have set $\psi = \psi_0 = b - 2\pi f_c\tau$. The vector of the received signal then becomes

$$\mathbf{y}(t) = \rho e^{j\psi}\sqrt{2P_s}\sum_k c_k g_T(t-kT-\tau)e^{j2\pi f_c t}\mathbf{a}(\phi) + \mathbf{n}(t) = r(t)\mathbf{a}(\phi) + \mathbf{n}(t) \quad (4.4)$$

The steering vector $\mathbf{a}(\phi)$ in (4.4) can be either $\mathbf{a}_{ULA}(\phi)$ of (2.5) or $\mathbf{a}_{UCA}(\phi)$ of (2.11). In the general approach, in (4.4) there are four unknown quantities in one symbol time T. They are grouped in the vector $\mathbf{u}[k] \triangleq \mathbf{u}[kT]$ defined as

$$\mathbf{u}[k] = [c_k, \boldsymbol{\rho}, \boldsymbol{\psi}, \boldsymbol{\phi}]^T \quad (4.5)$$

whereas the carrier frequency f_c is commonly considered as a known quantity over T_0 . The assumption of knowing the carrier frequency is reasonable since signal reception is usually carried out by estimating the frequency offset first and the other quantities of (4.5) subsequently. Thus, when estimating $\mathbf{u}[k]$, the carrier frequency offset has already been recovered and the original uncertainty of the carrier frequency is transparent at the second stage of estimation. This justifies the framework developed on the analytic signal with the assumption of knowing the signal carrier frequency.

When characterizing the parameter space two categories of parameters arise. In one case the parameters are random variables whose behaviour is governed by a probability density that represents the a priori knowledge of the parameters. The probability density function (pdf) is usually known. In the second case the parameters are unknown deterministic variables. For both kinds of variables there exists an ultimate inferior limit to the estimation accuracy of any unbiased estimator. This inferior limit is the well known Cramér Rao Bound (CRB). The derivation of the CRB of non random parameters is usually plain whilst it is more complicated when dealing with the pdfs of the random variables. In the presence of stochastic variables one can resort to the Modified CRB (MCRB) [31 – 32] to simplify the manipulation of the pdfs or to overcome the lack of knowledge of the pdfs. The MCRB is a lower bound that has been proven to be less than the CRB. The matter will be illustrated in the sequel with reference to the constellation symbols that can be known (pilot) or modulation symbols

(stochastic variables). In our treatment we assume PSK constellation points and we calculate the CRB when the symbols are pilots whereas we calculate the MCRB if they are data symbols. In both cases the deterministic unknown parameters of our interest are ρ, ψ and ϕ and the **FIM** [33] is

$$\mathbf{FIM} = \begin{pmatrix} J_{\rho\rho} & J_{\rho\psi} & J_{\rho\phi} \\ J_{\psi\rho} & J_{\psi\psi} & J_{\psi\phi} \\ J_{\phi\rho} & J_{\phi\psi} & J_{\phi\phi} \end{pmatrix} \tag{4.6}$$

In estimation models where one of the quantities of (4.6) is known instead, the framework scales easily by removing the row and the column corresponding to this quantity in the **FIM**.

Furthermore, we point out that all the unknown quantities are treated as constant quantities versus time for the overall duration of the observation interval T_0. As for T_0, we first focus on the situation of an observation interval equal to one symbol time T and consider the changes involved when T_0 extends to many symbol times afterwards. For ease of notation we omit the index *k* since its presence is clear by the context.

We dub CRB(u_v) the CR lower bound of any unbiased estimator of the unknown parameter u_v which is the entry of position *v* in the vector $[\rho, \psi, \phi]^T$. CRB(u_v) is found as the diagonal element at the position *(v,v)* of the inverse of the Fisher Information Matrix **FIM**, i.e.

$$CRB(u_v) = [FIM^{-1}]_{vv} \tag{4.7}$$

The matter then reduces to the computation of the **FIM**. There are two approaches to the derivation of the **FIM**. One is for direct derivation from the vector of continuous signals $\mathbf{y}(t)$; the other defines a finite-dimensional representation of $\mathbf{y}(t)$ and works on this representation instead of $\mathbf{y}(t)$. The former is the optimum approach by default since it exploits all the information about the quantities to estimate. On the other hand, the passage to a finite-dimension vector $\mathbf{z}$ is useful in practical estimation situations since it reduces the dimension of the observation space to the finite one of **z.** From the theoretical point of view, manipulating the observed space to draw $\mathbf{z}$ from $\mathbf{y}(t)$ poses the issue of the finite-dimensional accuracy. Equivalency

between the two approaches occurs if **z** captures all the information about the parameters that is present originally in $\mathbf{y}(t)$. Such a of known data symbols, Figure 4. 1 shows how the signal $\mathbf{y}(t)$ can be received and manipulated at the *m*-th antenna system branch to obtain the sufficient statistic **z**.

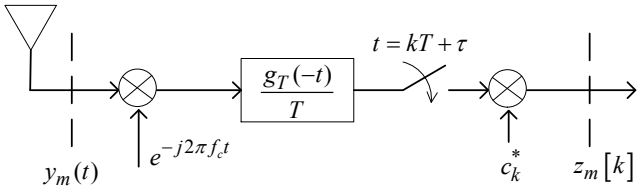

Figure 4. 1 - signal reception at the m-*th* branch

The samples $z_m[k]$ at the output of the matched filter are

$$z_m[k] = \rho e^{j\psi} e^{-j\boldsymbol{\beta}\cdot\mathbf{p}_m} + n_m[k] \tag{4.8}$$

The noise samples $n_m[k]$ are statistically independent Gaussian random variables

$$E\left\{n_m[k]n_{m'}^*[k']\right\} = \sigma^2\delta[k-k']\delta_{m,m'}$$

with zero mean and variance equal to

$$\sigma^2 = \frac{2N_0/T}{2P_s} = \frac{2}{\xi_s/N_0} \tag{4.9}$$

where δ indicates the Kronecker delta and $\xi_s = 2P_S T$ is the energy per symbol interval of the complex signal (4.1) with the signalling pulse (4.2) and PSK constellation symbols.

4.2 Derivation of the **FIM** *from the Sufficient Statistic*

Indicating with **z** the vector of the samples $z_m[k]$ taken at the branches of the array system, the entry *(v,w)* of the **FIM** can be computed as

$$J_{u_v u_w} = -E_{\mathbf{z}}\left\{\frac{\partial^2 \ln p(\mathbf{z}/\mathbf{u})}{\partial u_v \partial u_w}\right\} \tag{4.10}$$

In (4.10) $p(\mathbf{z}/\mathbf{u})$ is the probability density function of the vector **z** for a given **u** and the stochastic expectation $E_{\mathbf{z}}$ is actually carried out versus the

noise samples ($E_{\mathbf{z}} = E_{\mathbf{n}}$). In fact from (4.8) one can see that $z_m / \mathbf{u}$ is a Gaussian variable with the same second order statistic as $n_m[k]$ and with mean value equal to $ae^{j\psi}e^{j\boldsymbol{\beta}\cdot\mathbf{p}_m}$. When $T_0 = T$, the probability density function $p(\mathbf{z}/\mathbf{u})$ is

$$p(\mathbf{z}/\mathbf{u}) = \left(\frac{1}{\sigma\sqrt{2\pi}}\right)^M \exp\left\{-\frac{1}{2\sigma^2}\sum_{m=0}^{M-1}\left|z_m[k] - \rho e^{j\psi}e^{-j\boldsymbol{\beta}\cdot\mathbf{p}_m}\right|^2\right\} =$$

$$= \left(\frac{1}{\sigma\sqrt{2\pi}}\right)^M \exp\left\{-\frac{1}{2\sigma^2}\left(\mathbf{z}[k] - \rho e^{j\psi}\mathbf{a}(\boldsymbol{\phi})\right)^H\left(\mathbf{z}[k] - \rho e^{j\psi}\mathbf{a}(\boldsymbol{\phi})\right)\right\} \tag{4.11}$$

and its logarithm

$$\ln(p(\mathbf{z}/\mathbf{u})) = C - \frac{1}{2\sigma^2}\left(\mathbf{z}[k] - \rho e^{j\psi}\mathbf{a}(\boldsymbol{\phi})\right)^H\left(\mathbf{z}[k] - \rho e^{j\psi}\mathbf{a}(\boldsymbol{\phi})\right)$$

where C indicates a constant term versus the unknown parameters of $\mathbf{u}$. Thus one can consider the log likelihood function $\Delta(\mathbf{z}/\mathbf{u})$

$$\Delta(\mathbf{z}/\mathbf{u}) = -\frac{1}{2\sigma^2}\left(\mathbf{z}[k] - \rho e^{j\psi}\mathbf{a}(\boldsymbol{\phi})\right)^H\left(\mathbf{z}[k] - \rho e^{j\psi}\mathbf{a}(\boldsymbol{\phi})\right) \tag{4.12}$$

By computing all the derivatives of (4.12) as indicated in (4.10) (see Appendix B for the mathematical details) we get the **FIM.**

4.3 CRB for DOA with ULA Systems

The **FIM** of ULA systems is

$$\mathbf{FIM} = \begin{pmatrix} \frac{M}{\sigma^2} & 0 & 0 \\ 0 & \frac{M\rho^2}{\sigma^2} & -2\pi\frac{f_c}{c}d\sin\phi\frac{M(M-1)}{2}\frac{\rho^2}{\sigma^2} \\ 0 & -2\pi\frac{f_c}{c}d\sin\phi\frac{M(M-1)}{2}\frac{\rho^2}{\sigma^2} & \left(2\pi\frac{f_c}{c}d\sin\phi\right)^2\frac{M(M-1)(2M-1)}{6}\frac{\rho^2}{\sigma^2} \end{pmatrix} \tag{4.13}$$

From (4.13), it is clear the block diagonal form of the **FIM**, with a block amplitude **A** that is associated to entries of **u** concerning the amplitude of

$\mathbf{y}(t)$ and a block phase $\boldsymbol{\Theta}$ that is associated to the entries of $\mathbf{u}$ concerning the phases (ψ and ϕ) of $\mathbf{y}(t)$ instead. Thus we write

$$\mathbf{FIM} = \begin{pmatrix} \mathbf{A} & \mathbf{0} \\ \mathbf{0} & \boldsymbol{\Theta} \end{pmatrix} \tag{4.14}$$

The wanted CRBs are computed through the inversion of (4.13)-(4.14). In particular, the CR lower bound for DOA estimation is

$$CRB_{ULA}(\phi) = \frac{J_{\psi\psi}\det(\mathbf{A})}{\det(\mathbf{A})\det(\boldsymbol{\Theta})} = \frac{J_{\psi\psi}}{\det(\boldsymbol{\Theta})} = \frac{12}{\left(2\pi\frac{f_c}{c}d\sin\phi\right)^2 M(M^2-1)\frac{\rho^2}{\sigma^2}}$$

The signal to noise ratio SNR of the received signal at the symbol interval kT is given by

$$\frac{\rho^2}{\sigma^2} = \frac{\rho^2}{2/(\xi_s/N_0)} = \frac{\rho^2\xi_s}{2N_0} = \frac{1}{2}\frac{E_s}{N_0} \tag{4.15}$$

In (4.15) E_s is the energy of the received symbol. The CRB for DOA estimation becomes

$$CRB(\phi) = \frac{24}{\left(2\pi\frac{f_c}{c}d\sin\phi\right)^2 M(M^2-1)}\frac{1}{\frac{E_s}{N_0}} \tag{4.16}$$

In Figure 4. 2 we plotted the square root of (4.16) in degrees, with the inter sensor offset d equal to half a wavelength (standard ULA). The DOA ϕ is 90° and the channel attenuation is $\rho^2 = 1$. Figures 4.3 show the CRB for different directions of arrivals and different values of the SNR of the incident signal. In fact, ULA systems exhibit a strong dependency of the DOA estimation performance from the direction of arrival itself. This is a direct consequence of the anisotropic arrangement of the array sensors. (4.16) shows that the function $CRB_{ULA}(\phi)$ has its minimum at broadside $\phi = 90°$, and increases progressively with ϕ that moves from broadside to end-fire. The end-fire positions, $\phi = 0°$ and $\phi = 180°$, are DOAs for which the $CRB_{ULA}(\phi)$ is infinitely large.

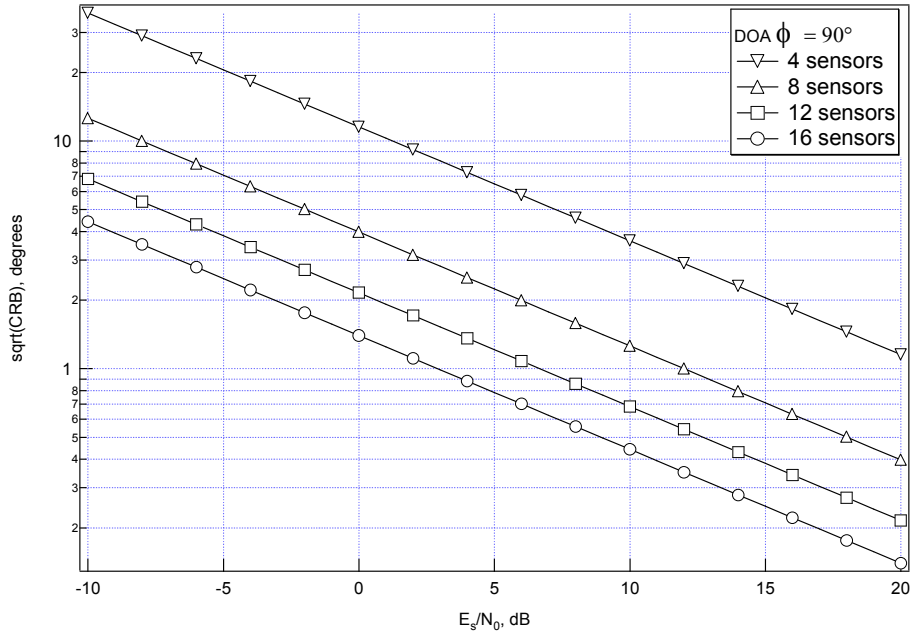

Figure 4. 2 – CRB on DOA of standard ULA systems

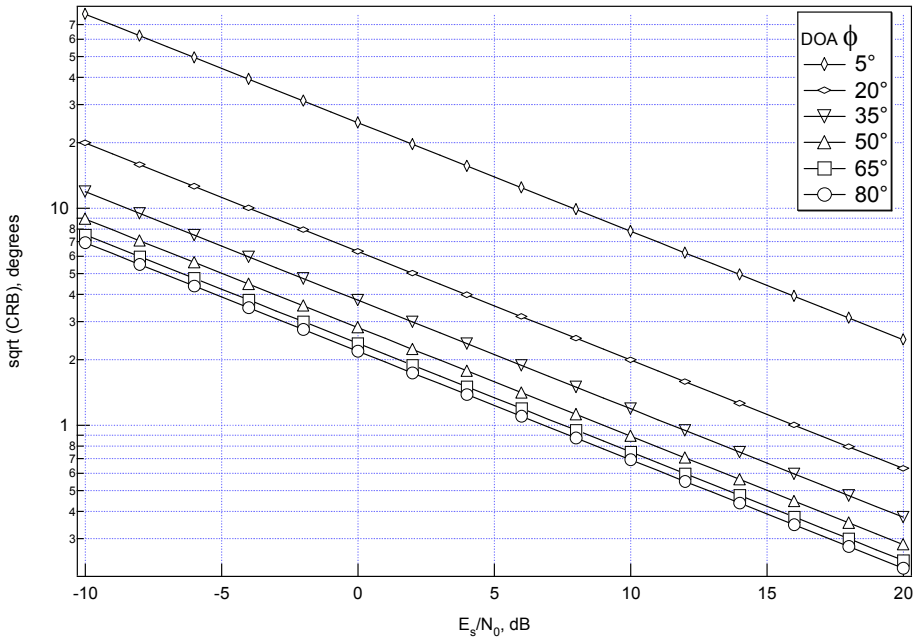

Figure 4. 3a – CRB of a 12 sensors ULA system versus SNR and DOA

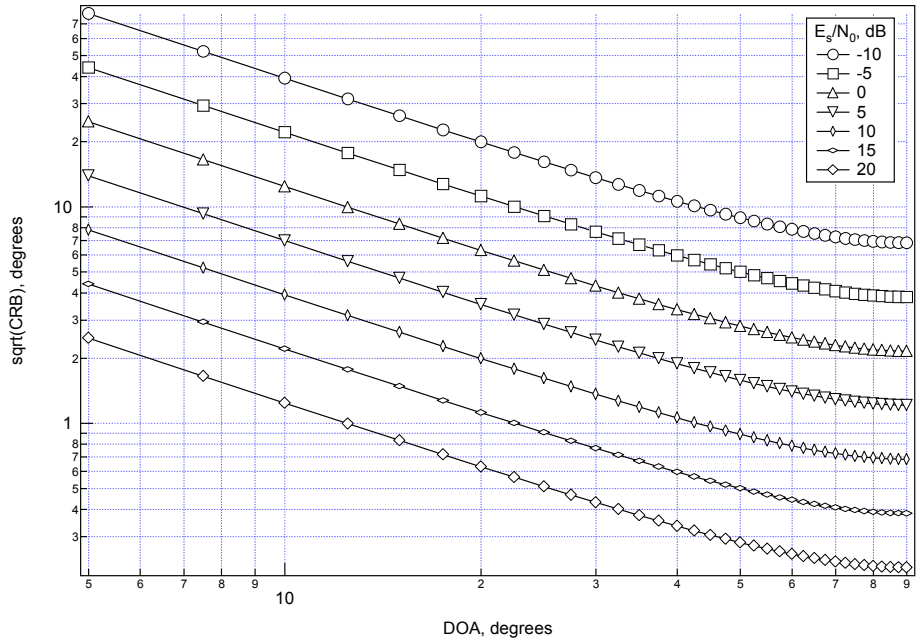

Figure 4.3b – CRB of a 12 sensors ULA system versus DOA and SNR

4.4 CRB for DOA with UCA Systems

The **FIM** of UCA systems is

$$\mathbf{FIM} = \begin{pmatrix} \frac{M}{\sigma^2} & 0 & 0 \\ 0 & \frac{M\rho^2}{\sigma^2} & 0 \\ 0 & 0 & \left(\frac{2\pi R}{\lambda}\right)^2 \frac{\rho^2}{\sigma^2} \sum_{m=0}^{M-1} \cos\phi_m{}^2 \end{pmatrix}$$

The CRB on the direction of arrival is

$$CRB_{UCA}(\phi) = \frac{2}{\left(\frac{2\pi R}{\lambda}\right)^2 \sum_{m=0}^{M-1} \cos^2\left(m\frac{2\pi}{M}\right)\frac{E_s}{N_0}} \tag{4.17}$$

By substituting R given in (2.10) in (4.17) the expression of the CRB becomes

$$CRB_{UCA}(\phi) = \frac{8}{\pi^2} \frac{\left(1 - \cos^2\left(\frac{\pi}{M}\right)\right)}{\sum_{m=0}^{M-1} \cos^2\left(\frac{2\pi}{M}\right) \frac{E_s}{N_0}} \tag{4.18}$$

Unlike ULA, UCA systems show an isotropic CRB versus the DOA The uniform circular disposition of sensors ensures isotropic estimation capability. In Figure 4. 4 we plotted the square root of (4.18) with $\rho^2 = 1$.

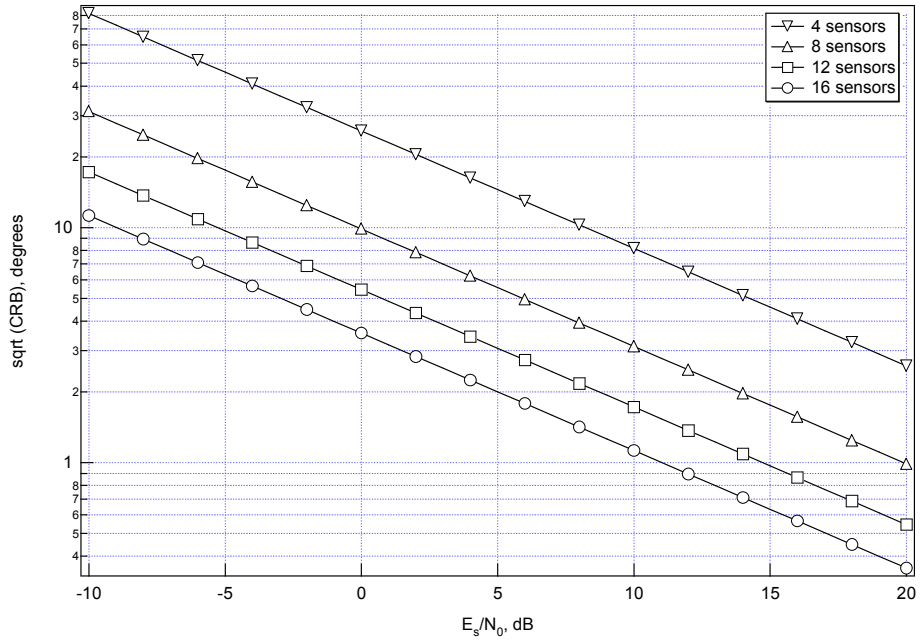

Figure 4. 4 – CRB on DOA of UCA systems

When comparing ULA versus UCA systems one notice that UCA systems have the advantage of a CRB that is not affected by the source arrival angle, but suffer from noise sensitivity. Even a relatively large number of sensors like 12 or 16, which is unrealistic in real antenna systems, would not be able of lowering down the performance accuracy below 1° with a SNR of 10 dB over an AWGN channel and no interfering sources (on a single-symbol observation time). In general we can state that the DOA CRB of UCA

systems is higher than the one of ULA systems. By contrast, the CRB of ULA systems is not isotropic versus the source direction of arrival is robust to noise, at least in a wide region of source directions of arrivals distant from end fire. With narrow band sources, the only ways to boost the performance is in hardware/spatial domain by increasing the number of sensors or in time domain by extending the observation interval to more symbol times. How the CRB varies with the number of array elements is immediately evident by looking at the CRB formulas. The dependency of the CRB from the observation interval T_0 is briefly treated in the next section.

4.5 Extension of the Observation Time to more Symbol Intervals

(4.16) gives the CRB in one symbol interval *T*. When the condition of quasi-stationary channel is true, the observation interval T_0 can be extended up to a certain number *K* of symbol intervals *T* during which the channel does not vary significantly. It can be seen easely that

$$CRB_{T_0=KT} = \frac{1}{K} CRB_{T_0=T}$$

To see this, suppose to use a PSK constellation. With $T_0 = KT$ the vector $\mathbf{z}_K$ of the samples at the output of the array system is the collection of *K* times the vector $\mathbf{z}$ taken *T* by *T*

$$\mathbf{z}_K = \left[\mathbf{z}[k], \mathbf{z}[k+1], ..., \mathbf{z}[k-2], \mathbf{z}[k+K-1]\right]^T$$

Because of the statistical independence of the noise samples, the probability density function of $\mathbf{z}_K$ is

$$p(\mathbf{z}_K / \mathbf{u}) = \left[\left(\frac{1}{\sigma\sqrt{2\pi}} \right)^M \exp\left\{ -\frac{1}{2\sigma^2} \sum_{m=0}^{M-1} \left| z_m[k] - \rho e^{j\psi} e^{j\boldsymbol{\beta}\cdot\mathbf{p}_m} \right|^2 \right\} \right]^K = p(\mathbf{z} / \mathbf{u})^K$$

Thus the following identities conclude the proof

$$\mathbf{FIM}\big|_{T_0=KT} = K\, \mathbf{FIM}\big|_{T_0=T} \quad \text{and} \quad \mathbf{FIM}\big|_{T_0=KT}^{-1} = \frac{1}{K} \mathbf{FIM}\big|_{T_0=T}^{-1}$$

4.6 Derivation of the **FIM** *from the Continuous Time Observation Space*

The derivation of the **FIM** has been conducted so far through the notion of the sufficient statistic $\mathbf{z}$ that has been introduced in lieu of the infinite-dimensional observation space represented by the vector of waveforms $\mathbf{y}(t)$. The approach to the CRB through direct manipulation of $\mathbf{y}(t)$ is managed by replacing the probability density function $p(\mathbf{z}/\mathbf{u})$ in (4.10) with the likelihood function $L(\mathbf{u})$ that is defined as in [33]

$$\begin{aligned} L(\mathbf{u}) &= \exp\left\{-\frac{1}{4N_0}\int_{T_0}\left|\mathbf{y}(t)-E\{\mathbf{y}(t)\}\right|^2 dt\right\} \\ &= \exp\left\{-\frac{1}{4N_0}\int_{T_0}\left|\mathbf{y}(t)-r(t)\mathbf{a}(\boldsymbol{\phi})\right|^2 dt\right\} \end{aligned} \tag{4.19}$$

from which it can be seen that the entry *(v,w)* of the **FIM** can be calculated as

$$J_{u_v u_w} = \frac{1}{2N_0}\int_{T_0}\mathrm{Re}\left\{\frac{\partial}{\partial u_w}\left[r(t)\mathbf{a}(\boldsymbol{\phi})\right]^H \frac{\partial}{\partial u_v} r(t)\mathbf{a}(\boldsymbol{\phi})\right\} dt \tag{4.20}$$

and also

$$J_{u_v u_v} = \frac{1}{2N_0}\int_{T_0}\left|\frac{\partial}{\partial u_v} r(t)\mathbf{a}(\boldsymbol{\phi})\right|^2 dt \tag{4.21}$$

In appendix B, it is shown that (4.20) and (4.21) lead to the same **FIM** as in (4.13), and this justifies why the vector $\mathbf{z}$ that we defined in (4.8) was considered to be a sufficient statistic.

4.7 MCRB: Estimation with Unknown Data Symbols

We now analyse the case of a data modulated signal and derive the MCRB of the direction of arrival. Suppose to split the entries of $\mathbf{u}$ in two sub-vectors $[\mathbf{u}_s, \mathbf{u}_d]$: $\mathbf{u}_s$ gathers the stochastic variables ($\{c_k\}$ here) of $\mathbf{u}$ whilst $\mathbf{u}_d$ contains the deterministic parameters of $\mathbf{u}$. We are interested in estimating $\mathbf{u}_d$. The **FIM** is computed in a way similar to (4.10), that is

$$J_{u_v u_w} = -E_{\mathbf{z}}\left\{\frac{\partial^2 \ln p(\mathbf{z}/\mathbf{u}_d)}{\partial u_v \partial u_w}\right\} \qquad u_v, u_w \in \mathbf{u}_d \tag{4.22}$$

In (4.22), $p(\mathbf{z}/\mathbf{u}_d)$ is the probability density function of the observed statistic $\mathbf{z}$ for a fixed $\mathbf{u}_d$ and the stochastic expectation $E_{\mathbf{z}}$ is to carry out versus the noise. In the presence of the other stochastic variables $\mathbf{u}_s$, $p(\mathbf{z}/\mathbf{u}_d)$ is found as

$$p(\mathbf{z}/\mathbf{u}_d) = \int_{-\infty}^{\infty} p(\mathbf{z}/\mathbf{u}_d, \mathbf{u}_s) p(\mathbf{u}_s) d\mathbf{u} \tag{4.23}$$

where $p(\mathbf{u}_s)$ denotes the pdf of $\mathbf{u}_s$. The conditional probability density function of the sufficient statistic $\mathbf{z}$ given $[\mathbf{u}_s, \mathbf{u}_d]$, $p(\mathbf{z}/\mathbf{u}_d, \mathbf{u}_s)$, is usually available, as for instance for Gaussian channels. Unfortunately, it can happen that either the integration in (4.23) or the expectation in (4.22) is impossible to calculate in close form. We call Modified **FIM**, (**MFIM**), the **FIM** that we use for the MCRB. Its entry is

$$J^M_{u_v u_w} = -E_{\mathbf{z}}\left\{\frac{\partial^2 \ln p(\mathbf{z}/\mathbf{u}_d, \mathbf{u}_s)}{\partial u_v \partial u_w}\right\} \qquad u_v, u_w \in \mathbf{u}_d$$

and the expectation $E_{\mathbf{z}}$ is to carry out versus both the noise and $\mathbf{u}_s$.
Similarly to (4.11), $p(\mathbf{z}/\mathbf{u}_d, \mathbf{u}_s)$ is

$$p(\mathbf{z}/\mathbf{u}_d, \mathbf{u}_s) = \left(\frac{1}{\sigma\sqrt{2\pi}}\right)^M \exp\left\{-\frac{1}{2\sigma^2}\sum_{m=0}^{M-1}\left|z_m[k] - \rho c_k e^{j\psi} e^{j\boldsymbol{\beta}\cdot\mathbf{p}_m}\right|^2\right\}$$

With easy manipulations it can be shown that

$$\mathbf{MFIM} = E\left\{|c_k|^2\right\}\mathbf{FIM} = \mathbf{FIM} \tag{4.24}$$

where the last equality in (4.24) holds for PSK constellation symbols. (4.24) states that the MCRB of any non random parameter calculated with modulation symbols is equal to the CRB attainable with pilot symbols. Thus referring to the DOA as an example, one can interpret (4.24) as follows. When DOA estimation is performed on pilot symbols, if an efficient estimator exists it will achieve the CRB (4.16). When instead estimation is performed on modulation symbols, if an efficient estimator exists it will

achieve a minimum variance curve that coincides with (4.16) only if the approximation of the MCRB is tight.

Chapter V. CRB for DOA of OFDM Data Signals

5.1 CRB of Parameter Estimation with Waveforms having Orthogonal Derivatives

In this section we tackle the problem of estimating N_u deterministic parameters $\mathbf{u}=\left[u_0,...,u_v,...,u_w,...,u_{N_u-1}\right]^T$ through the observation of N **u**-bearing signals $\left\{s_i(t;\mathbf{u})\right\}_{i=0,...,N-1}$ in the presence of additive white Gaussian noise. The hypothesis about the N waveforms is that their derivatives versus the vector **u** are orthogonal

$$\int_{T_0}\frac{\partial s_i(t;\mathbf{u})}{\partial u_v}\frac{\partial s_l^*(t;\mathbf{u})}{\partial u_w}dt=\begin{cases}0 & i\neq l\\ A_i & i=l\end{cases} \tag{5.1}$$

where T_0 indicates the estimation time. With N=1 we have the traditional estimation of a set of unknown quantities by observing one waveform corrupted by white Gaussian noise. With the extension to a generic number N of waveforms, we aim to study how the estimation of **u** attainable when the observation space includes all the set of waveforms $\left\{s_i(t;\mathbf{u})\right\}_{i=0,...,N-1}$ is related to the estimation of **u** attainable when one observes only one of the N functions. That is, if one characterizes the estimation of **u** from the observation of one waveform $s_i(t;\mathbf{u})$, how the estimation of **u** can related to the observation of more waveforms. The problem can be stated as follows. The observed signal is

$$y(t)=s(t;\mathbf{u})+n(t) \tag{5.2}$$

where $n(t)$ is AWGN with zero mean and PSD $2N_0$ and $s(t;\mathbf{u})$ is

$$s(t;\mathbf{u})=\sum_{i=0}^{N-1}s^{(i)}(t;\mathbf{u}) \tag{5.3}$$

We call $\mathbf{FIM}_N$ the **FIM** resulting from the joint observation of all the waveforms $\left\{s_i(t;\mathbf{u})\right\}_{i=0,...,N-1}$ and $\mathbf{FIM}_i$ the **FIM** associated to the function

$s_i(t;\mathbf{u})$. We point out that in our estimation model, the vector of unknowns $\mathbf{u}$ to be estimated as well as all the waveforms $\{s_i(t;\mathbf{u})\}_{i=0,\ldots,N-1}$ are deterministic quantities, and the stochastic part of the model is due to the presence of the white Gaussian noise. It can be shown that

$$\mathbf{FIM}_N^{-1} = \left(\sum_{i=0}^{N-1} \mathbf{FIM}_i \right)^{-1} \tag{5.4}$$

To prove this we start by deriving our **FIM** from the time continuous representation of the observation space because the hypothesis (5.1) has been formulated in terms of continuous time waveforms. Thus we follow this approach and write the likelihood function $L(\mathbf{u})$ as

$$L(\mathbf{u}) = \exp\left\{ -\frac{1}{2\sigma_n^2} \int_{T_0} \left| y(t) - E\{y(t)\} \right|^2 dt \right\} = \exp\left\{ -\frac{1}{2\sigma_n^2} \int_{T_0} \left| y(t) - s(t;\mathbf{u}) \right|^2 dt \right\}$$

from which the entry *(v,w)* of the **FIM** is found to be

$$J_{u_v u_w} = \frac{1}{\sigma_n^2} \int_{T_0} \mathrm{Re}\left\{ \frac{\partial}{\partial u_v} s(t;\mathbf{u}) \frac{\partial}{\partial u_w} s^*(t;\mathbf{u}) \right\} dt \tag{5.5}$$

When only one function of the set, let us say $s^i(t;\mathbf{u})$, is taken , we have

$$J^i_{u_v u_w} = \frac{1}{\sigma_n^2} \int_{T_0} \mathrm{Re}\left\{ \frac{\partial}{\partial u_v} s_i(t;\mathbf{u}) \frac{\partial}{\partial u_w} s_i^*(t;\mathbf{u}) \right\} dt$$

In the case of *N* waveforms instead, we substitute (5.3) in (5.5) to get

$$J^N_{u_v u_w} = \frac{1}{\sigma_n^2} \int_{T_0} \mathrm{Re}\left\{ \frac{\partial}{\partial u_v} s(t;\mathbf{u}) \frac{\partial}{\partial u_w} s^*(t;\mathbf{u}) \right\} dt =$$

$$= \frac{1}{\sigma_n^2} \int_{T_0} \mathrm{Re}\left\{ \frac{\partial}{\partial u_v} \sum_{i=0}^{N-1} s_i(t;\mathbf{u}) \frac{\partial}{\partial u_w} \sum_{l=0}^{N-1} s_l^*(t;\mathbf{u}) \right\} dt =$$

$$= \frac{1}{\sigma_n^2} \int_{T_0} \mathrm{Re}\left\{ \sum_{i=0}^{N-1} \frac{\partial}{\partial u_v} s_i(t;\mathbf{u}) \sum_{l=0}^{N-1} \frac{\partial}{\partial u_w} s_l^*(t;\mathbf{u}) \right\} dt =$$

$$= \frac{1}{\sigma_n^2} \int_{T_0} \mathrm{Re}\left\{ \sum_{i=0}^{N-1} \left[\frac{\partial}{\partial u_v} s_i(t;\mathbf{u}) \frac{\partial}{\partial u_w} s_i^*(t;\mathbf{u}) + \frac{\partial}{\partial u_v} s_i(t;\mathbf{u}) \sum_{l=0, l\neq i}^{N-1} \frac{\partial}{\partial u_w} s_l^*(t;\mathbf{u}) \right] \right\} dt =$$

$$= \frac{1}{\sigma_n^2} \int_{T_0} \sum_{i=0}^{N-1} \mathrm{Re}\left\{ \frac{\partial}{\partial u_v} s_i(t;\mathbf{u}) \frac{\partial}{\partial u_w} s_i^*(t;\mathbf{u}) + \frac{\partial}{\partial u_v} s_i(t;\mathbf{u}) \sum_{l=0, l\neq i}^{N-1} \frac{\partial}{\partial u_w} s_l^*(t;\mathbf{u}) \right\} dt =$$

$$= \frac{1}{\sigma_n^2} \sum_{i=0}^{N-1} \int_{T_0} \mathrm{Re}\left\{ \frac{\partial}{\partial u_v} s_i(t;\mathbf{u}) \frac{\partial}{\partial u_w} s_i^*(t;\mathbf{u}) + \frac{\partial}{\partial u_v} s_i(t;\mathbf{u}) \sum_{l=0, l\neq i}^{N-1} \frac{\partial}{\partial u_w} s_l^*(t;\mathbf{u}) \right\} dt =$$

$$= \frac{1}{\sigma_n^2} \sum_{i=0}^{N-1} \left[\int_{T_0} \mathrm{Re}\left\{ \frac{\partial}{\partial u_v} s_i(t;\mathbf{u}) \frac{\partial}{\partial u_w} s_i^*(t;\mathbf{u}) \right\} dt + \right.$$

$$\left. + \int_{T_0} \mathrm{Re}\left\{ \frac{\partial}{\partial u_v} s_i(t;u) \sum_{l=0, l\neq i}^{N-1} \frac{\partial}{\partial u_w} s_l^*(t;u) \right\} dt \right] =$$

$$= \frac{1}{\sigma_n^2} \sum_{i=0}^{N-1} \left[\int_{T_0} \mathrm{Re}\left\{ \frac{\partial}{\partial u_v} s_i(t;\mathbf{u}) \frac{\partial}{\partial u_w} s_i^*(t;\mathbf{u}) \right\} dt + \right.$$

$$\left. + \mathrm{Re}\left\{ \int_{T_0} \frac{\partial}{\partial u_v} s_i(t;\mathbf{u}) \sum_{l=0, l\neq i}^{N-1} \frac{\partial}{\partial u_w} s_l^*(t;\mathbf{u}) dt \right\} \right] =$$

$$= \sum_{i=0}^{N-1} \left[J^i_{u_v u_w} + \frac{1}{\sigma_n^2} \mathrm{Re}\left\{ \sum_{l=0, l\neq i}^{N-1} \int_{T_0} \frac{\partial}{\partial u_v} s_i(t;\mathbf{u}) \frac{\partial}{\partial u_w} s_l^*(t;\mathbf{u}) dt \right\} \right] \qquad (5.6)$$

If the set of waveforms $\{s_i(t;\mathbf{u})\}_{i=0,\ldots,N-1}$ is such that

$$\sum_{i=0}^{N-1} \mathrm{Re}\left\{ \sum_{l=0, l\neq i}^{N-1} \int_{T_0} \frac{\partial}{\partial u_v} s_i(t;\mathbf{u}) \frac{\partial}{\partial u_w} s_l^*(t;\mathbf{u}) dt \right\} = 0, \qquad \forall i \neq j \qquad (5.7)$$

the observations of **u** among the **u**-bearing waveforms are uncoupled and one gets

$$J^{N}_{u_v u_w} = \sum_{i=0}^{N-1} J^{i}_{u_v u_w}$$

Since the mathematical manipulation has been developed with generic unknowns u_v and u_w, we can conclude that if (5.7) holds true

$$\mathbf{FIM}_N = \sum_{i=0}^{N-1} \mathbf{FIM}_i \tag{5.8}$$

It easy to recognise that the hypothesis (5.1) is a sufficient condition for (5.7) to happen. In fact, under (5.1) the individual integral in (5.7) is zero for any pairs of functions *(i,l),* with $i \neq l$, the overall sum is zero for any fixed index *i*, and the theorem is proved.

When the estimation model is scalar the **FIM** is a scalar quantity that corresponds to the inverse of the CRB. Thus with a self explanatory notation (5.8) becomes

$$CRB_N^{-1} = \sum_{i=0}^{N-1} CRB_i^{-1} \tag{5.9}$$

The theorem that we have derived in this section is of practical interest in several estimation problems in wireless communications. In the next section we will discuss an example of application of the theorem to the DOA estimation of OFDM signals impinging on antenna array systems and we will show a counter example to the theorem to show that it is not trivial.

We conclude this paragraph by pointing out two conditions, which are useful in the sequel, under which the hypothesis (5.1) holds true. They are:

i) $\{s_i(t;\mathbf{u})\}_{i=0,\ldots,N-1}$ is a set of orthogonal functions

ii) the derivative of each function component is proportional to the function itself for all the unknowns

$$\frac{\partial s_i(t;\mathbf{u})}{\partial u_v} = \boldsymbol{\gamma} s_i(t;\mathbf{u}) \qquad \begin{matrix} i = 0,\ldots,N\text{-}1 \\ v = 0,\ldots,N_u\text{-}1 \end{matrix} \tag{5.10}$$

where γ is a constant quantity versus time.

5.2 DOA Estimation of OFDM Signals over AWGN Channel

Estimation of the DOA of OFDM signals impinging on antenna arrays is an example of application of the results of the previous section. The analytic OFDM signal can be written as

$$s(t) = \sqrt{\frac{2P_S}{N}} \sum_k \sum_{i=0}^{N-1} c_{k,i} e^{j2\pi f_i (t-kT)} p(t-kT) \qquad (5.11)$$

where N is the number of FFT points, $T = T_{FFT} + T_G$ is the overall OFDM symbol length given as the sum of the effective FFT time plus the duration of the cyclic prefix. Indicating with f_0 the frequency of the lowest Sub Carrier (SC) and with $\Delta f = 1/T_{FFT}$ the subcarrier spacing, $f_i = f_0 + i\Delta f$ represents the frequency of the i-*th* SC. $\{c_{k,i}\}$ are the constellation points {data, pilot, null} that modulate the sub-carriers. It is reasonable to suppose that the data streams of different sub-carriers are statistically independent

$$E\left\{c_{k,i} c_{k,l}^*\right\} = \begin{cases} E_c & i = l \\ 0 & otherwise \end{cases}$$

Moreover, $p(t)$ is an ideal signalling pulse

$$p(t-kT) = \begin{cases} 1 & kT \le t \le kT + T_{FFT} + T_G \\ 0 & otherwise \end{cases}$$

To fix the scenario we analyse the case of Gaussian channel, with direction of arrival ϕ of the OFDM source in the *x*-*y* Cartesian plane. For simplicity we concentrate on ULA systems. The OFDM signal is the sum of N narrowband PAM signals with carriers $\{f_i\}_{i=0,\ldots,N-1}$ that are orthogonal to each other. With this in mind, we try to exploit the background of the narrow band signals to treat the broadband signals generated through the OFDM technique. In particular we use the simplification (2.4), regarding the reception of narrowband signals with antenna arrays, to all the SCs of the received OFDM signal. In general, with the same formalism used for narrow band signals, the noiseless reference OFDM signal received at reference spot of the antenna system is

$$r(t) = \sum_{k} \sum_{i=0}^{N-1} \boldsymbol{\mu}_i (t - kT) e^{j2\pi f_i (t-kT)}$$

if the *i*-th data modulation bearing signal $\boldsymbol{\mu}_i(t-kT)$ does not vary over $\max\{\tau_m\}$, the signals captured by the array sensors at the frequency f_i during the signalling interval T, are the signal $\boldsymbol{\mu}_i(t-kT)$ with different phase rotations. In operating conditions in which this happens, the noiseless component of the OFDM signal received at the array element *m*, $r_m(t)$, is

$$r_m(t) = \boldsymbol{\alpha} \sqrt{\frac{2P_S}{N}} \sum_{k} \sum_{i=0}^{N-1} c_{k,i} e^{j2\pi f_i (t-\boldsymbol{\tau}-kT)} e^{j2\pi \frac{f_i}{c} md \cos \boldsymbol{\phi}} p(t - \boldsymbol{\tau} - kT) \quad (5.12)$$

A convenient way of writing the vector of the *M* OFDM signals received at the *M* elements of the array

$$\mathbf{y}(t) = [y_0(t), y(t)_1, ..., y(t)_{M-2}, y_{M-1}(t)]^T$$

is on a SC basis. For this purpose, we introduce the array manifold of the ULA systems in the direction ϕ at the frequency f_i

$$\mathbf{a}^i_{ULA}(\phi) = \left[1, e^{j2\pi \frac{f_i}{c} d \cos\phi}, ..., e^{j(M-2)2\pi \frac{f_i}{c} d \cos\phi}, e^{j(M-1)2\pi \frac{f_i}{c} d \cos\phi} \right]^T$$

so as the signal component of the i-*th* SC received at the array element *m*, that we indicate with $r^i_m(t)$, is

$$r^i_m(t) = \alpha \sqrt{\frac{2P_s}{N}} \sum_{k} c_{k,i} e^{j2\pi f_i (t-\tau-kT)} p(t - \tau - kT) e^{j2\pi \frac{f_i}{c} md \cos\phi} = r^i(t) e^{j2\pi \frac{f_i}{c} md \cos\phi}$$

and the vector collecting $r^i_m(t)$ at all sensors

$$\mathbf{r}^i(t) = [r^i_0(t), r^i_1(t), ..., r(t)^i_{M-2}, r^i_{M-1}(t)]^T$$

can be written as

$$\mathbf{r}^i(t) = \alpha \sqrt{\frac{2P_s}{N}} \sum_{k} c_{k,i} e^{j2\pi f_i (t-\tau-kT)} p(t - \tau - kT) \mathbf{a}^i_{ULA}(\phi) = r(t) \mathbf{a}^i_{ULA}(\phi) \quad (5.13)$$

The (noisy) vector $\mathbf{y}(t)$ of the received OFDM signal becomes

$$\mathbf{y}(t) = \sum_{i=0}^{N-1} \mathbf{r}^i(t;\phi) + \mathbf{n}(t) \quad (5.14)$$

In (5.14) we have highlighted the dependency of the vectors $\mathbf{r}^i(t)$ from ϕ and we have introduced the noise vector $\mathbf{n}(t)$.

As seen with narrowband signals, in general, there is a certain number of unknowns to be estimated in the received signal (5.14). The presence of each unknown affects the estimation accuracy of the other unknowns as it is possible to realise by looking at the **FIM**. In the following we focus on the estimation of the DOA ϕ only. The considerations that follow may apply to the other parameters to estimate and however the general view of more unknowns is of straightforward derivation bearing in mind the study of impinging narrowband sources of Section 1.5.

(5.13) shows that, consistently with the narrow band domain, the received vector of the SC i, $\mathbf{r}^i(t)$, carries the DOA information in the antenna steering vector at the frequency f_i of the SC itself as if the individual SC were transmitted separately from the other SCs. In the context of OFDM incident signals, the theorem of Section 5.1 permits the composition of the CRB of DOA of the wideband OFDM signal through the CRBs of the DOA estimations performed over the narrowband SCs.

We now explain how the estimation model of (5.14) fits the one considered in the theorem whose observed signal is given in (5.2). The DOA ϕ is the deterministic parameter to estimate. It spans over the set of waveforms $\left\{\mathbf{r}^i(t;\phi)\right\}_{i=0,\ldots,N-1}$. The time continuous observation space $\mathbf{y}(t)$ in (5.14) actually is a vector form of (5.2). Clearly, the scalar correspondence of (5.2) is with each entry of the vector $\mathbf{y}(t)$. The hypothesis (5.1) has to be put in a vector form and concerns the derivatives of $\left\{\mathbf{r}^i(t;\phi)\right\}_{i=0,\ldots,N-1}$ versus the parameter to estimate. We develop the integral in (5.1) when T_0 is one OFDM symbol time under the hypothesis of perfect timing alignment.

$$\int_{k\mathrm{T}+\boldsymbol{\tau}}^{k\mathrm{T}+\mathrm{T}+\boldsymbol{\tau}} \frac{\partial \mathbf{r}^i(t)^H}{\partial \boldsymbol{\phi}} \frac{\partial \mathbf{r}^l(t)}{\partial \boldsymbol{\phi}} dt \quad = \tag{5.15}$$

$$= |\boldsymbol{\alpha}|^2 c_{k,i}^* c_{k,l} e^{j2\boldsymbol{\pi}(\boldsymbol{\tau}+kT)(f_i-f_l)} \left(\frac{\partial \mathbf{a}^i(\boldsymbol{\phi})}{\partial \boldsymbol{\phi}}\right)^H \frac{\partial \mathbf{a}^l(\boldsymbol{\phi})}{\partial \boldsymbol{\phi}} \int_{k\mathrm{T}+\boldsymbol{\tau}}^{k\mathrm{T}+\mathrm{T}+\boldsymbol{\tau}} e^{j2\boldsymbol{\pi} f_i t} e^{-j2\boldsymbol{\pi} f_l t} dt$$

For any pairs *(i,l)* of distinct sub carriers the orthogonality property of the exponential functions $\left\{e^{j2\pi f_i t}\right\}_{i=0,\ldots,N-1}$ ensures the orthogonality of the derivatives, thus the hypothesis is met. It is easy to verify that the conditions i) and ii) of Section 5.1 are met in deriving (5.15) and that the same applies if the derivatives in (5.15) are calculated versus the other unknown quantities of the vector $\mathbf{u} = [a, \varphi, \phi]^T$. The result of (5.15) is that the estimates of the DOA are uncoupled among the SCs. Thus, they can be composed following a parallel combination to yield the DOA estimation of the broadband signal.

A question now arises on whether the SCs are pilots or modulation SCs. For pilot SCs we have the CRB, for data SCs we have the MCRB. The number of available pilot SCs may vary significantly in real wireless communications systems and two situations are possible. It can be that all the SCs are pilots. This happens for instance during the preamble of the MAC frames that is composed of a few, maybe only one, known OFDM training patterns for the sake of signal synchronization, channel status estimation and antenna weights control operations [34]. Or, as for instance during the payload of the data frame, it can be that only a tiny subset of SCs are pilots. When the pilot SCs are merged in the data SCs one can wonder what is the estimation performance if the observation is limited to the pilot SCs only. So far we have focused on the analysis of the (M)CRB of the OFDM signal by focusing on the continuous time representation of the received signal $\mathbf{y}(t)$. When dealing with the analytic signal $\mathbf{y}(t)$ the separation of the SC would be artificial. But the problem makes sense in real receivers where the SCs are split after down-conversion and FFT demodulation so as an observation sub-space made of pilot SCs becomes available in the form of signal samples which are used for estimation. Thus one can think of shifting to the base band analysis and use the portion of sufficient statistic representing the pilot sub-space. Following the analysis of the narrow band signals, it is easy to realise that the operations of the down-

conversion and FFT demodulation carried out in the OFDM receivers preserve the information that is present in $\mathbf{y}(t)$ and the vector of samples [4]

$$\mathbf{z}[k] = \sum_{i=0}^{N-1} \alpha c_{k,i} \mathbf{a}_{ULA}^{i}(\phi) + \mathbf{n}[k] \tag{5.16}$$

compose a sufficient statistic. In (5.16) $\mathbf{n}[k]$ is a vector of M statistically independent random white Gaussian noise variable with zero mean and variance

$$\frac{2N_0}{2P_s T_{FFT}} = \frac{2N_0}{E_{OFDM}}$$

Where E_{OFDM} is the energy transmitted per OFDM symbol. We are interested into the part of the sum of (5.16) where the index i runs on the pilot SCs. This portion of the sufficient statistic is mapped in the group of pilot SCs of the analytic signal $\mathbf{y}(t)$ that we indicate with $\mathbf{y}^p(t)$. We can now apply the theorem of Section 5.1 to $\mathbf{y}^p(t)$ as if the $\mathbf{y}(t)$ were composed of $\mathbf{y}^p(t)$ only and derive the CRB of the observation sub-space of the noisy pilot samples $\mathbf{z}^p[k]$.

Indicating with N_p the number of pilot SCs and introducing the symbol p to indicate pilot we have that the **FIM** of the pilot portion of the OFDM signal is the sum of the **FIM**s of the pilot SCs

$$\mathbf{FIM}_{OFDM}^{p} = \sum_{i=0}^{N_p-1} \mathbf{FIM}_{SC_i^p} \tag{5.17}$$

With reference to the matrix notation presented in (4.13) and (4.14)

$$CRB(\boldsymbol{\phi})_{OFDM}^{p} = \frac{J_{\boldsymbol{\psi}\boldsymbol{\psi}-OFDM}^{p}}{\det\left(\boldsymbol{\Pi}_{OFDM}^{p}\right)}$$

with

$$J_{\boldsymbol{\psi}\boldsymbol{\psi}-OFDM}^{p} = \sum_{i=0}^{N_p-1} J_{\boldsymbol{\psi}\boldsymbol{\psi}-SC_i^p} = N_p \frac{|\boldsymbol{\alpha}|^2 \left(2P_s T_{FFT}/N\right)}{2N_0} M$$

and

$$\mathbf{\Pi}_{OFDM}^{p}=\sum_{i=0}^{N-1}\mathbf{\Pi}_{SC_i^p}=|\boldsymbol{\alpha}|^2\frac{\left(2P_sT_{FFT}/N\right)}{2N_0}\times$$

$$\times\begin{pmatrix} MN_p & -\dfrac{2\pi d\sin\boldsymbol{\phi}}{c}\dfrac{M(M-1)}{2}\displaystyle\sum_{i=0}^{N_p-1}f_i \\ -\dfrac{2\pi d\sin\boldsymbol{\phi}}{c}\dfrac{M(M-1)}{2}\displaystyle\sum_{i=0}^{N_p-1}f_i & \left(\dfrac{2\pi d\sin\boldsymbol{\phi}}{c}\right)^2\dfrac{M(M-1)(2M-1)}{6}\displaystyle\sum_{i=0}^{N_p-1}f_i^2 \end{pmatrix}$$

where we have highlighted the received SNR per SC

$$SNR_{SC}=|\boldsymbol{\alpha}|^2\frac{\left(2P_sT_{FFT}/N\right)}{2N_0}=\frac{|\boldsymbol{\alpha}|^2}{2}\left(\frac{E_s}{N_0}\right)_{SC}$$

After some manipulations we get the final expression

$$CRB(\boldsymbol{\phi})_{OFDM}^{p}=\frac{MN_p}{\left(\dfrac{2\pi d\sin\boldsymbol{\phi}}{c}\right)^2\left[N_pMQ_2(M)\displaystyle\sum_{i=0}^{N_p-1}f_i^2-Q^2(M)\left(\sum_{i=0}^{N_p-1}f_i\right)^2\right]SNR_{SC}} \tag{5.18}$$

In (5.18) we have used the abbreviations

$$Q(M)=M(M-1)/2$$

and

$$Q_2(M)=M(M-1)(2M-1)/6$$

We note that if $N_p=N$, (5.18) gives the CRB of the DOA estimation on OFDM known symbols.

We now conclude the paragraph with an example of estimation problem, which is close to the one analysed throughout this document, to which the application of the theorem is not possible since the hypothesis of the theorem is not met. Suppose we want to estimate the reference carrier frequency f_0 of the OFDM signal. We repeat the calculation as in (5.15) and differentiate versus f_0.

$$\int_{k\mathrm{T}+\boldsymbol{\tau}}^{k\mathrm{T}+\mathrm{T}+\boldsymbol{\tau}}\frac{\partial\mathbf{r}^i(t)^H}{\partial f_0}\frac{\partial\mathbf{r}^l(t)}{\partial f_0}dt\ \propto\int_{k\mathrm{T}+\boldsymbol{\tau}}^{k\mathrm{T}+\mathrm{T}+\boldsymbol{\tau}}\sum_{m=0}^{M-1}\left[2\pi(t-kT-\boldsymbol{\tau}-\boldsymbol{\tau}_m)\right]^2e^{j2\pi\frac{(l-i)}{T_{FFT}}t}dt$$

We find out that the integral is not zero, and in turn, the cross sum (5.7) is generally not zero meaning that the observations are coupled among the SCs. The difference with the estimation of $\mathbf{u}=[a,\varphi,\phi]^T$ is that when differentiating the exponential function versus f_0

$$\frac{\partial e^{j2\pi f_i t}}{\partial f_0} = e^{j2\pi \frac{i}{T_{FFT}} t} \frac{\partial e^{j2\pi f_0 t}}{\partial f_0} = j2\pi t e^{j2\pi f_i t} = \gamma(t) e^{j2\pi f_i t}$$

one notes that $\gamma(t)$ comes out as a function of time instead of as a constant quantity versus time γ, i.e. the condition ii) highlighted in Section 5.1 is not met.

5.2.1 Numerical Example: IEEE802.15.3c OFDM

As a practical example of DOA estimation of OFDM sources, we consider the IEEE 802.15.3c wireless standard, for which an OFDM signal transmission in the 60 GHz (57-66 GHz) free band with a channel bandwidth from 1 GHz to 5GHz is being considered.

We first verify that the assumption (2.4) is true at the frequencies at stake. With an inter-sensor spacing d of half a wavelength ($\lambda = 5\ mm$) and 10 sensors, the linear size L of a ULA system is

$$L = \frac{(M-1)}{2} \frac{c}{60\ GHz} \simeq 22{,}5\ mm$$

$\max\{\tau_m\}$ is experienced when the wave impinges from $\phi = 0°$ or $\phi = 180°$ and corresponds to the time that the wave front takes to propagate from one end sensor to the other end sensor

$$\max\{\tau_m\} = \frac{L}{c} = \frac{(M-1)}{2} \frac{1}{60\ GHz} \simeq 75 \times 10^{-12}\ s$$

The complex envelope of the OFDM signal can be considered constant during $\max\{\tau_m\}$ if

$$T_{OFDM} \gg \max\{\tau_m\} \tag{5.19}$$

With a channel bandwidth $B = 5\ GHz$ and $N = 256$ SCs the OFDM symbol duration is

$$T_{OFDM} \simeq \frac{1}{2(B/N)} \simeq 2{,}58\times10^{-8}\ s$$

and the approximation (2.4) holds true. Note that (5.19) poses an upper limit to the data rate of OFDM; the maximum signalling rate per single SC can be expressed as

$$(B/N)_{\max} = \frac{1}{20\max\{\tau_m\}} \simeq 667\ Mbaud$$

which is significantly higher than the signalling rate of IEEE 802.15.3c OFDM indeed. .A similar conclusion can be drawn with UCA systems. For UCA systems the constraint on the signalling rate is

$$\max\{\tau_m\} = \frac{2R}{c} = \frac{1}{c}\frac{\lambda/2}{\sqrt{\left(1-\cos\left(\frac{\pi}{10}\right)^2\right)}} \simeq 27\times10^{-12}\,s$$

and (5.19) is verified.

Let us focus on ULA systems and change N_p with N with obvious meaning of the implications. To simplify the expression, we note that $B/f_0 \simeq 0.08 \ll 1$ and make the following approximations in (5.18)

$$\sum_{i=0}^{N-1} f_i \simeq Nf_0 \quad \text{and} \quad \sum_{i=0}^{N-1} f_i^2 \simeq Nf_0^2 \tag{5.20}$$

from which it yields

$$CRB(\boldsymbol{\phi})_{\substack{IEEE802.15.3c\\OFDM}} \simeq \frac{1}{N}\frac{24}{\left(2\pi\frac{f_0}{c}d\sin\boldsymbol{\phi}\right)^2 M(M^2-1)\left(\frac{E_s}{N_0}\right)_{SC}} \tag{5.21}$$

The interpretation of (5.21) is that the (M)CRB of IEEE 802.15.3c OFDM sources decreases linearly with the number of SCs. To be more general, one can refer the DOA (M)CRB to any of the SCs of the OFDM source and for both UCA and ULA systems write

$$CRB(\boldsymbol{\phi})_{\substack{IEEE802.15.3c\\OFDM}} \simeq \frac{1}{N} CRB(\boldsymbol{\phi})_{\substack{IEEE\,802.15.3c\\OFDM-SC_i}} \tag{5.22}$$

In Figures 5.1 we have plotted the square root of (5.22) in the cases of ULA and UCA systems, respectively, by varying the number of pilot SCs N_p that

are present in the OFDM signal. The decrease of the DOA (M)CRB by increasing the signal source bandwidth, although predictable, is

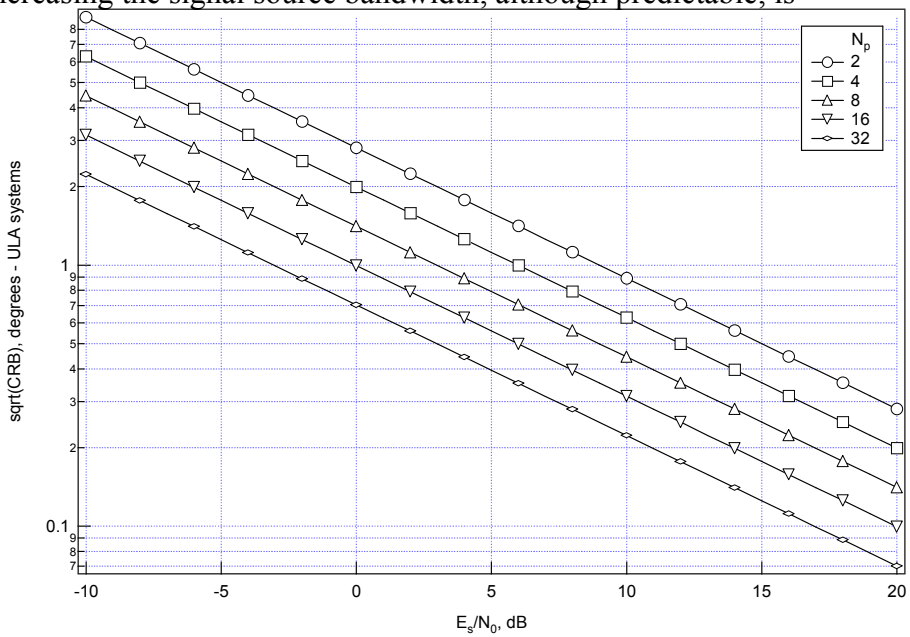

Figure 5. 1a – CRB on DOA of OFDM signals versus N_p , ULA systems with 8 sensors

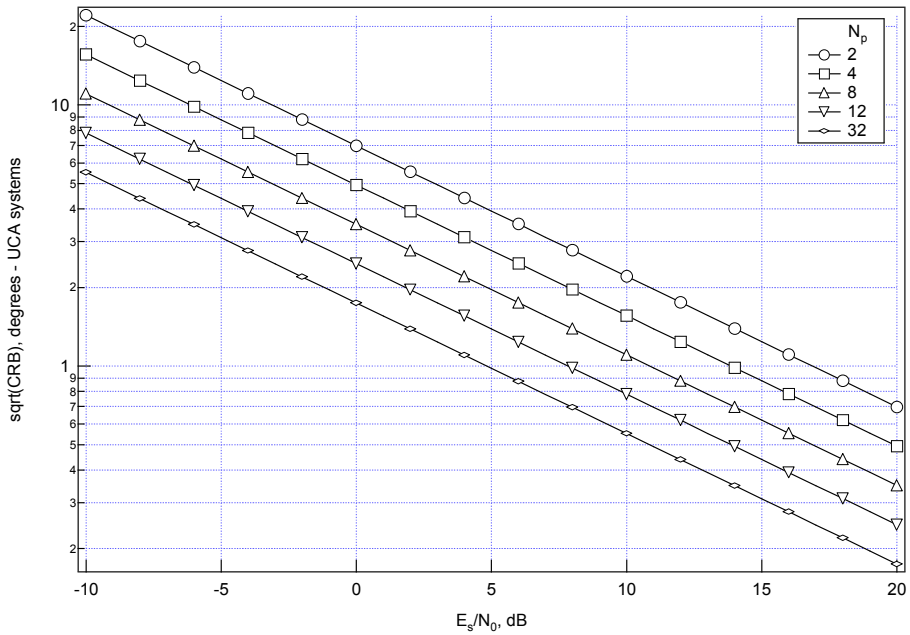

Figure 5.1b – CRB on DOA of OFDM signals versus N_p , UCA systems with 8 sensors

particularly important for UCA systems. ULA systems outperform UCA systems in DOA estimation but the use of more bandwidth determines increased values of estimation accuracy so as, unlike narrowband signals, the performance achieved by UCA systems for broadband applications can be satisfying. For instance, with a reasonable low number of pilot SCs of 8, the standard deviation is slightly above 1° at 10 dB of SNR with 8 sensors. This property together with the isotropic radiation patter make UCA systems worth considering for wideband applications

5.2.2 Comparison between OFDM Signals and Monocarrier Signals

In the previous sections we have approached the CRB for DOA estimation of wideband OFDM signal sources by means of the narrow band array model. The signal bandwidth is an important parameter for the application of such a model. The insight of adopting the narrow band array model stems from the structure of the OFDM signal whose wideband feature is achieved by maintaining a signalling interval T_{OFDM} that is N times lower than the signal interval of the input data stream. Thus, the significant signal bandwidth for the purpose of applying the narrowband DOA estimation model is the subcarrier bandwidth B/N instead of the overall bandwidth B of the OFDM signal. In other words, the narrowband array model can be applied to the OFDM signal if it applicable to its narrowband subcarriers. The advantage of OFDM signals is the independency of the narrow band array model from the overall bandwidth occupied by the signal. This point can be understood by comparing the theory developed for the multicarrier OFDM signal with the analysis of a monocarrier signal having a same bandwidth B . The matter is explained with reference to the numerical example of the *mm*-wave communications at 60 GHz. As seen the CRB for

DOA estimation of OFDM signals performed on N_p pilot subcarriers out of N subcarriers is

$$CRB(\boldsymbol{\phi})_{\substack{IEEE802.15.3c \\ OFDM}} \simeq \frac{1}{N_p} \frac{24}{\left(2\pi \frac{f_0}{c} d \sin \boldsymbol{\phi}\right)^2 M(M-1)^2} \frac{1}{SNR_{SC}} \quad (5.23)$$

where the signal to noise ratio of one subcarrier is

$$SNR_{SC} = \frac{\left(2P_s T_{FFT} / N\right)}{N_0}$$

We want to compare (5.23) with the CRB attainable by observing N_p known symbols out of N symbol intervals of a monocarrier signal source having the same bandwidth B of the OFDM signal. We suppose that the channel is quasi-stationary over N symbol times. The monocarrier signal has the form

$$s(t) = \sqrt{2P_s} \sum_k c_k p\left(t - \frac{T_{FFT}}{N}\right) e^{j2\pi f_0 t} \quad (5.24)$$

The CRB on one symbol time for narrow band single carrier signals is (4.16) that is

$$CRB_{MC}(\phi) = \frac{24}{\left(2\pi \frac{f_0}{c} d \sin \phi\right)^2 M(M^2-1) \frac{E_s}{N_0}}$$

where the energy per symbol E_s is $2P_s \frac{T_{FFT}}{N}$. If the observation time lasts N_p symbols times the CRB becomes

$$CRB_{MC}(\phi) = \frac{1}{N_p} \frac{24}{\left(2\pi \frac{f_0}{c} d \sin \phi\right)^2 M(M^2-1) \frac{2P_s T_{FFT} / N}{N_0}} \quad (5.25)$$

which is identical to (5.23). A difference between the two results however emerges from the analysis of the hypotheses that stay behind (5.23) and (5.25). We repeat here the requirement of the narrow band array model that is

$$\max\{\tau_m\} \ll T \quad (5.26)$$

where T is the symbol time interval. For standard ULA systems and OFDM signals (5.26) can be written as

$$\frac{(M-1)}{2f_o} << T_{FFT} = \frac{N}{2B} \tag{5.27}$$

which, as seen in the previous sections, is largely respected. Under (5.27) we have derived the general expression of the CRB (5.18) which simplifies in (5.23) if

$$\frac{B}{f_0} \ll 1$$

that is true also for large values of B such as 5 GHz at the reference carrier frequency of 60 GHz. On the other hand, the requirement (5.26) for the signal (5.24) is

$$\frac{(M-1)}{2f_o} << \frac{T_{FFT}}{N} = \frac{1}{2B} \tag{5.28}$$

which differs from (5.27) because the symbol time duration of the mono carrier signal (5.24) is *1/N*-th of the OFDM symbol interval T_{FFT}. If f_0 is given as a system parameter one gets the following constraint on the product $(M-1)B$

$$f_0 \gg (M-1)B \tag{5.29}$$

which for OFDM signal is instead

$$f_0 \gg (M-1)\frac{B}{N} \tag{5.30}$$

(5.29) is plotted in Figure 5. 2 with a factor 10 for much greater.

Since the maximum channel bandwidth B decreases with M that increases, the dependency (5.29) and (5.30) between B and M provides an upper limit to either of these quantities when the other is fixed. In our numerical example for instance, with a six sensors array, the narrow band array model is no longer applicable to the wideband mono carrier signals if these have a bandwidth larger than 1.2 GHz. This is an important drawback of the model given the availability of bandwidth in this portion of spectrum. When the signal bandwidth is such that the narrow band array model cannot be used, we have to resort to the more complex wideband array model in which a

tapped-delay line is present on each branch of the array. By contrast, the presence of N in (5.30) ensures that the narrow band array model can be applied to OFDM signals having a bandwidth B larger than 1.2 GHz that are the ones of interest in the 60 GHz bandwidth.

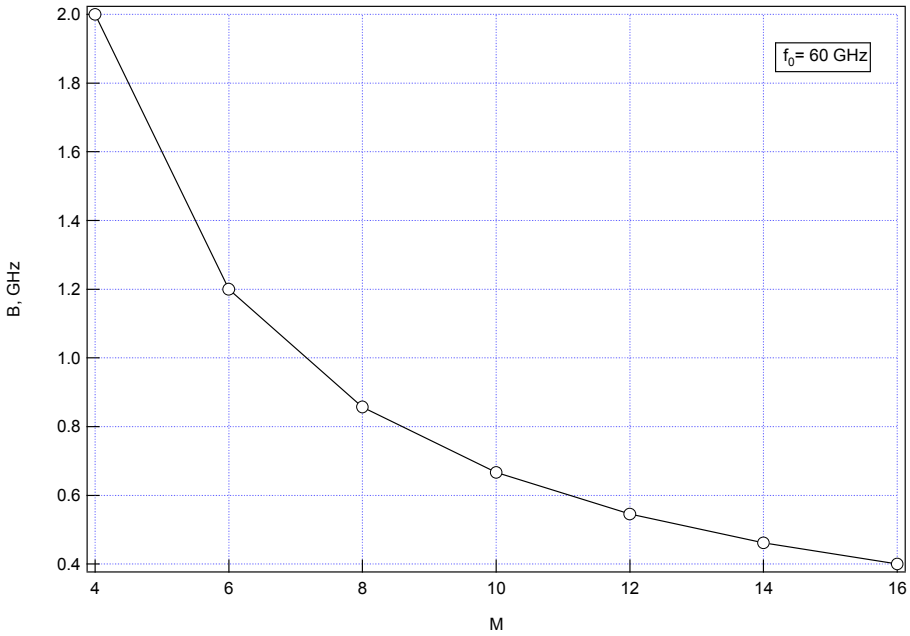

Figure 5. 2 – B versus M for monocarrier signals

5.3 DOA Estimation of OFDM Signals over Frequency Selective Channel

In Section 5.1 the DOA estimation problem has been studied in the case of Gaussian channel. In (5.12) the complex-valued channel frequency response of the narrow band signals

$$\alpha = \rho e^{jb} \tag{5.31}$$

has been applied unchanged to the wideband OFDM signal so that all the SCs undergo the same attenuation and phase shift. The DOA model corresponding to (5.31) is an optical one in the sense that it assumes that only one ray of the source reaches the receiver. The hypothesis is founded especially at the high frequencies of the *mm*-wave WPANs. Actually, this

model can be considered as the schematic of a more accurate description of the channel with LOS where the power of the received signal is spread in angle because of scattered (local and far) replicas, but with a dominant concentration around one particular direction, the one of the LOS. This channel is described by the cluster channel model [2] [35]. In the following we extend the analysis of the CRB for DOA considering this channel characterization as the general case.

Under the assumption of quasi static channel during the transmission of the *k*-th OFDM signal, the received signal from the *m*-tue to thh antenna at the *i*-th tone of the *k*-th OFDM symbol time can be expressed as

$$z_m[k,i] = H[k,i]c_{k,i}e^{j2\pi\frac{f_i}{c}md\cos\phi} + n_m[k,i] \tag{5.32}$$

where $H[k,i]$ denotes the channel frequency response of the sub-channel *i* during the block *k*. With this modelling, $H[k,i]$ is a complex unknown quantity

$$H[k,i] = \left|H[k,i]\right| e^{j\angle H[k,i]}$$

In (5.32) $n_m[k,i]$ is a complex white Gaussian noise sample with zero mean ad variance (5.33). It comes from the white Gaussian noise sample function at the sensor *m*.

$$\sigma_{SC}^2 = \frac{2N_0}{2P_S T_{FFT}/N} \tag{5.33}$$

We assume that the DOA estimation is performed through N_p pilot subcarriers, thus, from this point onward, the index *i* denotes pilot sub-carriers (the constellations symbols $c_{k,i}$ are removed). The samples $z_m[k,i]$ can be grouped per SC to form N_p vectors of size *Mx1* each.

$$\mathbf{z}[k,i] = H[k,i]\mathbf{a}_{ULA}^i(\phi) + \mathbf{n}[k,i], \qquad i = 0,..., N_p - 1$$

from which we form the $MN_p x1$ vector of all the samples $z_m[k,i]$ available

$$\mathbf{z}[k]=\begin{bmatrix}\mathbf{z}[k,0]\\ \vdots\\ \mathbf{z}[k,i]\\ \vdots\\ \mathbf{z}[K,N-1]\end{bmatrix} \tag{5.34}$$

In $\mathbf{z}[k]$ there are $2N_p+1$ unknowns. The tuple of the unknowns $\mathbf{u}$ is composed of N_p amplitudes $|H[k,i]|$ and N_p phases $\angle H[k,i]$ of channel frequency response, and the DOA ϕ. The derivation of the **FIM** can be calculated from (4.10)

$$J_{u_v u_w}=-E_{\mathbf{n}}\left\{\frac{\partial^2 \ln p(\mathbf{z}/\mathbf{u})}{\partial u_v \partial u_w}\right\}$$

To compute the CRB for DOA we consider the $(N_p+1)x(N_p+1)$ block $\mathbf{\Pi}$ of the **FIM** which is related to the unknowns regarding the phases of $\mathbf{u}$ to estimate as highlighted in (4.14). The mathematical details of the computation of the entries of $\mathbf{\Theta}$ are in Appendix B.3. For the sake of compacting the expression of $\mathbf{\Theta}$ we introduce the positions (5.35), (5.36) and (5.37).

$$\Theta_{l,l}=\frac{M\left|H\left[k,N_p-l\right]\right|^2}{\sigma_{SC}^2}, \qquad l=1,...,N_p \tag{5.35}$$

$$\Theta_{N_p+1,l}=\Theta_{l,N_p+1}=-2\pi\frac{f_{N_p-l}}{c}d\sin\phi\frac{M(M-1)}{2}\frac{\left|H\left[k,N_p-l\right]\right|^2}{\sigma_{SC}^2}, \qquad l=1,...,N_p \tag{5.36}$$

$$\Theta_{N_p+1,N_p+1}=\frac{M(M-1)(2M-1)}{6}\sum_{i=0}^{N_p-1}\left(2\pi\frac{f_i}{c}d\sin\phi\right)^2\frac{\left|H\left[k,i\right]\right|^2}{\sigma_{SC}^2} \tag{5.37}$$

The matrix $\mathbf{\Theta}$ is

$$\boldsymbol{\Theta} = \begin{pmatrix} \Theta_{1,1} & 0 & 0 & \cdots & 0 & \Theta_{1,N_p+1} \\ 0 & \Theta_{2,2} & 0 & \cdots & 0 & \Theta_{2,N_p+1} \\ 0 & 0 & \ddots & 0 & \vdots & 0 \\ \vdots & \vdots & 0 & \Theta_{N_p-1,N_p-1} & 0 & \Theta_{N_p-1,N_p+1} \\ 0 & 0 & \cdots & 0 & \Theta_{N_p,N_p} & \Theta_{N_p,N_p+1} \\ \Theta_{N_p+1,1} & \Theta_{N_p+1,2} & \cdots & \Theta_{N_p+1,N_p-1} & \Theta_{N_p+1,N_p} & \Theta_{N_p+1,N_p+1} \end{pmatrix} \tag{5.38}$$

We proceed the analysis with the simplification that $f_i \simeq f_0$ which has been introduced in (5.20) for the proposed OFDM signal format of the IEEE 802.15.3c standard. We want to prove that the CRB for DOA of OFDM signals propagating through frequency selective channel and detected by a linear-phased array is

$$CRB(\boldsymbol{\phi}) \simeq \frac{24}{\left(2\boldsymbol{\pi}\frac{f_0}{c} d \sin\boldsymbol{\phi}\right)^2 M(M^2-1) \sum_{i=0}^{N_p-1} \left(\frac{E_s}{N_0}\right)_{SC_i}} \frac{1}{} \tag{5.39}$$

The SNR of the *i*-th subcarrier in (5.39) is

$$\left(\frac{E_s}{N_0}\right)_{SC_i} = 2\frac{\left|H[k,i]\right|^2}{\boldsymbol{\sigma}_{SC}^2} \tag{5.40}$$

We note that (5.39) generalizes the results of Section 5.2.1 which are valid for signal propagation over AWGN channel. With flat channel frequency response in fact, the SNRs of the SCs are equal to each other because

$$\left|H[k,i]\right|^2 = \boldsymbol{\rho}^2 \qquad i = 0,..,N_p-1$$

and (5.39) coincides with (5.21).

To prove (5.39) we proceed by means of the Principle of Induction. The idea is to demonstrate that (5.39) is valid for a general number of subcarriers. First we state that (5.39) holds true if $N_p = 1$. With one subcarrier only, (5.39) and (4.16) coincide once recognized the correspondence regarding the channel response at the frequency of interest in (5.40) and (4.15),

$$\left|H\left[k,i\right]\right|^2 = \boldsymbol{\rho}^2$$

and the correspondence regarding the signalling interval in (5.33) and (4.9)

$$\frac{T_{FFT}}{N} = T$$

The first step of the Principle of Induction is proved.

We suppose that (5.39) holds true with N_p-1 subcarriers and it remains to demonstrate that it holds true with N_p subcarriers as well. To do this we denote with $\boldsymbol{\Theta}^{N_p-1}$ the matrix $\boldsymbol{\Theta}$ at the step N_p-1 and with $\boldsymbol{\Theta}^{N_p}$ the matrix $\boldsymbol{\Theta}$ at the step N_p. From (5.38) the CRB for DOA at the step N_p is

$$CRB\left(\phi\right)_{\boldsymbol{\Theta}^{N_p}} = \frac{cof\left(\Theta_{N_p+1,N_p+1}\right)}{\det\left(\boldsymbol{\Theta}^{N_p}\right)} \tag{5.41}$$

where $cof\left(\Theta_{N_p+1,N_p+1}\right)$ indicates the cofactor of the element Θ_{N_p+1,N_p+1}.

$$cof\left(\Theta_{N_p+1,N_p+1}\right) = \prod_{l=1}^{N_p}\Theta_{l,l} = \prod_{l=1}^{N_p}\frac{M\left|H\left[k,N_p-l\right]\right|^2}{\sigma_{SC}^2} \tag{5.42}$$

For the determinant of $\boldsymbol{\Theta}^{N_p}$ we have

$$\det\left(\boldsymbol{\Theta}^{N_p}\right) = \Theta_{1,1}\times cof\left(\Theta_{1,1}\right) + \left(-1\right)^{N_p+2}\Theta_{Np+1,1}\times cof\left(\Theta_{Np+1,1}\right) \tag{5.43}$$

The term $cof\left(\Theta_{1,1}\right)$ in (5.43) is tied to the determinant of $\boldsymbol{\Theta}^{N_p-1}$ as

$$cof\left(\Theta_{1,1}\right) = \det\left(\boldsymbol{\Theta}^{N_p-1}\right) + \left(2\pi\frac{f_0}{c}d\sin\phi\right)^2\frac{M\left(M-1\right)\left(2M-1\right)}{6}\frac{\left|H\left[k,N_p-1\right]\right|^2}{\sigma_{SC}^2}\prod_{l=2}^{N_p}\Theta_{l,l} \tag{5.44}$$

while the term $cof\left(\Theta_{Np+1,1}\right)$, as is possible to see by inspection, is

$$cof\left(\Theta_{Np+1,1}\right) = \left(-1\right)^{N_p+1}\Theta_{Np+1,1}\prod_{l=2}^{N_p}\Theta_{l,l} \tag{5.45}$$

By substituting (5.44) and (5.45) in (5.43) one gets

$$\det\left(\boldsymbol{\Theta}^{N_p}\right)=\Theta_{1,1}\det\left(\boldsymbol{\Theta}^{N_p-1}\right)+$$

$$+\left(2\pi\frac{f_0}{c}d\sin\phi\right)^2\frac{M\left(M-1\right)\left(2M-1\right)}{6}\frac{\left|H\left[k,N_p-1\right]\right|^2}{\sigma_{SC}^2}\prod_{l=1}^{N_p}\Theta_{l,l}+$$

$$-\left(\Theta_{Np+1,1}\right)^2\prod_{l=2}^{N_p}\Theta_{l,l}$$

that can be further simplified with the use of

$$\det\left(\boldsymbol{\Theta}^{N_p}\right)=\frac{M\left|H\left[k,N_p-1\right]\right|^2}{\sigma_{SC}^2}\det\left(\boldsymbol{\Theta}^{N_p-1}\right)+$$

$$+\left(2\pi\frac{f_0}{c}d\sin\phi\right)^2\frac{\left|H\left[k,N_p-1\right]\right|^2}{\sigma_{SC}^2}\frac{M\left(M^2-1\right)}{12}\prod_{l=1}^{N_p}\frac{M\left|H\left[k,N_p-l\right]\right|^2}{\sigma_{SC}^2} \tag{5.46}$$

In (5.46) the $\det\left(\boldsymbol{\Theta}^{N_p}\right)$ has been expressed through the $\det\left(\boldsymbol{\Theta}^{N_p-1}\right)$.

By writing (5.41) and (5.42) in the case N_p-1 subcarriers we find the following expression of the $\det\left(\boldsymbol{\Theta}^{N_p-1}\right)$

$$\det\left(\boldsymbol{\Theta}^{N_p-1}\right)=\frac{\prod_{l=2}^{N_p}\frac{M\left|H\left[k,N_p-l\right]\right|^2}{\sigma_{SC}^2}}{CRB\left(\phi\right)_{\boldsymbol{\Theta}^{N_p-1}}} \tag{5.47}$$

where $CRB\left(\phi\right)_{\boldsymbol{\Theta}^{N_p-1}}$ indicates the CRB for DOA at the step N_p-1. By deriving $CRB\left(\phi\right)_{\boldsymbol{\Theta}^{N_p-1}}$ from (5.39), the determinant of $\boldsymbol{\Theta}^{N_p-1}$ becomes

$$\det\left(\boldsymbol{\Theta}^{N_p-1}\right)\simeq\left(2\boldsymbol{\pi}\frac{f_0}{c}d\sin\boldsymbol{\phi}\right)^2\frac{M(M^2-1)}{24}\sum_{i=0}^{N_p-2}\left(\frac{E_s}{N_0}\right)_{SC_i}\prod_{l=2}^{N_p}\frac{M\left|H\left[k,N_p-l\right]\right|^2}{\boldsymbol{\sigma}_{SC}^2} \tag{5.48}$$

Moreover by using (5.40) and rearranging the index of the summation in (5.48) we obtain

$$\det\left(\boldsymbol{\Theta}^{N_p-1}\right) \simeq \left(2\pi \frac{f_0}{c} d \sin\boldsymbol{\phi}\right)^2 \frac{M(M^2-1)}{12} \left(\sum_{l=2}^{N_p} \frac{\left|H\left[k, N_p - l\right]\right|^2}{\boldsymbol{\sigma}_{SC}^2}\right) \prod_{l=2}^{N_p} \frac{M\left|H\left[k, N_p - l\right]\right|^2}{\boldsymbol{\sigma}_{SC}^2} \tag{5.49}$$

We can now substitute the $\det\left(\boldsymbol{\Theta}^{N_p-1}\right)$ given (5.49) in (5.46) and get

$$\det\left(\boldsymbol{\Theta}^{N_p}\right) \simeq \left(2\pi \frac{f_0}{c} d \sin\boldsymbol{\phi}\right)^2 \frac{M(M^2-1)}{12} \left(\sum_{l=1}^{N_p} \frac{\left|H\left[k, N_p - l\right]\right|^2}{\boldsymbol{\sigma}_{SC}^2}\right) \prod_{l=1}^{N_p} \frac{M\left|H\left[k, N_p - l\right]\right|^2}{\boldsymbol{\sigma}_{SC}^2} \tag{5.50}$$

From (5.50) and (5.42) the CRB for DOA at the step N_p is $CRB(\phi)_{\boldsymbol{\Theta}^{N_p}}$ of (5.41) becomes

$$CRB(\phi)_{\boldsymbol{\Theta}^{N_p}} \simeq \frac{1}{\left(2\pi \frac{f_0}{c} d \sin\phi\right)^2 \frac{M(M^2-1)}{12} \left(\sum_{l=1}^{N_p} \frac{\left|H\left[k, N_p - l\right]\right|^2}{\sigma_{SC}^2}\right)}$$

that becomes identical to (5.39) by using (5.40) and re-indexing the summation from l=1,..,N_p to i=0,...,N_p-1. This concludes the proof.

5.4 Comparison of the CRB for DOA with the Simulation Analysis Results

With the simulation analysis of the IEEE 802.15.3c MAC phased-array controller throughput of Section 3, we have gained insight into the impact of the array controller performance onto the network throughput performance. The quantity that we have chosen to represent the array controller performance is the standard deviation of the simulated Gaussian DOA estimator used by the array system to perform beamforming. We have then investigated how the throughput of the wireless links of WPNAs adopting IEEE 802.15.3c MAC is affected by the this second order statistics if ULA or UCA systems are employed for narrow beam communication. In

particular, we have pinpointed the turning values of the standard deviation at which the drop of the throughput due to misponting is less than 5% of the error free channel capacity.

We are now able to relate the information about the standard deviation of the simulated DOA estimator with the theoretical information represented by the CRB for DOA in order to understand whether the design of the IEEE 802.15.3 c MAC phased array controller throughput based on DOA estimation is feasible or not. For this purpose, let us consider Figure 5. 1a and Figure 5. 1b that plot the CRB (sqrt(CRB) in degrees) on DOA for a 8-element ULA and a 8-element UCA, respectively. For ULA systems we can see that already 2 pilot symbols are enough to meet the requirement of $\sigma_G = 2.8°$ .We remind however that Figure 5. 1a refers to a broadside standard ULA while the CRB degrades close to end-fire. For instance, from Figure 4. 3 one sees that with 12 sensors in the array the number of pilots needed to achieve a CRB less than 3° when the DOA to estimate is 5°, is at least 10 at 0 dB and 3 at 10dB. For UCA systems the CRB is isotropic with the DOA. As is seen, 4 pilots ensure a CRB below 5.5° at 0 dB SNR. At 10 dB the goal is achieved with 2 pilots.

The analysis can be repeated in the case of more directive arrays. As seen, the requirements on σ_G become stricter when increasing the array size. At the same time however, the performance achievable by the DOA estimators is expected to improve as the CRB decreases when increasing the number of elements in the array. In general, we can state that 12-16 pilot SCs ensure negligible throughput losses due to mispointnig, It is a reasonable number for the OFDM format of the 60 GHz WPANs.

Table 5. 1 reports some details of one IEEE 802.15.3c OFDM proposal.

- 256 point FFT
- 216 Data carriers, 16 pilot carriers, 24 NULL
- Channel Bandwidth = 750MHz
- Symbol Time = 384ns
- Guard Interval = 1/8 Symbol Time= 48ns

Table 5. 1- OFDM system parameters of 802.15.3c proposal

Data Rate (Mbit/s)	Modulation	Coding Rate	Coded bits per subcarrier (Nbpsc)	Coded bits per OFDM symbol (Ncbps)	Data bits per OFDM symbol (Ndbps)
281	BPSK	1/2	1	216	108
421	BPSK	3/4	1	216	162
562	QPSK	1/2	2	432	216
843	QPSK	3/4	2	432	324
1,125	16-QAM	1/2	4	864	432
1.687	16-QAM	3/4	4	864	648
2,250	64-QAM	2/3	6	1296	864
2.531	64-QAM	5/6	6	1296	972

For comparison sake, we have reported in Table 5. 2 the parallel details of the 802.11a PHY

- 52 point FFT
- 48 Data carriers, 4 pilot carriers
- Channel Bandwidth = 20 MHz
- Symbol Time (BPSK) = 4 μs
- Guard Interval = 0.8 μs

Table 5. 2- OFDM system parameters of 802.11a

Data Rate (Mbit/s)	Modulation	Coding Rate	Coded bits per subcarrier (Nbpsc)	Coded bits per OFDM symbol (Ncbps)	Data bits per OFDM symbol (Ndbps)
6	BPSK	1/2	1	48	24
9	BPSK	3/4	1	48	36
12	QPSK	1/2	2	96	48
18	QPSK	3/4	2	96	72
24	16-QAM	1/2	4	192	96
36	16-QAM	3/4	4	192	144
48	64-QAM	2/3	6	288	192
54	64-QAM	3/4	6	288	216

Conclusions and Developments

In this work we have studied the use of adaptive array systems in 60 GHz UWB-OFDM Personal Area Network Transceivers. The study has been conducted by simulations and theoretical analysis. Two sensor arrangements have been considered, ULA and UCA.

We have designed and implemented into the network simulators ns-2 a IEEE 802.15.3c MAC array-phased controller throughput that makes use of a DOA estimator. Simulations have been run to assess the impact of the array controller performance onto the achievable throughput of the wireless link. Requirements about the standard deviation of the DOA estimator have been drawn.

On the other hand, we have found the CRB for DOA estimation of impinging 60 GHz OFDM sources in the simple case of the LOS scenario.

By comparing the DOA estimation requirements obtained by simulation against the CRB on DOA we can state that the use of adaptive antennas is possible. The requirements can be fulfilled with 12-16 pilot subcarriers starting from a SNR of 0 dB. This is true for the most common configurations of the antenna directivity for both ULA and UCA.

Another indication of our study is that UCA systems may gain new consideration in wideband applications. ULA systems have the two drawbacks, the end-fire and the DOA-dependent estimation performance. By contrast UCA systems exhibit the favourable feature of isotropic DOA estimation. Their CRB on DOA is generally worse than ULA. For single carrier applications their performance may be not enough.

For wideband applications instead, at the cost of a signal overhead of the same order of the ones typically already in use for estimating other quantities of the received signal, their DOA estimation performance grows and becomes sufficient.

The developments of our analysis may go in many directions. Some could be the study of the behaviour of directional transceivers in no-LOS and obstructed-LOS scenarios, the system analysis with the inclusion of interference as this could be present and captured by either the main lobe or the sidelobes of the array pattern, and the design of Spatial Division Multiple Access (SDMA) techniques to increase the system capacity.

Appendix A: Analytic White Gaussian Noise

In this appendix we characterize the analytic white Gaussian noise. It is a complex white noise process

$$n(t) = n_R(t) + jn_I(t)$$

whose imaginary component $n_I(t)$ can be thought as obtained by filtering the real noise process $n_R(t)$ through a Hilbert filter

$$n_I(t) = n_R(t) \otimes h_H(t) \tag{6.1}$$

where $h_H(t)$ denotes the Hilbert impulse response

$$h_H(t) = \frac{1}{\pi t}$$

The frequency response of the Hilbert filter is

$$H_H(f) = -j\,\mathrm{sgn}(f)$$

where $\mathrm{sgn}(x)$ is the well known sign function. The PSD of $S_{n_R}(f)$ of $n_R(t)$ is flat and equal to $N_0/2$ over the bandwidth of the modulated signal with a carrier frequency f_0 as shown in Figure a. 1.

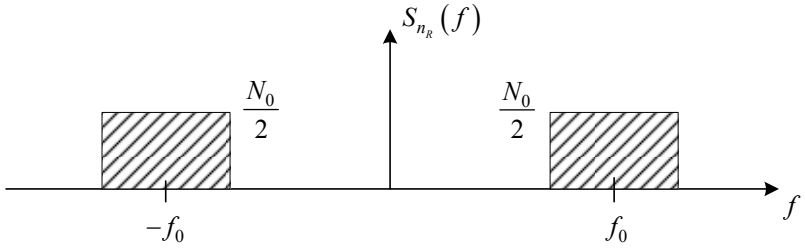

Figure a. 1 PSD of $n_R(t)$

The PSD of $n_I(t)$ is

$$S_{n_I}(f) = S_{n_R}(f)\left|H_H(f)\right|^2 = S_{n_R}(f) \tag{6.2}$$

The PSD of the analytic process $n(t)$ is made up of $S_{n_R}(f)$ and $S_{n_I}(f)$ and of the cross PSDs between $n_R(t)$ and $n_I(t)$ that we have indicated with $S_{n_R n_I}(f)$ and $S_{n_I n_R}(f)$. The autocorrelation function of $n(t)$ is

$$R(\tau) = E\left\{n(t+\tau)n^*(t)\right\}$$

With the use of (6.1), it can be decomposed into the autocorrelation functions involving $n_R(t)$ and $n_I(t)$ as follows

$$R(\tau) = R_{n_R}(\tau) + R_{n_I}(\tau) + j[R_{n_I n_R}(\tau) - R_{n_R n_I}(\tau)] \tag{6.3}$$

The autocorrelation functions introduced in (6.3) are defined as

$$R_{n_R}(\tau) = E\left\{n_R(t+\tau)n_R^*(t)\right\} \tag{6.4}$$

$$R_{n_I}(\tau) = E\left\{n_I(t+\tau)n_I^*(t)\right\}$$

$$R_{n_I n_R}(\tau) = E\left\{n_I(t+\tau)n_R^*(t)\right\}$$

$$R_{n_R n_I}(\tau) = E\left\{n_R(t+\tau)n_I^*(t)\right\}$$

We now show how $R_{n_I}(\tau)$, $R_{n_I n_R}(\tau)$ and $R_{n_R n_I}(\tau)$ can be expressed in terms of the autocorrelation function of $n_R(t)$ (6.4). From (6.2) we have

$$R_{n_I}(\tau) = \mathcal{F}^{-1}\left\{S_{n_I}(f)\right\} = \mathcal{F}^{-1}\left\{S_{n_R}(f)\right\} = R_{n_R}(\tau)$$

where the notation $\mathcal{F}^{-1}\{\bullet\}$ represents the inverse Fourier transform. Moreover, as for the cross autocorrelation functions we have

$$R_{n_I n_R}(\tau) = E\left\{\left[\int_{-\infty}^{\infty} n_R(t+\tau-\alpha)h_H(\alpha)d\alpha\right] n_R(t)\right\}$$

$$= \int_{-\infty}^{\infty} E\left\{n_R(t+\tau-\alpha)n_R(t)\right\}h_H(\alpha)d\alpha =$$

$$= \int_{-\infty}^{\infty} R_{n_R}(\tau-\alpha)h_H(\alpha)d\alpha = R_{n_R}(\tau) \otimes h_H(\tau)$$

and

$$R_{n_R n_I}(\tau) = E\left\{n_R(t+\tau)\int_{-\infty}^{\infty} n_R(t-\alpha)h_H(\alpha)d\alpha\right\} =$$

$$= \int_{-\infty}^{\infty} E\{n_R(t+\tau)n_R(t-\alpha)\}h_H(\alpha)d\alpha = \int_{-\infty}^{\infty} R_{n_R}(\tau+\alpha)h_H(\alpha)d\alpha$$

$$= R_{n_R}(-\tau) \otimes h_H(-\tau) = -R_{n_R}(\tau) \otimes h_H(\tau) = -R_{n_I n_R}(\tau)$$

where we have used the properties that $R_{n_R}(\tau)$ is an even function whereas $h_H(\tau)$ is an odd function. Thus, $R(\tau)$ becomes

$$R(\tau) = 2\left[R_{n_R}(\tau) + jR_{n_R}(\tau) \otimes h_H(\tau) \right]$$

from which we get the PSD of $n(t)$ that is depicted in Figure a. 2.

$$S_n(f) = 2\left[1 + \mathrm{sgn}(f)\right] S_{n_R}(f)$$

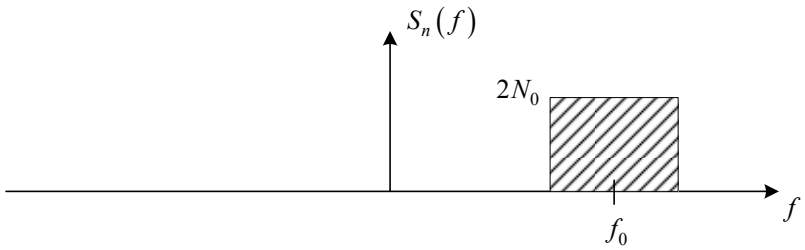

Figure a. 2 - PSD of the analytic white Gaussian noise process $n(t)$

Appendix B: FIM Computation

B.1 Derivation of the FIM *from the sufficient statistic z of narrow band signals*

In the following we show the mathematical derivation of the **FIM** (4.13) from the sufficient statistic (4.8). We used the log likelihood function (4.12)

$$\Delta(\mathbf{z}/\mathbf{u}) = -\frac{1}{2\sigma^2}\left(\mathbf{z}[k] - \rho e^{j\psi}\mathbf{a}(\phi)\right)^H \left(\mathbf{z}[k] - \rho e^{j\psi}\mathbf{a}(\phi)\right)$$

and derive any entries of the **FIM** (4.6) through the definition of entry (4.10). It is useful to recall a few identities that are recurrent in the computation:

$$\mathbf{a}(\phi)^H \mathbf{a}(\phi) = M \tag{7.1}$$

$$E_{\mathbf{n}}\left\{\mathbf{z}[k] - \rho e^{j\psi}\mathbf{a}(\phi)\right\} = 0 \tag{7.2}$$

Moreover, indicating with $\dot{\mathbf{a}}(\phi)$ the derivative vector of $\mathbf{a}(\phi)$ versus the DOA ϕ

$$\dot{\mathbf{a}}(\phi) \triangleq \frac{\partial \mathbf{a}(\phi)}{\partial \phi}$$

for ULA systems we have:

$$\mathbf{a}_{ULA}(\phi)^H \dot{\mathbf{a}}_{ULA}(\phi) = -j\sum_{m=0}^{M-1} 2\pi \frac{f_c}{c} md \sin\phi = -j2\pi \frac{f_c}{c} d \sin\phi \frac{M(M-1)}{2} \tag{7.3}$$

$$\begin{aligned} \dot{\mathbf{a}}_{ULA}(\phi)^H \dot{\mathbf{a}}_{ULA}(\phi) &= \sum_{m=0}^{M-1}\left(2\pi \frac{f_c}{c} md \sin\phi\right)^2 = \\ &= \left(2\pi \frac{f_c}{c} d \sin\phi\right)^2 \frac{M(M-1)(2M-1)}{6} \end{aligned} \tag{7.4}$$

whereas for UCA systems we have:

$$\mathbf{a}_{UCA}(\phi)^H \dot{\mathbf{a}}_{UCA}(\phi) = \left[-\sin\phi \sum_{m=0}^{M-1} \cos\phi_m + \cos\theta \sum_{m=0}^{M-1} \sin\phi_m\right] \frac{2\pi R}{\lambda} = 0 \tag{7.5}$$

$$\begin{aligned} \dot{\mathbf{a}}_{UCA}(\phi)^H \dot{\mathbf{a}}_{UCA}(\phi) &= \left(\frac{2\pi R}{\lambda}\right)^2 \sum_{m=0}^{M-1} \left(-\sin\phi\cos\phi_m + \cos\phi\sin\phi_m\right)^2 = \\ &= \left(\frac{2\pi R}{\lambda}\right)^2 \sum_{m=0}^{M-1} \cos\phi_m{}^2 = \left(\frac{2\pi}{\lambda}\right)^2 \sum_{m=0}^{M-1} \sin\phi_m{}^2 \end{aligned} \tag{7.6}$$

In (7.6) we have used the simplifications ($M > 2$):

$$\sum_{m=0}^{M-1} \cos\phi_m{}^2 = \sum_{m=0}^{M-1} \sin\phi_m{}^2$$

and

$$\sum_{m=0}^{M-1} \cos\phi_m \sin\phi_m = 0$$

- $J_{\rho\rho}$:

$$\frac{\partial \Delta(\mathbf{z}/\mathbf{u})}{\partial \rho} = \frac{1}{2\sigma^2}\left\{\left(e^{j\psi}\mathbf{a}(\phi)\right)^H \left(\mathbf{z}[k] - \rho e^{j\psi}\mathbf{a}(\phi)\right) + \right.$$

$$\left. + \left(z[k] - \rho e^{j\psi} a(\phi)\right)^H \left(e^{j\psi} a(\phi)\right)\right\} =$$

$$= \frac{1}{\sigma^2}\mathrm{Re}\left\{\left(e^{j\psi} a(\phi)\right)^H \left(z[k] - \rho e^{j\psi} a(\phi)\right)\right\}$$

$$\frac{\partial^2 \Delta(\mathbf{z}/\mathbf{u})}{\partial^2 \rho} = \frac{1}{\sigma^2}\mathrm{Re}\left\{\left(e^{j\psi}\mathbf{a}(\phi)\right)^H \left(-e^{j\psi}\mathbf{a}(\phi)\right)\right\} = -\frac{M}{\sigma^2}$$

Thus,

ULA and UCA: $$J_{\rho\rho} = -E_{\mathbf{n}}\left\{\frac{\partial^2 \Delta(\mathbf{z}/\mathbf{u})}{\partial^2 \rho}\right\} = \frac{M}{\sigma^2}$$

- $J_{\rho\psi} = J_{\psi\rho}$:

$$\frac{\partial}{\partial \psi}\frac{\partial \Delta(\mathbf{z}/\mathbf{u})}{\partial \rho} = \frac{1}{\sigma^2}\mathrm{Re}\left\{\left(je^{j\psi}\mathbf{a}(\phi)\right)^H \left(\mathbf{z}[k] - \rho e^{j\psi}\mathbf{a}(\phi)\right) + \right.$$

$$\left. + \left(e^{j\psi}\mathbf{a}(\phi)\right)^H \left(-j\rho e^{j\psi}\mathbf{a}(\phi)\right)\right\}$$

From (7.1) and (7.2) one gets

ULA and UCA: $$J_{\rho\psi} = -E_{\mathbf{n}}\left\{\frac{\partial}{\partial \psi}\frac{\partial \Delta(\mathbf{z}/\mathbf{u})}{\partial \rho}\right\} = 0$$

- $J_{\rho\phi} = J_{\phi\rho}$:

$$\frac{\partial}{\partial \phi}\frac{\partial \Delta(\mathbf{z}/\mathbf{u})}{\partial \rho} = \frac{1}{\sigma^2}\mathrm{Re}\left\{\left(e^{j\psi}\dot{\mathbf{a}}(\phi)\right)^H\left(\mathbf{z}[k]-\rho e^{j\psi}\mathbf{a}(\phi)\right)+\right.$$

$$\left.+\left(e^{j\psi}\mathbf{a}(\phi)\right)^H\left(\rho e^{j\psi}\dot{\mathbf{a}}(\phi)\right)\right\}$$

From (7.2) and (7.3) for ULA systems and from (7.2) and (7.5) one gets

ULA and UCA: $J_{\rho\phi} = -E_{\mathbf{n}}\left\{\frac{\partial}{\partial \phi}\frac{\partial \Delta(\mathbf{z}/\mathbf{u})}{\partial \rho}\right\} = 0$

- $J_{\psi\phi} = J_{\phi\psi}$:

$$\frac{\partial}{\partial \phi}\frac{\partial \Delta(\mathbf{z}/\mathbf{u})}{\partial \psi} = \frac{1}{\sigma^2}\mathrm{Re}\left\{\left(j\rho e^{j\psi}\dot{\mathbf{a}}(\phi)\right)^H\left(\mathbf{z}[k]-\rho e^{j\psi}\mathbf{a}(\phi)\right)+\right.$$

$$\left.+\left(j\rho e^{j\psi}\mathbf{a}(\phi)\right)^H\left(-\rho e^{j\psi}\dot{\mathbf{a}}(\phi)\right)\right\}$$

from (7.2) and (7.3) one gets

ULA: $J_{\psi\phi} = -E_{\mathbf{n}}\left\{\frac{\partial}{\partial \phi}\frac{\partial \Delta(\mathbf{z}/\mathbf{u})}{\partial \psi}\right\} = -2\pi\frac{f_c}{c}d\sin\phi\frac{M(M-1)}{2}\frac{\rho^2}{\sigma^2}$

and from (7.2) and (7.5) it yields

UCA: $J_{\psi\phi} = -E_{\mathbf{n}}\left\{\frac{\partial}{\partial \phi}\frac{\partial \Delta(\mathbf{z}/\mathbf{u})}{\partial \psi}\right\} = 0$

- $J_{\psi\psi}$:

$$\frac{\partial \Delta(\mathbf{z}/\mathbf{u})}{\partial \psi} = \frac{1}{2\sigma^2}\left\{\left(j\rho e^{j\psi}\mathbf{a}(\phi)\right)^H\left(\mathbf{z}[k]-\rho e^{j\psi}\mathbf{a}(\phi)\right)+\right.$$

$$\left.+\left(\mathbf{z}[k]-\rho e^{j\psi}\mathbf{a}(\phi)\right)^H\left(j\rho e^{j\psi}\mathbf{a}(\phi)\right)\right\}=$$

$$=\frac{1}{\sigma^2}\mathrm{Re}\left\{\left(j\rho e^{j\psi}\mathbf{a}(\phi)\right)^H\left(\mathbf{z}[k]-\rho e^{j\psi}\mathbf{a}(\phi)\right)\right\}$$

$$\frac{\partial^2 \Delta(\mathbf{z}/\mathbf{u})}{\partial^2 \psi} = \frac{1}{\sigma^2}\mathrm{Re}\left\{\left(-\rho e^{j\psi}\mathbf{a}(\phi)\right)^H\left(\mathbf{z}[k]-\rho e^{j\psi}\mathbf{a}(\phi)\right)+\right.$$

$$\left.+\left(j\rho e^{j\psi}\mathbf{a}(\phi)\right)^H\left(-j\rho e^{j\psi}\mathbf{a}(\phi)\right)\right\}$$

From (7.1) and (7.2) one gets

ULA and UCA: $$J_{\psi\psi} = -E_{\mathbf{n}}\left\{\frac{\partial^2 \Delta(\mathbf{z}/\mathbf{u})}{\partial^2 \psi}\right\} = M\frac{\rho^2}{\sigma^2}$$

- $J_{\phi\phi}$:

$$\frac{\partial \Delta(\mathbf{z}/\mathbf{u})}{\partial \phi} = \frac{1}{2\sigma^2}\left\{\left(\rho e^{j\psi}\dot{\mathbf{a}}(\phi)\right)^H\left(\mathbf{z}[k]-\rho e^{j\psi}\mathbf{a}(\phi)\right)+\right.$$

$$\left.+\left(\mathbf{z}[k]-\rho e^{j\psi}\mathbf{a}(\phi)\right)^H\left(\rho e^{j\psi}\dot{\mathbf{a}}(\phi)\right)\right\}=$$

$$=\frac{1}{\sigma^2}\mathrm{Re}\left\{\left(\rho e^{j\psi}\dot{\mathbf{a}}(\phi)\right)^H\left(\mathbf{z}[k]-\rho e^{j\psi}\mathbf{a}(\phi)\right)\right\}$$

$$\frac{\partial^2 \Delta(\mathbf{z}/\mathbf{u})}{\partial^2 \phi} = \frac{1}{\sigma^2} \mathrm{Re}\left\{ \left(\rho e^{j\psi} \ddot{\mathbf{a}}(\phi) \right)^H \left(\mathbf{z}[k] - \rho e^{j\psi} \mathbf{a}(\phi) \right) + \right.$$

$$\left. + \left(\rho e^{j\psi} \dot{\mathbf{a}}(\phi) \right)^H \left(-\rho e^{j\psi} \dot{\mathbf{a}}(\phi) \right) \right\}$$

where $\ddot{\mathbf{a}}(\phi)$ is defined as

$$\ddot{\mathbf{a}}(\phi) \triangleq \frac{\partial \mathbf{a}(\phi)}{\partial \phi}$$

Form (7.2) and (7.4) one gets
ULA:

$$J_{\phi\phi} = -E_{\mathbf{n}} \left\{ \frac{\partial^2 \Delta(\mathbf{z}/\mathbf{u})}{\partial^2 \phi} \right\} = \left(2\pi \frac{f_c}{c} d \sin\phi \right)^2 \frac{M(M-1)(2M-1)}{6} \frac{\rho^2}{\sigma^2}$$

and from (7.2) and (7.6) for UCA Systems it yields
UCA:

$$J_{\phi\phi} = -E_{\mathbf{n}} \left\{ \frac{\partial^2 \Delta(\mathbf{z}/\mathbf{u})}{\partial^2 \phi} \right\} = \left(\frac{2\pi R}{\lambda} \right)^2 \frac{\rho^2}{\sigma^2} \sum_{m=0}^{M-1} \cos\phi_m{}^2 = \left(\frac{2\pi R}{\lambda} \right)^2 \frac{\rho^2}{\sigma^2} \sum_{m=0}^{M-1} \sin\phi_m{}^2$$

B.2 Derivation of the **FIM** *from the analytic signal y(t) of narrow band signals*

The likelihood function to consider when the analysis is conducted with the analytic signal $\mathbf{y}(t)$ is

$$L(\mathbf{u}) = \exp\left\{ -\frac{1}{2\sigma^2} \int_{T_0} \left| \mathbf{y}(t) - E\{\mathbf{y}(t)\} \right|^2 dt \right\} =$$

$$= \exp\left\{ -\frac{1}{4N_0} \int_{T_0} \left| \mathbf{y}(t) - r(t)\mathbf{a}(\boldsymbol{\phi}) \right|^2 dt \right\}$$

and the entry of the **FIM** is

$$J_{u_v u_w} = -E_{\mathbf{y}} \left\{ \frac{\partial^2 \ln L(\mathbf{u})}{\partial u_v \partial u_w} \right\} = \frac{1}{4N_0} \int_{T_0} E_{\mathbf{y}} \left\{ \frac{\partial^2}{\partial u_v \partial u_w} \left| \mathbf{y}(t) - r(t)\mathbf{a}(\phi) \right|^2 \right\}$$

thus

$$\frac{\partial \left|\mathbf{y}(t)-r(t)\mathbf{a}(\phi)\right|^2}{\partial u_v}=\left[-\frac{\partial r(t)\mathbf{a}(\phi)}{\partial u_v}\right]^H\left[\mathbf{y}(t)-r(t)\mathbf{a}(\phi)\right]+$$

$$+\left[\mathbf{y}(t)-r(t)\mathbf{a}(\phi)\right]^H\left[-\frac{\partial r(t)\mathbf{a}(\phi)}{\partial u_v}\right]$$

and

$$\frac{\partial^2 \left|\mathbf{y}(t)-r(t)\mathbf{a}(\phi)\right|^2}{\partial u_w \partial u_v}=\left[-\frac{\partial^2 r(t)\mathbf{a}(\phi)}{\partial u_w \partial u_v}\right]^H\left[\mathbf{y}(t)-r(t)\mathbf{a}(\phi)\right]+$$

$$+\left[-\frac{\partial r(t)\mathbf{a}(\phi)}{\partial u_v}\right]^H\left[-\frac{\partial r(t)\mathbf{a}(\phi)}{\partial u_w}\right]+\left[-\frac{\partial r(t)\mathbf{a}(\phi)}{\partial u_w}\right]^H\left[-\frac{\partial r(t)\mathbf{a}(\phi)}{\partial u_v}\right]+$$

$$+\left[\mathbf{y}(t)-r(t)\mathbf{a}(\phi)\right]^H\left[-\frac{\partial^2 r(t)\mathbf{a}(\phi)}{\partial u_v \partial u_w}\right]$$

When computing the stochastic expectation, we note that

$$E_{\mathbf{y}}\left\{\mathbf{y}(t)-r(t)\mathbf{a}(\phi)\right\}=0$$

and obtain

$$J_{u_v u_w}=\frac{1}{2N_0}\int_{T_0}\mathrm{Re}\left\{\left[\frac{\partial r(t)\mathbf{a}(\phi)}{\partial u_w}\right]^H\frac{\partial r(t)\mathbf{a}(\phi)}{\partial u_v}\right\}dt$$

which for diagonal elements gives

$$J_{u_v u_v}=\frac{1}{2N_0}\int_{T_0}\left|\frac{\partial r(t)\mathbf{a}(\phi)}{\partial u_v}\right|^2 dt$$

We proceed with ULA systems and omit the development of the framework for UCA systems.

- $J_{\rho\rho}$:

$$\frac{\partial r(t)\mathbf{a}(\phi)}{\partial \rho}=e^{j\psi}\sqrt{2P_s}\sum_k c_k g_T(t-kT-\tau)e^{j2\pi f_c t}\mathbf{a}(\phi)$$

$$\left|\frac{\partial r(t)\mathbf{a}(\phi)}{\partial \rho}\right|^2 = 2P_s \sum_k c_k^* g_T(t-kT-\tau) \sum_h c_h g_T(t-hT-\tau)\mathbf{a}(\phi)^H \mathbf{a}(\phi) =$$

$$= 2P_s M \sum_k |c_k|^2 g_T^2(t-kT-\tau)$$

$$J_{\rho\rho} = \frac{1}{2N_0} \int_{kT+\tau}^{kT+T+\tau} 2P_s M \sum_k |c_k|^2 g_T^2(t-kT-\tau)dt = M \frac{2P_s T}{2N_0} = \frac{M}{\sigma^2}$$

- $J_{\rho\psi} = J_{\psi\rho}$:

$$\left[\frac{\partial r(t)\mathbf{a}(\phi)}{\partial \rho}\right]^H \frac{\partial r(t)\mathbf{a}(\phi)}{\partial \psi} =$$

$$= j2P_s \rho \sum_k c_k^* g_T(t-kT-\tau) \sum_h c_h g_T(t-hT-\tau)\mathbf{a}(\phi)^H \mathbf{a}(\phi) =$$

$$= j2P_s M \rho \sum_k |c_k|^2 g_T^2(t-kT-\tau)$$

$$J_{\rho\psi} = \frac{1}{2N_0} \int_{kT+\tau}^{kT+T+\tau} \mathrm{Re}\left\{ j2P_s \rho M \sum_k |c_k|^2 g_T^2(t-kT-\tau) \right\} dt = 0$$

- $J_{\rho\phi} = J_{\phi\rho}$:

$$\left[\frac{\partial r(t)\mathbf{a}(\phi)}{\partial \rho}\right]^H \frac{\partial r(t)\mathbf{a}(\phi)}{\partial \phi} =$$

$$= 2P_s \rho \sum_k c_k^* g_T(t-kT-\tau) \sum_h c_h g_T(t-hT-\tau)\mathbf{a}(\phi)^H \dot{\mathbf{a}}(\phi) =$$

$$= 2P_s\rho\sum_k |c_k|^2 g_T^2(t-kT-\tau)\left[-j2\pi\frac{f_c}{c}d\sin\phi\frac{M(M-1)}{2}\right]$$

$$J_{\rho\phi} = \int_{kT+\tau}^{kT+T+\tau} \mathrm{Re}\left\{2P_s\rho\sum_k |c_k|^2 g_T^2(t-kT-\tau)\right.$$

$$\left.\left[-j2\pi\frac{f_c}{c}d\sin\phi\frac{M(M-1)}{2}\right]\right\}dt = 0$$

- $J_{\psi\psi}$:

$$\frac{\partial r(t)\mathbf{a}(\phi)}{\partial\psi} = j\rho e^{j\psi}\sqrt{2P_s}\sum_k c_k g_T(t-kT-\tau)e^{j2\pi f_c t}\mathbf{a}(\phi)$$

$$\left|\frac{\partial r(t)\mathbf{a}(\phi)}{\partial\psi}\right|^2 = 2P_s\rho^2\sum_k c_k^* g_T(t-kT-\tau)\sum_h c_h g_T(t-kT-\tau)\mathbf{a}(\phi)^H\mathbf{a}(\phi) =$$

$$= 2P_s M\rho^2\sum_k |c_k|^2 g_T^2(t-kT-\tau)$$

$$J_{\psi\psi} = \frac{1}{2N_0}\int_{kT+\tau}^{kT+T+\tau}\mathrm{Re}\left\{2P_s M\rho^2\sum_k |c_k|^2 g_T^2(t-kT-\tau)\right\}dt = M\rho^2\frac{2P_s T}{2N_0} = \frac{M\rho^2}{\sigma^2}$$

- $J_{\psi\phi} = J_{\phi\psi}$:

$$\left[\frac{\partial r(t)\mathbf{a}(\phi)}{\partial\psi}\right]^H\frac{\partial r(t)\mathbf{a}(\phi)}{\partial\phi} =$$

$$= -j\rho^2 2P_s\sum_k c_k^* g_T(t-kT-\tau)\sum_h c_h g_T(t-kT-\tau)\mathbf{a}(\phi)^H\dot{\mathbf{a}}(\phi) =$$

$$= -j\rho^2 2P_s\sum_k |c_k|^2 g_T^2(t-kT-\tau)\left[-j2\pi\frac{f_c}{c}d\sin\phi\frac{M(M-1)}{2}\right]$$

$$J_{\psi\phi} = \frac{1}{2N_0} \int_{kT+\tau}^{kT+T+\tau} \mathrm{Re}\left\{ -\rho^2 2P_s \sum_k |c_k|^2 \, g_T^2(t-kT-\tau) \right.$$

$$\left. \left[2\pi \frac{f_c}{c} d \sin\phi \frac{M(M-1)}{2} \right] \right\} dt =$$

$$= -\frac{2\rho^2 P_s T}{2N_0} \left[2\pi \frac{f_c}{c} d \sin\phi \frac{M(M-1)}{2} \right] = -2\pi \frac{f_c}{c} d \sin\phi \frac{M(M-1)}{2} \frac{\rho^2}{\sigma^2}$$

- $J_{\phi\phi}$:

$$\frac{\partial r(t)\mathbf{a}(\phi)}{\partial \phi} = \rho e^{j\psi} \sqrt{2P_s} \sum_k c_k g_T(t-kT-\tau) e^{j2\pi f_c t} \dot{\mathbf{a}}(\phi)$$

$$\left| \frac{\partial r(t)\mathbf{a}(\phi)}{\partial \phi} \right|^2 = \rho^2 2P_s \sum_k c_k^* g_T(t-kT-\tau) \sum_h c_k g_T(t-kT-\tau) \dot{\mathbf{a}}(\phi)^H \dot{\mathbf{a}}(\phi) =$$

$$= \rho^2 2P_s \sum_k |c_k|^2 \, g_T^2(t-kT-\tau) \left(2\pi \frac{f_c}{c} d \sin\phi \right)^2 \frac{M(M-1)(2M-1)}{6}$$

$$J_{\phi\phi} = \frac{1}{2N_0} \int_{kT+\tau}^{kT+T+\tau} \mathrm{Re}\left\{ \rho^2 2P_s \sum_k |c_k|^2 \, g_T^2(t-kT-\tau) \right.$$

$$\left. \left(2\pi \frac{f_c}{c} d \sin\phi \right)^2 \frac{M(M-1)(2M-1)}{6} \right\} =$$

$$= \left(2\pi \frac{f_c}{c} d \sin\phi \right)^2 \frac{M(M-1)(2M-1)}{6} \frac{\rho^2}{\sigma^2}$$

B.3 Derivation of the **FIM** *for OFDM Signals in the case of Frequency Selective Channels*

The log likelihood function $\Delta(\mathbf{z}/\mathbf{u})$ for single carrier signals (4.12) can be written as follows

$$\Delta(\mathbf{z}/\mathbf{u}) = -\frac{1}{2\sigma_{SC}^2}\left(\mathbf{z}[k]-E\{\mathbf{z}[k]\}\right)^H\left(\mathbf{z}[k]-E\{\mathbf{z}[k]\}\right)$$

where $\mathbf{z}[k]$ is the *1xN$_p$M* vector given in (5.34), σ_{SC}^2 is the thermal noise variance given in (5.33) and $E\{\mathbf{z}[k]\}$ is the statistical mean value of $\mathbf{z}[k]$. The statistical expectation is calculated versus the thermal noise and gives the following *1xN$_p$M* vector

$$E\{\mathbf{z}[k]\} = \begin{bmatrix} H[k,0]\mathbf{a}_{ULA}^{0}(\phi) \\ \vdots \\ H[k,i]\mathbf{a}_{ULA}^{i}(\phi) \\ \vdots \\ H[k,i]\mathbf{a}_{ULA}^{N_p-1}(\phi) \end{bmatrix}$$

The tuple *1x(2N$_p$+1)* $\mathbf{u}$ of unknown parameters in $\mathbf{z}[k]$ is

$$\mathbf{u} = \begin{bmatrix} |H[k,0]| \\ \vdots \\ |H[k,N_p-1]| \\ \angle H[k,0] \\ \vdots \\ \angle H[k,N_p-1] \\ \phi \end{bmatrix}$$

The elements of the **FIM** are calculated through

$$J_{u_v u_w} = -E_{\mathbf{n}}\left\{\frac{\partial^2 \ln \Delta(\mathbf{z}/\mathbf{u})}{\partial u_v \partial u_w}\right\} \tag{7.7}$$

The application of (7.7) is easy by noting that differentiating $\mathbf{z}[k]$ and $E\{\mathbf{z}[k]\}$ versus the unknown parameters specific of the sub-carrier *i*, i.e.

$|H[k,i]|$ and $\angle H[k,i]$, are zero in those positions related to the specific unknowns, $|H[k,j]|$ and $\angle H[k,j]$, of any other sub-carrier *j*, with $j \neq i$. For instance $u_v = |H[k,i]|$ yields

$$\frac{\partial \mathbf{z}[k]}{\partial |H[k,i]|} = \left[(0 \ \cdots \ 0) \ \cdots \ (0 \ \cdots \ 0) \ \ \frac{\partial \mathbf{z}^T[k,i]}{\partial |H[k,i]|} \ \ (0 \ \cdots \ 0) \ \cdots \ (0 \ \cdots \ 0) \right]^T$$

and

$$\frac{\partial E\{\mathbf{z}[k]\}}{\partial |H[k,i]|} = \left[(0 \ \cdots \ 0) \ \cdots \ (0 \ \cdots \ 0) \ \ \frac{\partial E\{\mathbf{z}^T[k,i]\}}{\partial |H[k,i]|} \ \ (0 \ \cdots \ 0) \ \cdots \ (0 \ \cdots \ 0) \right]^T$$

Bearing this in mind, the computation of (7.7) simplifies by observing that

O1) The cross derivatives versus the amplitudes and phases of the channel frequency responses of distinct sub-carriers, i.e. *i*-th sub-carrier and *j*-th subcarrier, with $i \neq j$, are null.

O2) The derivatives versus the unknowns of a same sub-carrier, develop in the same way as the corresponding derivatives of narrow band signals of Appendix B.1. Hence, we can reuse the results of Appendix B.1.

The expressions of entries of the **FIM** are listed next.

- $u_v = |H[k,i]|$ and $u_w = |H[k,i]|$

$$J_{|H[k,i]|,|H[k,i]|} = \frac{M}{\sigma_{SC}^2}$$

which corresponds to $J_{\rho\rho}$ of Appendix B.1.

- $u_v = |H[k,i]|$ and $u_w = |H[k,j]|$ with $j \neq i$,

$$J_{|H[k,i]|,|H[k,j]|} = 0$$

because of the observation O1.

- $u_v = |H[k,i]|$ and $u_w = \angle H[k,i]$

$$J_{|H[k,i]|,\angle H[k,i]} = 0$$

which corresponds to $J_{\rho\psi}$ of Appendix B.1.

- $u_v = |H[k,i]|$ and $u_w = \angle H[k,j]$ with $j \neq i$,

$$J_{|H[k,i]|,\angle H[k,j]} = 0$$

because of the observation O1.

- $u_v = |H[k,i]|$ and $u_w = \phi$

$$J_{|H[k,i]|,\phi} = 0$$

because of the observation O1 when $j \neq i$ and by using the results about $J_{\rho\phi}$ of Appendix B.1 when $j = i$.

In the following we have listed the results related to the block **Θ** of the **FIM** which is of interest for the computation of the CRB for DOA.

- $u_v = \angle H[k,i]$ and $u_w = \angle H[k,i]$

$$J_{\angle H[k,i],\angle H[k,i]} = \frac{M|H[k,i]|^2}{\sigma_{SC}^2}$$

which corresponds to $J_{\psi\psi}$ of Appendix B.1.

- $u_v = \angle H[k,i]$ and $u_w = \angle H[k,j]$ with $j \neq i$,

$$J_{\angle H[k,i],\angle H[k,j]} = 0$$

because of the observation O1.

- $u_v = \angle H[k,i]$ and $u_w = \phi$

$$J_{\angle H[k,i],\phi} = -2\pi \frac{f_i}{c} d \sin\phi \frac{M(M-1)}{2} \frac{|H[k,i]|^2}{\sigma_{SC}^2}$$

which corresponds to $J_{\psi\phi}$ of Appendix B.1.

- $u_v = \phi$ and $u_w = \phi$

$$J_{\phi,\phi} = \frac{M(M-1)(2M-1)}{6} \sum_{i=0}^{N_p-1} \left(2\pi \frac{f_i}{c} d \sin\phi\right)^2 \frac{|H[k,i]|^2}{\sigma_{SC}^2}$$

where each element of the summation corresponds to the corresponding entry $J_{\phi,\phi}$ of Appendix B.1.

References

[1] IEEE 802.15.3: Wireless Medium Access Control (MAC) and Physical Layer (PHY) Specifications for Personal Area Networks. (WPANs).

[2] IEEE 802.15 Working Group for WPAN, http://www.802.15.org/15/.

[3] WiMedia Alliance, http://www.wimedia.org.

[4] R. Parsad, OFDM for Wireless Communications Systems, Artech House, 2004.

[5] J.C Liberti Jr., T.S. Rappaport, *Smart Antennas for Wireless Communications*, Prentice Hall, New York, 1999.

[6] C.H. Doan, S. Emami, D.A.Sobel, A.M. Niknejad, and R.W. Brodersen, "Design Considerations for 60GHz CMOS Radios," *IEEE Communications Magazine*, vol. 42, no 12, pp. 132-140, 2004.

[7] M. R. Williamson, G. E. Athanasiadou and A. R. Nix, "Investigating the Effects of Antenna Directivity on Wireless Indoor Communications at 60 GHz," *In proceeding of 8th IEEE International Symposium on Personal, Indoor and Mobile Radio Communications (PIMRC'97),* vol. 2, pp. 635-639, Sept. 1997.

[8] H. Xu, V. Kukshya and T.S. Rappaport, "Spatial and Temporal Characteristics of 60 GHz Indoor Channels," *Journal on Selected Areas in Communications*, vol. 20, no. 3, pp. 620-630, 2002.

[9] L. Bao and J. Garcia-Luna-Aceves, "Transmission Scheduling in Ad Hoc Networks with directional Antennas," *In proceedings of the 8th Annual International Conference on Mobile Computing and Networking (ACM/MOBICOM '02)*, pp 48-58, Sept. 2002.

[10] T. Spyropoulos and C. S. Raghavendra, "ADAPT: A Media Access Control Protocol for Mobile Ad Hoc Networks Using Adaptive Array Antennas*," In proceedings of the 15th IEEE International Symposium on*

Personal, Indoor, and Mobile Radio Communications (PIMRC '04), vol. 2, pp. 370-374, Sept. 2004.

[11] H. Singh and S. Singh, "A MAC Protocol Based on Adaptive Beamforming for Ad Hoc Networks," *In proceedings of the 14th IEEE International Symposium on Personal, Indoor, and Mobile Radio Communications (PIMRC '03)*, vol. 2, pp 7-10, Sept. 2003.

[12] H. Singh and S. Singh, "Smart-802.11b MAC protocol for use with Smart Antennas," *In proceedings of the IEEE 2004 International Conference on Communications (ICC '04)*, vol. 6, pp. 3686-3688, June 2004.

[13] H. Sing and S. Singh, "DOA-ALOHA: Slotted Aloha for Ad Hoc Networking Using Smart Antennas," *In Proceedings of the 58th Vehicular Technology Conference (VCT '03-Fall)*, vol. 5, pp. 2804-2808, Oct. 2003.

[14] M. Takai, J. Martin, R. Bagrodia, and A. Ren, "Directional Virtual Carrier Sensing for Directional Antennas in Mobile Ad Hoc Networks," *In proceedings of the 3rd ACM International Symposium on Mobile Ad Hoc Networking & Computing (MobiHoc '02)*, pp. 183-193, June 2002.

[15] Z. Zhan, "Pure Directional Transmission and Reception Algorithms in Wireless Ad Hoc Networks with Directional Antennas," *In proceedings of the IEEE 2005 International Conference on Communications (ICC '05)*, vol. 5, pp. 3386-3390, May 2005.

[16] A. Nasipuri, S. Ye and R. E. Hiromoto, "A MAC Protocol for Mobile Ad Hoc Networks Using Directional Antennas," *In proceedings of the IEEE Wireless Communications and Networking Conference 2000 (WCNC '00)*, vol. 3, pp. 1214-1219, Sept. 2000.

[17] R. R. Choudhury, X. Yang, N. R. Ramanathan and H. Vaidya, "On Designing MAC Protocols for Wireless Networks Using Directional

Antennas," *IEEE Transactions on Mobile Computing*, vol. 5, Issue 5, pp 477-491, May 2006.

[18] T. Korakis, G. Jakllar and L. Tassiulas, "CDR-MAC: A Protocol for Full Exploitation of Directional Antennas in Ad Hoc Wireless Networks," *to appear on IEEE Transactions on Mobile Computing*.

[19] R. Ramanathan, J. Redi, C. Santivanez, D. Wiggings and S. Polit, "Ad Hoc Networking with Directional Antennas: A Complete System Solution," *IEEE Journal on Selected Areas in Communications*, vol. 23, issue 3, pp. 496-506, March 2005.

[20] D. A. Fittipaldi, S. Skafidas and M. Luise, "IEEE 802.15.3c Medium Access Controller Throughput for Phased Array Systems," *to appear in proceedings of the 18th IEEE International Symposium on Personal, Indoor, and Mobile Radio Communications (PIMRC '07)*, Sept. 2007.

[21] M. Demirhan, IEEE 802.15.3 MAC model for ns-2, http://www.winlab.rutgers.edu/~demirhan.

[22] M. A. Doron and E. Doron, "Wavefield Modelling and Array Processing Part III-Resolution Capacity," *IEEE Transactions on Signal Processing*, vol. 42, pp. 2571-2580, Oct. 1994.

[23] U. Baysal and R. L. Moses, "Source Localization with Isotropic Wideband Arrays," *In proceedings of the IEEE International Conference on Acoustics, Speech and Signal Processing 2002 (ICASSP '02)*, vol. 3, pp. 3045-3048, May 2002.

[24] H. Krim and M. Viterbi, "Two decades of Array Signal Processing Research: The Parametric Approach," *IEEE Signal Processing Magazine*, vol. 13, issue 4, pp. 67-94, July 1996.

[25] Stutzman, W. L., and G.A. Thiele, *Antenna Theory and Design*. John Wiley and Sons, 1998.

[26] L. Josefsson and P. Persson *Conformal Antenna Array Theory and Design*,Wiley-IEEE Press, March 2006.

[27] J.D. Kraus, *Antennas*, McGraw-Hill, New York, 1988.

[28] C.A. Balanis, *Antenna Theory: Analysis and Design*, John Wiley & Sons, New York, 1982.

[29] J. Ward and R.T. Compton "Improving the Performance of a Slotted Aloha Packet Radio Network with Adaptive Array," *IEEE Transactions on Communications*, vol. 40, pp. 292-300, Feb. 1992.

[30] TG3c Channel Modelling Sub-committee Final Report IEEE 15-07-0584-00-003c.

[31] A. N. D'Andrea, U. Mengali and R. Reggiannini, "The Modified Cramer-Rao Bound and Its Application to Synchronization Problems," *IEEE Transactions on Communications*, vol. 42, pp. 1391-1399, Feb.-Apr. 1994.

[32] F. Gini, R. Reggiannini and U. Mengali, "The Modified Cramér-Rao Bound in Vector Parameter Estimation," *IEEE Transactions on Communications*, vol. 46, pp. 52-60, Jan. 1998.

[33] H. Van Trees, *Detection, Estimation and Modulation Theory*, *Part I*. Wiley, New York, 1967.

[34] R. Van Nee, G. Awater, M. Morikura, H. Takanashi, M. Webster, K. W. Halford, "New High Rate Wireless Standards," *IEEE Communications Magazine*, vol. 30, no. 2, pp. 82-88, Dec. 1999.

[35] C. –C. Chong, C, –M. Tan, D. I. Laursenson, S. McLaughlin, M. A. Beach and A. R. Nix, "A New Statistical Wideband Spatio-Temporal Channel Model for 5-GHz Band WLAN Systems," *IEEE Journal on Selected Areas in Communications*, vol. 21, no. 2, pp. 139-150, Feb. 2003.